Developmental Cell

CellPress

Article

EYA protein complex is required for Wntless retrograde trafficking from endosomes to Golgi

Hilal Ahmad Reshi,[1,2] Raghavender Medishetti,[3] Aishwarya Ahuja,[4] Deepa Balasubramanian,[5] Kavita Babu,[4] Manish Jaiswal,[5] Kiranam Chatti,[3] and Subbareddy Maddika[1,6,*]

[1]Laboratory of Cell Death & Cell Survival, Centre for DNA Fingerprinting and Diagnostics (CDFD), Uppal, Hyderabad 500039, India
[2]Graduate Studies, Regional Centre for Biotechnology, Faridabad 121001, India
[3]Dr. Reddy's Institute of Life Sciences (DRILS), University of Hyderabad Campus, Hyderabad 500046, India
[4]Centre for Neuroscience, Indian Institute of Science (IISc), Bangalore 560012, India
[5]Tata Institute of Fundamental Research, Hyderabad 500046, India
[6]Lead contact
*Correspondence: msreddy@cdfd.org.in
https://doi.org/10.1016/j.devcel.2024.05.021

SUMMARY

Retrograde transport of WLS (Wntless) from endosomes to *trans*-Golgi network (TGN) is required for efficient Wnt secretion during development. However, the molecular players connecting endosomes to TGN during WLS trafficking are limited. Here, we identified a role for Eyes Absent (EYA) proteins during retrograde trafficking of WLS to TGN in human cell lines. By using worm, fly, and zebrafish models, we found that the EYA-secretory carrier-associated membrane protein 3 (SCAMP3) axis is evolved in vertebrates. EYAs form a complex and interact with retromer on early endosomes. Retromer-bound EYA complex recruits SCAMP3 to endosomes, which is necessary for the fusion of WLS-containing endosomes to TGN. Loss of EYA complex or SCAMP3 leads to defective transport of WLS to TGN and failed Wnt secretion. EYA mutations found in patients with hearing loss form a dysfunctional EYA-retromer complex that fails to activate Wnt signaling. These findings identify the EYA complex as a component of retrograde trafficking of WLS from the endosome to TGN.

INTRODUCTION

Wnt ligands are secreted morphogens that engage the frizzled and LRP (low-density-lipoprotein receptor-related proteins) receptors in the neighbouring cells, induce Wnt signaling, and upregulate the transcription of genes associated with proliferation, polarity, and differentiation.[1,2] After synthesis in the endoplasmic reticulum (ER), Wnts are lipidated by porcupine and get complexed with Wntless (WLS)/GPR177, a GPCR-like transmembrane protein that helps its anterograde movement toward the cell surface.[3–5] Although Wnts are secreted into the extracellular medium, WLS undergoes recycling via clathrin-mediated endocytosis.[6] A hetero-trimeric protein complex VPS26-VPS35-VPS29 called retromer along with a sorting nexin, SNX3 tethers to the surface of the early endosomes via PI3P lipids and directs WLS movement to the *trans*-Golgi network (TGN).[7,8] Thus, WLS becomes available for additional rounds of Wnt transport in Wnt-secretory cells.[9,10] Although conserved oligomeric Golgi (COG) complex, SNX3, GCC185, and SNARES regulate the capture and tethering of Golgi-bound vesicles,[11] the proteins that orchestrate the precise transport of WLS from endosomes to TGN are relatively unknown. Here, we demonstrate that Eyes Absent (EYA) proteins, along with a Golgi resident protein, secretory carrier-associated membrane protein 3 (SCAMP3), associate with retromer and lie at an interface between the two organelles to facilitate accurate trafficking of WLS from the endosome to the TGN.

The EYA proteins belong to a unique family of proteins that possess a distinct combination of biochemical activities such as serine/threonine phosphatase activity, tyrosine phosphatase activity, and transactivation activity in the same polypeptide.[12] Traditionally considered a part of the retinal determination (RD) network in *Drosophila* or a part of the Pax-Sox-Eya-Dach Network (PSEDN) in mammals, EYAs are involved in crucial stages of development, cell fate determination, and organogenesis.[13,14] Mutations in EYA genes lead to several disorders, including branchio-oto-renal (BOR) syndrome, late-onset sensorineural hearing loss, dilated cardiomyopathy, and congenital cataracts.[15–17] However, the underlying mechanisms defining the role of EYA proteins in these disorders are largely unknown.

EYAs have a highly conserved ~270 amino acid C-terminal EYA domain (ED) and a less conserved N-terminal domain that is enriched in proline, serine, and threonine (PST), motifs.[18] The ED harbors aspartyl-phosphotyrosine phosphatase activity and participates in protein-protein interactions, while as N-terminal domain includes motifs for serine/threonine phosphatase activity and helps in transactivation.[12,19,20] EYA proteins are bona fide cytoplasmic proteins that move to the nucleus after interacting

Please cite this article in press as: Reshi et al., EYA protein complex is required for Wntless retrograde trafficking from endosomes to Golgi, Developmental Cell (2024), https://doi.org/10.1016/j.devcel.2024.05.021

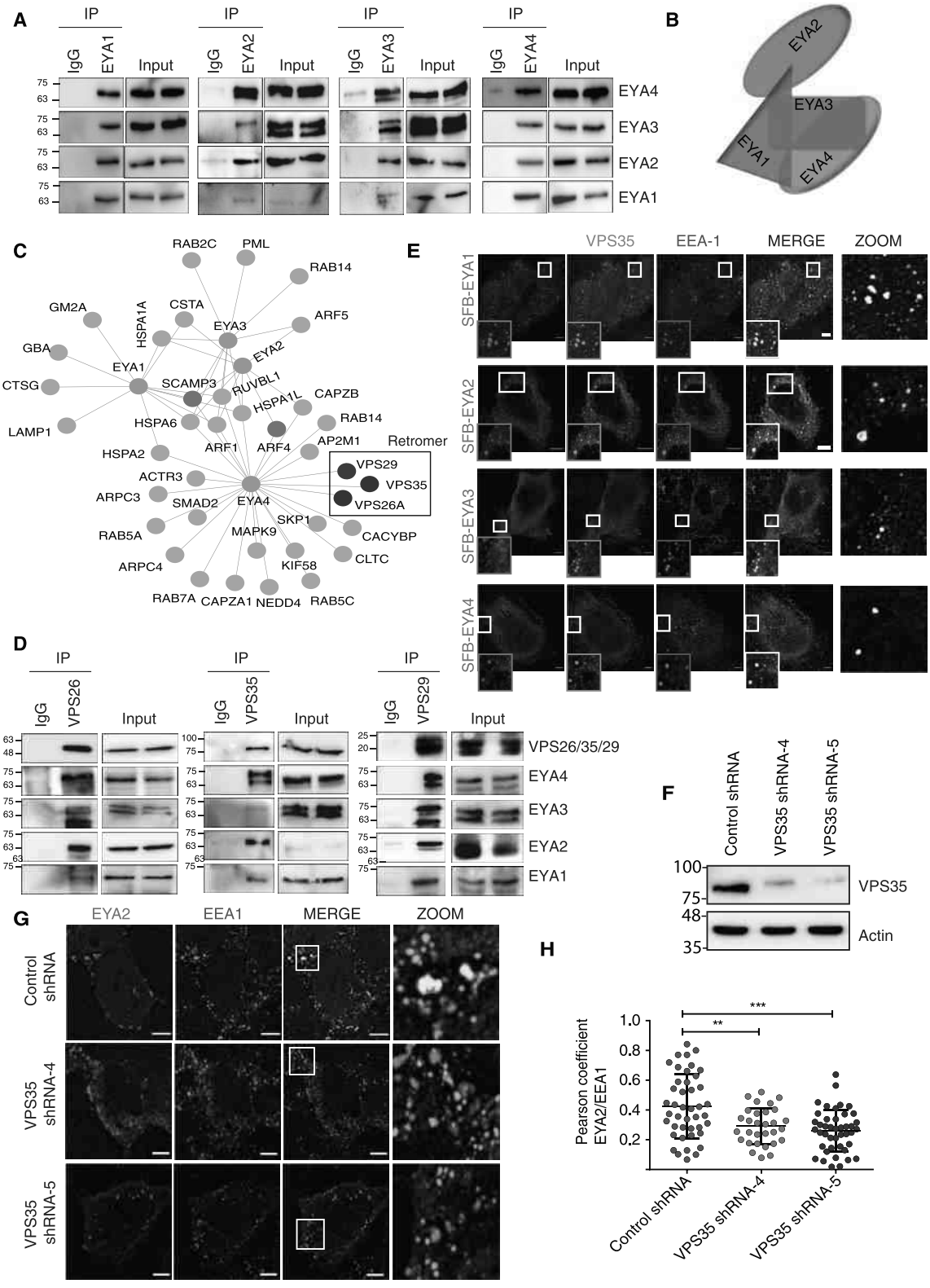

Figure 1. EYA proteins form a hetero-tetrameric complex that associates with retromer-SNX3

(A) Endogenous immunoprecipitations (IPs) with either immunoglobulin G (IgG) control or EYA-specific antibodies were carried out using 293T cell lysates. The endogenous interactions between EYA proteins were evaluated by immunoblotting using the indicated antibodies.

(legend continued on next page)

Please cite this article in press as: Reshi et al., EYA protein complex is required for Wntless retrograde trafficking from endosomes to Golgi, Developmental Cell (2024), https://doi.org/10.1016/j.devcel.2024.05.021

with homeodomain-containing SIX proteins and activate transcription from SIX-responsive elements.[21] EYA proteins are known to participate in limited cellular functions such as apoptosis and DNA repair.[22–24] Here, we identified an important cellular function for EYA proteins during vesicular trafficking. We demonstrate that EYA1-4 proteins interact with one another to form a hetero-tetrameric complex that facilitates retrograde transport of WLS cargo from endosomes to the TGN.

RESULTS

EYA phosphatase complex interacts with the retromer complex

To expand the cellular functions of EYA phosphatases, we analyzed the list of EYA1–4-associated proteins derived through an interaction proteomics approach in our earlier study.[25] Interestingly, we found that different EYA members were present in other EYA phosphatase complexes, possibly suggesting an assembly of multi-protein complex. For instance, EYA1 and EYA2 were present in the EYA4 complex, and EYA4 was present in EYA1 and EYA2 interactome list (Figure S1A). We confirmed the endogenous association of EYA1, EYA2, EYA3, and EYA4 with each other in cells (Figure 1A). Also, we validated the association of exogenously expressed EYA proteins with each other by performing co-immunoprecipitation experiments (Figures S1B–S1D). Next, to understand the architecture of the EYA complex involving all four EYA proteins, we performed *in vitro* binding experiments using bacterially purified recombinant maltose binding protein (MBP)- and His-tagged versions of EYAs. These experiments revealed direct interaction of EYA1 with EYA2, EYA3, 4; EYA2 with EYA1; EYA3 with EYA1, EYA4; and EYA4 with EYA1, EYA3 (Figures S1E–S1H). Together, our data revealed a multi-component complex containing all four members of the EYA family (Figure 1B). So far, EYA phosphatases have been studied individually, and their functions have been attributed to the monomeric state of EYAs. However, as we now identified that EYAs can exist in a hetero-tetrameric complex, we sought to identify the role of this complex in cells. Kyoto Encyclopedia of Genes and Genomes (KEGG) pathway enrichment analysis using pooled interactomes of all EYA proteins revealed several previously uncharacterized functions for EYAs, including ER processing, endocytosis, and retrograde signaling (Figure S1I). Interestingly, many EYA-associated proteins were found to be enriched in the secretory granules, intracellular membrane-bound organelles, and cytoplasmic vesicles (Figure S1J), suggesting a possible role for EYAs in vesicular trafficking. Indeed, several proteins with a key role in vesicular trafficking were found in EYA complexes (Figure 1C). Among these proteins, we consistently found retromer components in the EYA complex. By performing immunoprecipitation with specific antibodies, we established the interaction of EYA1–4 with retromer components VPS26, VPS29, and VPS35 (Figure 1D). Also, the association of all retromer components with the EYA complex was confirmed by using exogenously expressed EYA proteins (Figures S1K–S1M). Further, in our size-exclusion chromatography experiments, retromer components were co-eluted along with EYA proteins in higher molecular complexes (Figure S1N), suggesting that EYA and retromer complex proteins physically interact with each other and assemble a large complex in cells. All human EYA proteins have a well-conserved C terminal domain (CTD) along with a varied N terminus.[21] Next, to test whether EYA complex formation and its association with the retromer depends on the highly conserved CTD, we made CTD deletions of each EYA protein (Figure S1O) and tested for other EYA interactions. Deletion of EYA1 CTD led to the loss of its interaction with EYA3 but not with EYA2 and 4 (Figure S1P). CTD deletion of EYA2 does not affect its interaction with other EYAs (Figure S1Q). However, although the CTD of EYA3 is required for its interaction with all other EYAs (Figure S1R), the CTD of EYA4 is necessary for its interaction with EYA2 and EYA3 (Figure S1S). On the other hand, the C-terminal deletion mutants of EYA1, EYA2, and EYA3 but not EYA4 fail to interact with retromer (represented by VPS26) (Figures S1T–S1W), suggesting that CTD of EYA1–3 is necessary for their association with retromer. Together, our mapping data suggest that CTD of EYA1, 3, and 4 is required for EYA complex formation, and the CTD of EYA1–3 along with EYA4 N terminus is necessary for binding of retromer with EYA complex (Figure S1X).

Retromer complex localizes to early endosomes and sorts the cargoes to distinct routes of transport. We tested if EYA proteins via their association with the retromer complex localize to endosomes to function in cargo trafficking. Indeed, all EYA proteins displayed co-localization with retromer component VPS35 (Figure S1Y) as well as the early endosomal marker, EEA1 (Figures 1E and S1Z). Importantly, depletion of retromer component VPS35 in cells (Figure 1F) significantly reduced the co-localization of EYAs with EEA1 (Figures 1G and 1H), clearly suggesting that retromer binding is necessary for the recruitment of EYA complex to endosomes. Retromer associates with distinct SNX proteins to orchestrate the sorting of diverse cargo proteins

(B) The architecture of the EYA complex as determined from pull-down experiments using MBP and His-tagged versions of the EYA proteins is shown.
(C) A network of vesicular trafficking proteins associated with EYA1, EYA2, EYA3, and EYA4 is shown. The components of retromer (VPS26, VPS29, and VPS35) are highlighted.
(D) Endogenous IPs were carried out with either IgG control or antibodies against the components of retromer (VPS26, VPS29, and VPS35) using 293T lysates. Interactions of EYA proteins with retromer components were detected using the indicated antibodies.
(E) Localization of EYA proteins with retromer-coated (VPS35$^+$) early endosomes (EEA1) was studied using Carl Zeiss ELYRA Super-resolution microscope (63× oil immersion lens, NA 1.46). Scale bars, 5 μm. The triple-positive retromer and EYA-decorated early endosomes are highlighted.
(F) A western blot showing shRNA-mediated knockdown (KD) of the retromer component VPS35. The immunoblotting was done using a VPS35 antibody with actin as a loading control.
(G) The localization of EYA proteins (EYA2) to early endosomes (EEA1) in normal or VPS35-depleted 293T cells was assessed by imaging S protein-FLAG-Streptavidin binding peptide (SFB) tagged-EYA2-transfected cells using Carl Zeiss ELYRA Super-resolution microscope (63× oil immersion lens, NA 1.46). Scale bars, 5 μm.
(H) The co-localization of VPS35 with EEA1 was quantified by comparing Pearsons's co-relation coefficient for control or the VPS35 knockdown cells and plotting using GraphPad Prism software with ($n \geq 30$). The error bars represent standard deviation, $^{**}p < 0.01$, $^{***}p < 0.001$ (one-way ANOVA).

Please cite this article in press as: Reshi et al., EYA protein complex is required for Wntless retrograde trafficking from endosomes to Golgi, Developmental Cell (2024), https://doi.org/10.1016/j.devcel.2024.05.021

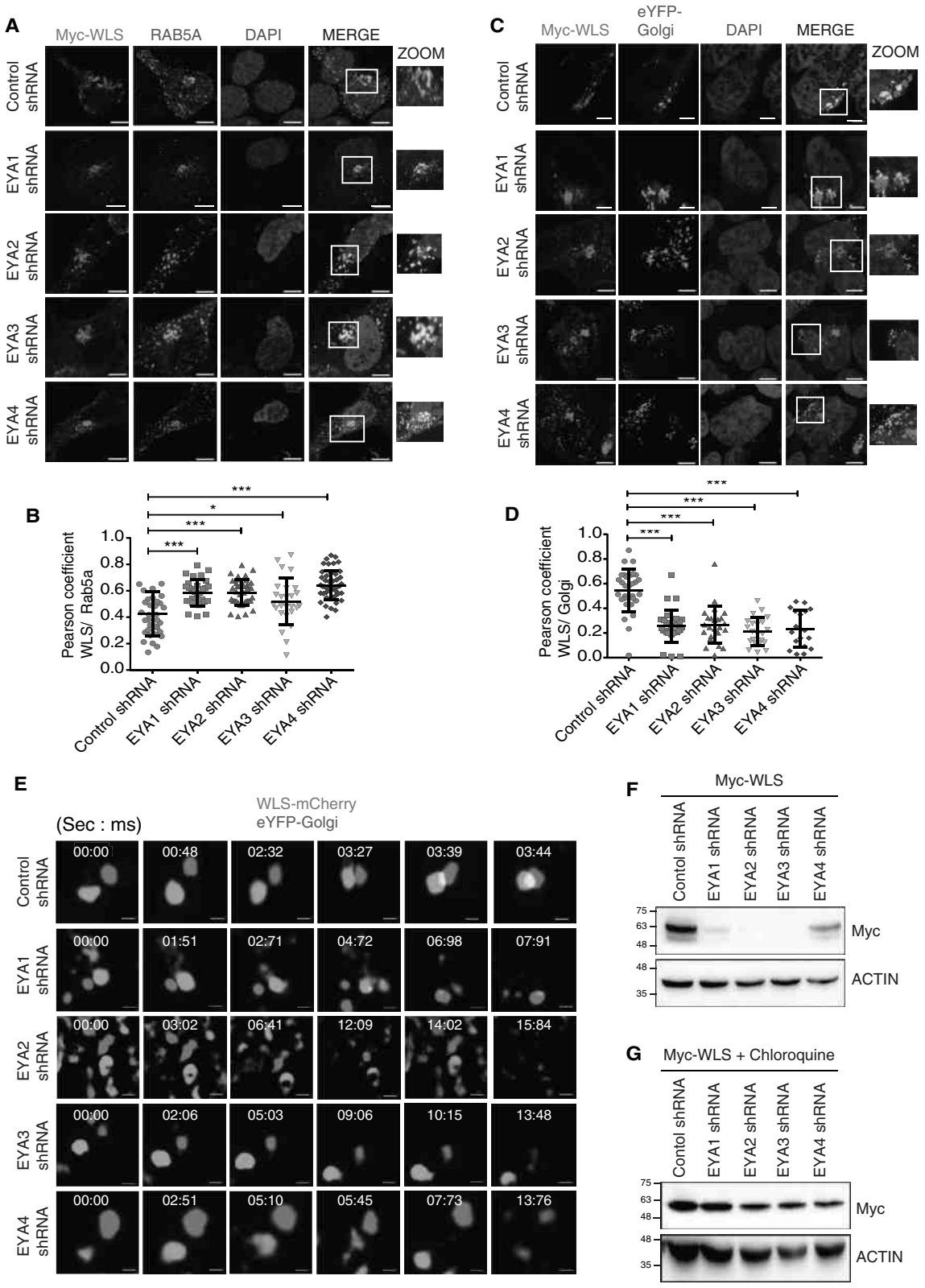

Figure 2. EYA depletion disrupts WLS movement from early endosomes to the *trans*-Golgi network

(A) Control or stable EYA knockdown 293T cells were transfected with Myc-Wntless. Localization of WLS with Rab5a endosomes was determined by confocal imaging (LSM 700, 63×, and NA 1.4) after co-staining with RAB5A and WLS antibodies. Scale bars, 10 μm.

(legend continued on next page)

into precise trafficking routes.[26] Whereas SNX1/2-SNX5/6-associated retromer complex mediates retrograde endosome-to-TGN trafficking of mannose 6-phosphate receptor, SNX27-retromer recycle cargoes such as β2 adrenergic receptor and GLUT1 to the plasma membrane, and retromer bound with SNX3 participates in retrograde trafficking of WLS to TGN. Although retromer component VPS26 interacts with different SNX proteins, none of the EYA proteins interacted with SNX1 and SNX27 (Figures S2A and S2B). Although EYA3 efficiently interacted with SNX5, other EYA proteins failed to associate with SNX5 (Figure S2C). However, all the EYA proteins readily interacted with SNX3 in cells (Figure S2D), thus suggesting that the EYA complex might have a critical role in the trafficking of SNX3-dependent cargoes in cells.

EYA complex facilitates WLS trafficking from endosome to TGN

WLS trafficking from endosome to TGN is dependent on the SNX3-retromer complex; however, the molecular players connecting retromer to TGN are unknown. Since we found the EYA complex's interaction specifically with retromer-SNX3, we hypothesized that the EYA complex may play an important role in linking endosomes to TGN during WLS trafficking. To test this hypothesis, we generated multiple stable cell lines each with a depletion of an individual EYA protein using specific short hairpin RNAs (shRNA) (Figures S2E–S2H) and tracked the localization of Myc-WLS with early endosomes, late endosomes, lysosomes, or TGN in normal and EYA-depleted conditions. Fixed-cell imaging analysis revealed a significant accumulation of WLS in early endosomes (marked with Rab5a) in all EYA-depleted cells in comparison with control cells (Figures 2A and 2B). Consequently, as evident from reduced co-localization with TGN markers, the fraction of WLS reaching TGN is severely compromised in EYA-depleted cells (Figures 2C and 2D). Furthermore, in our time-lapse experiments, we observed that mCherry-WLS punctae fuse readily with eYFP-Golgi punctae in normal cells, but such fusion events were rare in cells depleted for EYA proteins (Figure 2E; Video S1), thus clearly suggesting that EYA proteins are essential for WLS movement from early endosomes to TGN. Defective movement of WLS to TGN in EYA-depleted cells led to rerouting of cargo to the endo-lysosomal pathway as WLS is found to be significantly enriched in CD63 positive multi-vesicular bodies (Figures S2I and S2J) and LAMP2 positive lysosomes (Figures S2K and S2L) in these cells. The initial accumulation of WLS in lysosome is followed by degradation. After 30 h of expression, WLS levels were severely low in EYA-depleted cells, while its protein levels remained stable in control cells (Figure 2F). Importantly, the levels of WLS in EYA knockdown cells could, however, be rescued by treating the cells with chloroquine (a lysosomal inhibitor) for 6 h (Figure 2G), thus confirming the lysosomal pathway as a mode of cargo degradation in EYA-depleted cells. Depletion of individual EYAs led to the reduction of other EYA proteins (Figure S2M), suggesting that each EYA is necessary for a stable EYA complex. Nonetheless, not only individual EYA, depletion of all the EYAs together in cells produced similar defects in WLS trafficking such as delayed movement of cargo from endosome to TGN followed by rerouting to lysosomes in EYA-depleted cells (Figures S2N–S2S). WLS trafficking defects in EYA-depleted conditions are not restricted to transformed cells, as similar defects such as accumulation of WLS in endosomes (Figures S3A and S3B) without reaching TGN (Figures S3C and S3D) and further rerouting to lysosomes (Figures S3E and S3F) were observed in EYA-depleted primary retinal pigment epithelial cells (RPE1). To rule out the possibility that the observed WLS trafficking defect was an artifact of shRNA constructs used, we tested additional shRNAs that targeted different regions of the EYA transcripts. Defect in WLS trafficking to the TGN and accumulation in lysosomes is seen consistently with all the tested EYA shRNAs in RPE1 cells (Figures S3G and S3H). Together, these data indicate that the EYA complex is necessary to facilitate the accurate retrograde movement of WLS toward TGN from the endosome.

EYA depletion causes defective Wnt3a ligand secretion

Wntless cargo is important for the anterograde trafficking of lipidated Wnt3a from the Golgi toward the plasma membrane for secretion.[27] Since we demonstrated that the EYA complex is necessary for WLS movement to the TGN, we then assessed the effect of EYA depletion on Wnt3a in cells. Similar to the observations made in WLS defective cells earlier by Port et al.,[7] we found that Wnt3a is accumulated heavily in the form of distinct punctae in the cytoplasm of EYA-depleted cells (Figures 3A and 3B). Moreover, total internal reflection fluorescence (TIRF) surface microscopy revealed that a significantly low number of EGFP-Wnt3a reached the plasma membrane and its immediate cortical region in EYA knockdown cells as compared with the control cells (Figures 3C and 3D). Also, analysis of Wnt3a levels in the conditioned media by immunoblotting (Figure 3E) as well as ELISA (Figure 3F) suggested that loss of EYA components in cells led to defective secretion of Wnt3a ligand. Defective Wnt3a secretion in EYA-depleted cells may not be attributed to general secretion defect as the secreted levels of another protein Y-Box protein binding 1 (YB1) into the

(B) RAB5a co-localization with Myc-WLS was assessed by comparing the Pearson's correlation coefficient values of control or EYA knockdown cells ($n \geq 30$) using Zen Blue software. Error bars represent standard deviation, $^{***}p < 0.001$ (one-way ANOVA).

(C) Control 293T cells or those stably depleted for EYA proteins were co-transfected with Myc-WLS and eYFP-Golgi (a marker for *trans*-Golgi network) and imaged using a confocal microscope (LSM 700, 63×, and NA 1.4). Scale bars, 10 μm.

(D) Co-localization of WLS with Golgi was assessed using Pearson's correlation coefficient (for $n \geq 30$). Error bars represent SD, $^{*}p < 0.05$, $^{***}p < 0.001$ (one-way ANOVA).

(E) Control or EYA knockdown cells expressing WLS-mCherry and eYFP-Golgi were imaged in real-time using a Carl Zeiss ELYRA Super-resolution microscope (63× oil immersion lens, NA 1.46). The screenshots of individual punctae highlighting the fusion of WLS vesicles with Golgi are shown with the indicated time points. Scale bars, 2 μm.

(F and G) (F) Protein levels of Myc-WLS in control and EYA knockdown conditions were evaluated by immunoblotting in the absence or (G) presence of a lysosomal inhibitor, chloroquine. Actin was used as a loading control.

Please cite this article in press as: Reshi et al., EYA protein complex is required for Wntless retrograde trafficking from endosomes to Golgi, Developmental Cell (2024), https://doi.org/10.1016/j.devcel.2024.05.021

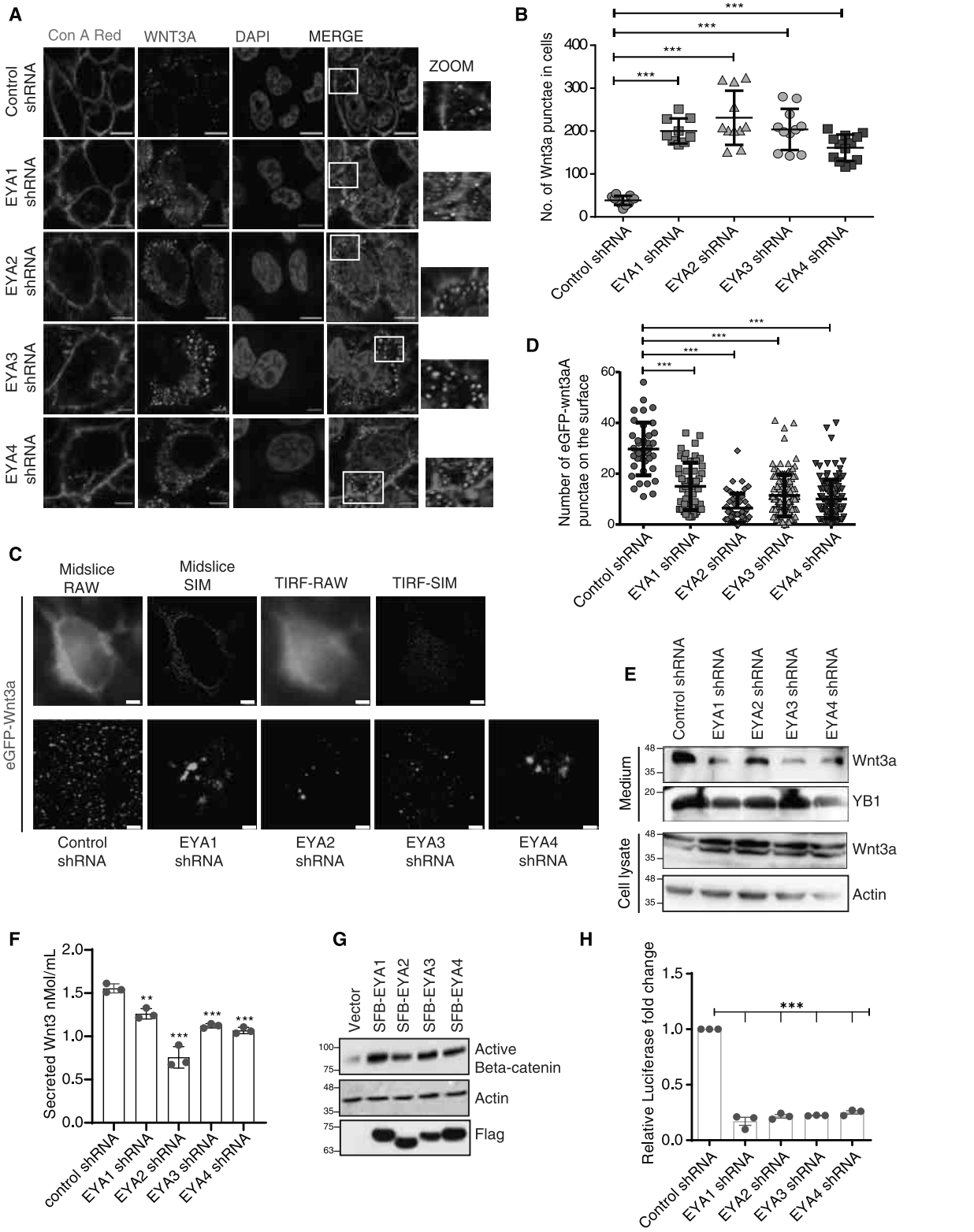

Figure 3. Loss of EYA hampers Wnt3a secretion from cells

(A) Control or EYA knockdown HeLa cells were immunostained using endogenous Wnt3a antibody, and the imaging was done using Carl Zeiss LSM 700 microscope (63×, oil immersion, NA 1.4). Scale bars, 10 μm. The peripheries of the cells were marked by fluorescent lectin, concanavalin A red.

(legend continued on next page)

medium did not show any significant changes upon EYA knockdown conditions. Next, we tested if EYA proteins, by enabling WLS-dependent Wnt secretion, functionally participate in Wnt signaling. Indeed, overexpression of any of the EYA1–4 led to enhanced active β-catenin levels in cells (Figures 3G and S4A) followed by augmented β-catenin-dependent luciferase activity (Figure S4B). The effect was observed even in a paracrine system where Wnt3a secretory and receiving systems were segregated. The addition of Wnt3a conditioned media from the cells expressing EYA proteins significantly enhanced the β-catenin-dependent luciferase activity in the receiving cells (Figure S4C). On the contrary, depletion of EYA complex components severely reduced β-catenin-dependent luciferase activity in cells (Figure 3H). Additional shRNAs targeting different regions of EYA transcripts further validated the importance of EYA presence in cells for activation of Wnt signaling (Figure S4D). As established above, the CTD of EYA proteins is necessary for EYA complex formation and its interaction with retromer. We further tested the effect of CTD loss in EYA proteins on Wnt signaling. Indeed, full-length EYAs but not their respective CTD truncated versions enhanced the β-catenin-dependent luciferase activity in cells (Figures S4E–S4H). This indicates that EYA complex formation as well as its association with retromer are important for activation of Wnt signaling in human cells.

EYA complex recruits SCAMP3 to sorting endosomes and connects it to retromer

We next sought to identify the molecular mechanism of how the EYA complex connects the endosome with TGN for WLS delivery. We analyzed the interactome data of EYA1–4 proteins and specifically searched for proteins that are present in the list of all 4 EYA protein complexes and possibly involved in vesicular trafficking. Among different vesicular trafficking proteins that are commonly found in all EYA complexes (Figure 4A), SCAMP3 is of particular interest. SCAMP3 is a transmembrane protein that is highly enriched in Golgi, and plasma membrane.[28] It is known to facilitate the movement of cargoes from the endosomes to the TGN[29] and also participates in post-Golgi recycling.[28] We confirmed the interaction of SCAMP3 with all 4 EYA proteins at the endogenous level (Figure 4B) as well as exogenously expressed proteins (Figure S5A). *In vitro* binding experiments using bacterially purified recombinant proteins indicated direct binding of SCAMP3 with EYA1 and 4, a weaker direct association with EYA3, and no direct interaction with EYA2 (Figure S5B). Interestingly, our interaction data suggest that it is the N terminus of EYA proteins that may be required for their binding with SCAMP3 and not the C-terminal domain as both the full-length EYAs and their respective ΔCTD versions bind SCAMP3 efficiently (Figure S5C). These data suggest that the EYA complex engages both SCAMP3 and retromer with distinct N-terminus and C-terminal regions, respectively, to properly tether the whole assembly to the surface of early endosomes. To further test if SCAMP3 binds to the EYA complex associated with retromer on endosomes, we checked the interaction of SCAMP3 with retromer components. SCAMP3 is found to efficiently interact with VPS26, VPS29, and VPS35 in cells (Figures 4C and S5D). As EYA complex is found to interact with SCAMP3 as well as retromer, we reasoned that EYA might be acting as a bridging complex to attach SCAMP3 to retromer-coated endosomes (Figure 4D). As predicted, the interaction of SCAMP3 with VPS26 (Figure 4E), VPS29 (Figure 4F), and VPS35 (Figure 4G) was severely reduced in EYA1–4-depleted cells in comparison with control cells. Moreover, immunofluorescence staining clearly demonstrated SCAMP3 co-localization with retromer components VPS26 (Figures S5E and S5F) and VPS35 (Figures S5G and S5H), which is severely compromised in EYA-depleted cells. These data suggest that SCAMP3 associates with the EYA-bound retromer complex at endosomes.

To further assess if SCAMP3 associates with sorting endosomes with assistance from EYA complex, we co-transfected 293T cells with GFP-SCAMP3 and Red Fluorescent Protein (RFP)-tagged RAB5A and time-tracked the fusion in real time. After initial contact, GFP-SCAMP3 vesicles are progressively recruited to RFP-RAB5A positive endosomes in control cells (Figure 5A; Video S2), whereas such events were not readily observed in EYA-depleted cells (Figure S5I; Video S3). EYA-dependent association of SCAMP3 with endosomes was further substantiated in our fixed-cell imaging experiments using another early endosomal marker. SCAMP3 readily co-localizes with EEA1, which is significantly reduced in EYA-depleted cells (Figures 5B and 5C). Further, real-time analysis of individual punctae using super-resolution microscopy demonstrated that

(B) The number of Wnt3a punctae inside the cells was counted using ImageJ software. Statistical significance was calculated using GraphPad Prism software ($n \geq 10$, one-way ANOVA, $^{***}p < 0.001$). Error bars represent SD.

(C) Control or EYA knockdown 293T cells were transfected with EGFP-Wnt3a. Raw images were captured using Carl Zeiss ELYRA Super-resolution microscope (63× oil immersion lens, NA 1.46) equipped with a TIRF imaging facility. The surface of the cells was focused by setting appropriate critical angles. The validation of the method was carried out by comparing these images with deconvoluted images of the cells taken as Z stacks and manually focusing the plasma membrane of the cells. Raw images along with TIRF-structured illumination microscopy (SIM) images showing surface localized Wnt3a for various conditions are shown. Scale bars, 5 and 2 μm for the upper and the lower panel, respectively.

(D) The number of EGFP-Wnt3a punctae present in sections on the plasma membrane after TIRF-SIM imaging was counted using ImageJ software and analyzed using GraphPad Prism ($n \geq 50$, one-way ANOVA, $^{***}p < 0.001$). Error bars represent SD.

(E) Conditioned media collected from either control or EYA knockdown cells was processed using Amicon ultrafilters, Millipore, with 30 kDa molecular weight cutoff (MWCO), and level of Wnt3a along with YB1 was detected by immunoblotting with specific antibodies.

(F) Wnt3a ELISA was used to measure the secreted Wnt3a levels. 96 well plates precoated with Wnt3a antibody were incubated with spent media from control or EYA knockdown stable cell lines. Wnt3a levels were determined by measuring the absorbance at 450 nm. The comparisons were plotted in GraphPad Prism using one-way ANOVA with n = 3 biological replicates, $^{***}p < 0.001$, and error bars representing SEM.

(G) Active-β-catenin levels in cells transfected with vector or different EYAs were determined by immunoblotting the cell lysates with specific antibodies. Actin was used as a loading control.

(H) The effect of EYA depletion on Wnt-dependent β-catenin transcriptional activity was measured using SuperTopFlash (STF) luciferase assay using Renilla luciferase as an internal control. Plot made using GraphPad Prism, n = 3 biological replicates, error bars represent standard error of the mean (SEM) with one-way ANOVA, $^{***}p < 0.001$.

Please cite this article in press as: Reshi et al., EYA protein complex is required for Wntless retrograde trafficking from endosomes to Golgi, Developmental Cell (2024), https://doi.org/10.1016/j.devcel.2024.05.021

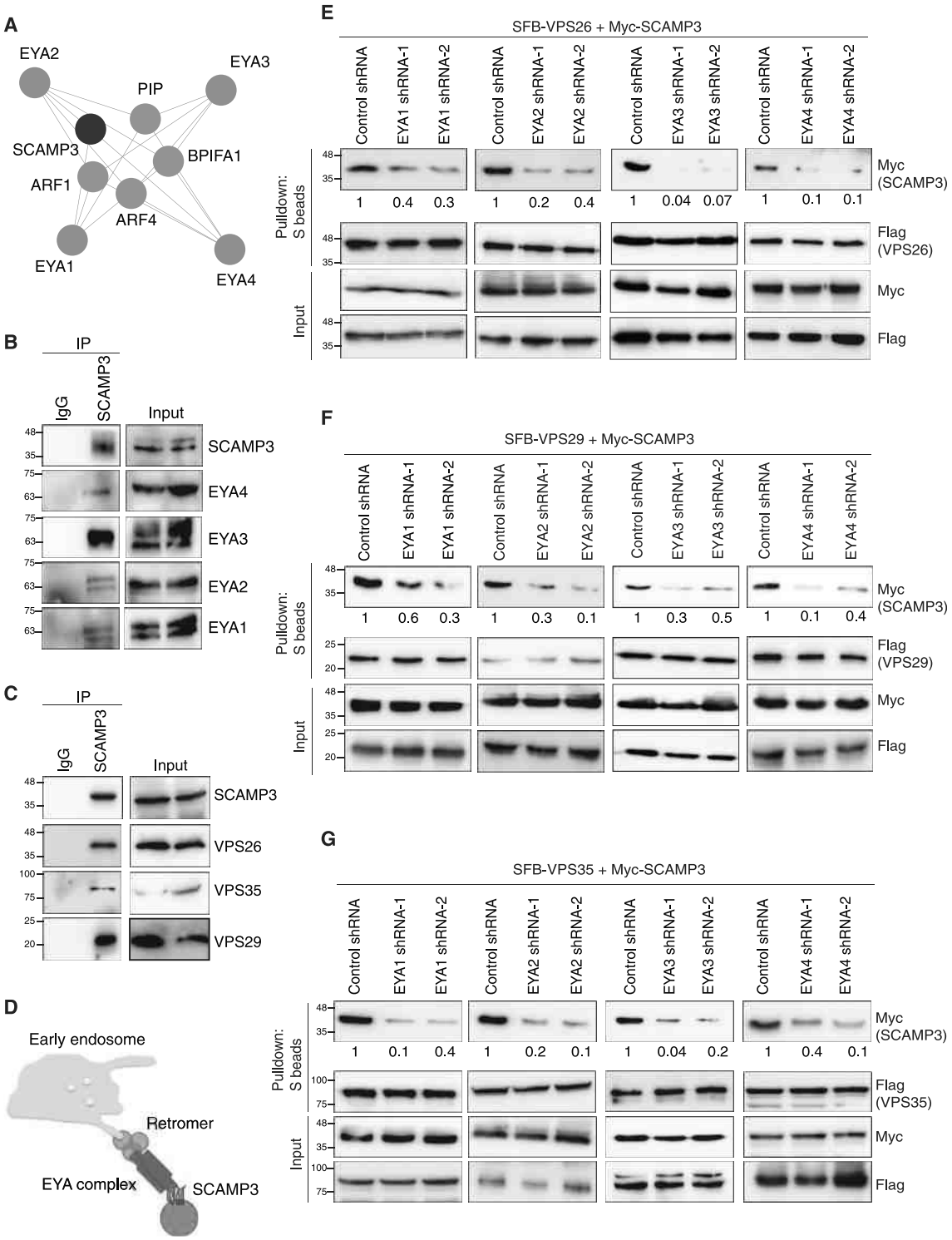

Figure 4. EYA complex bridges the retromer with SCAMP3

(A) Schematic showing vesicular trafficking proteins commonly found in the interactome of all the members of EYA complexes.

(B) Endogenous immunoprecipitation (IP) with either IgG control or SCAMP3-specific antibody was carried out using 293T cell lysates. The endogenous interaction between EYA proteins and SCAMP3 was evaluated by immunoblotting using the indicated antibodies.

(legend continued on next page)

WLS-mCherry and GFP-SCAMP3 fused in control cells, which is not observed in EYA-depleted cells (Figure 5D; Video S4). Also, triple immunofluorescence staining (WLS, EEA1, SCAMP3) experiments revealed that the EYA complex is essential for bringing SCAMP3 to WLS cargo-containing endosomes (Figure S5J). On the other hand, SCAMP3-decorated cargo vesicles fuse with the TGN, which is again dependent on the EYA complex (Figure 5E; Video S5). Together, these data suggest that the EYA complex binds to WLS-positive early endosomes via retromer and marks its surface with SCAMP3. The SCAMP3-positive WLS-containing endosomes are directed to merge with the TGN.

EYA-dependent SCAMP3 recruitment is essential for directing cargo to TGN

To determine if EYA-dependent recruitment of SCAMP3 is required for directing WLS cargo-containing endosomes toward TGN, we generated stable cell knockdowns of SCAMP3 in 293T cells (Figure 6A). Similar to EYA depletion, knockdown of SCAMP3 causes WLS accumulation in the early endosomes (Figures 6B and 6C). Cargo-containing vesicles derived from endosomes fail to fuse with TGN (Figure 6D; Video S6), leading to reduced WLS at TGN in SCAMP3-depleted cells (Figures S5K and S5L). Wntless trafficking defect toward TGN under SCAMP3 depletion was also replicated in primary RPE-1 cells (Figure S5M). Upon failure to be directed toward TGN in SCAMP3-depleted cells, WLS cargo is rerouted to late endosomes (Figures S5N and S5O) and lysosomes (Figures S5P and S5Q). Subsequently, the rerouted WLS undergoes lysosomal degradation in SCAMP3 depletion that could be rescued by treating the cells with chloroquine (Figure 6E). Consequent to the lack of carrier protein caused due to defective WLS movement to TGN from sorting endosomes, Wnt3a is accumulated in SCAMP3-depleted cells (Figures 6F and 6G). Akin to EYA knockdown, EGFP-Wnt3a reaching the plasma membrane is significantly reduced in SCAMP3 knockdown cells as compared with the control cells (Figures 6H and 6I). Furthermore, loss of SCAMP3 in cells led to defective secretion of the Wnt3a ligand (Figures 6J and S5R), thus phenocopying the loss of the EYA complex in cells. Depletion of SCAMP3 also resulted in reduced β-catenin activity (Figure 6K), suggesting an important role of SCAMP3 in Wnt signaling. Together, these data suggest that EYA-assisted recruitment of SCAMP3 is necessary for connecting endosomes with TGN during WLS trafficking.

EYA-SCAMP3 axis is an evolved mechanism in vertebrates

The role of retromer in regulating WLS trafficking has earlier been well documented in several model organisms including *C. elegans*[30] and *Drosophila melanogaster*.[10,31] As we established an important role of the EYA complex in retromer-dependent WLS trafficking in mammalian cells, we next sought to assess the physiological relevance of EYA proteins in other organisms. In *C. elegans*, the Wntless homolog, MIG-14 physically interacts with and targets Wnt/EGL-20 to the plasma membrane for secretion.[27] Compared with the wild type (WT), loss of *VPS35 (vps-35*, *hu68)* in *C. elegans* causes MIG-14 accumulation in intracellular compartments with an overall decrease in MIG-14 levels.[32] We tested if MIG-14 (WLS ortholog) is accumulated in *C. elegan*'s *Eya* and *Scm* (*SCAMP3 ortholog*) mutants. Surprisingly, no changes in MIG-14::GFP levels were observed in *Scm-1* and *Eya-1* mutants in comparison with the WT worms (Figures S6A–S6C). Wnt signaling has an important role in maintaining the polarity of anterior lateral microtubule (ALM) and posterior lateral microtubule (PLM) bipolar neurons. Disruption of Wnt signaling is known to cause polarity defects such as the reversal of polarity or the absence of anterior or posterior processes.[33] By scoring ALM and PLM defects, we further assessed if *Eya-1* and *Scm-1* affect Wnt signaling in worms. Although *VPS35 (hu68)* mutants show clear ALM and PLM polarity defects, no defects were observed in *Eya-1(ok654)* or *Scm-1(hd30)* mutants (Figures S6D–S6K and S6L). These data suggest that EYAs and SCAMP3 may not have a conserved role during WLS trafficking and Wnt signaling in *C. elegans*. On the other hand, we also assessed whether EYA-mediated WLS regulation is conserved in another model organism *Drosophila*. The intricate patterning of the *Drosophila* wing disc requires WLS-mediated secretion of the *Drosophila* homolog of Wnt-1, *Wingless* (*Wg*). Loss-of-function *Drosophila* WLS mutants show defective *Wg* secretion and cause *Wg* accumulation in the *Wg*-producing cells.[5,34] Although retromer is known to be an essential regulator of *Wg* secretion in *Wg*-producing cells,[35] such a role for either EYA or SCAMP3 has not been characterized. In the *Drosophila* imaginal disc, while the *VPS26* RNAi line ($vps26^{b}$) showed a noticeable accumulation of *Wg* in *Wg* secretory cells, no such change was visible in *Eya* ($eya^{cli\text{-}IID}$) or *Scam* ($scamp^{63A}$) depleted lines (Figure S6M). EYA proteins therefore seem to have no conserved role in WLS trafficking during Wnt signaling in either *C. elegans* or *Drosophila*. One reason for this could be that duplication of EYA proteins happened later in the evolution in higher organisms specifically from the clade Euteleostoma onward (Figures S6N and S6O). Also, interestingly, the N terminus of EYA proteins in these early non-vertebrate organisms display almost no homology with the human EYAs (Figure S6P). Since the N terminus of EYA proteins is critical for the binding of SCAMP3 and retromer (EYA4 N terminus), the changes in the N terminus plus the capability to assemble into a higher-order complex with four distinct EYA proteins to regulate WLS trafficking might be acquired by EYA proteins in vertebrates later in the evolution. To understand whether EYA- and SCAMP3-mediated WLS regulation and Wnt signaling is indeed an outcome of EYA complex formation evolved in the higher organisms, we resorted to a vertebrate model, zebrafish. Like humans, zebrafish have 4 Eya proteins that share considerable homology with their human counterparts. We generated mosaic knockouts

(C) Interaction of SCAMP3 with the components of retromer (VPS26, VPS29, and VPS35) was determined by immunoblotting with specific antibodies after performing endogenous IP with 293T cell lysates using Protein-G Sepharose beads coated either with IgG control or SCAMP3 antibody.

(D) Schematic illustration depicting the EYA complex as a bridge between the retromer tethered to the early endosomes and SCAMP3.

(E–G) (E) Stable control 293T cells or individual EYA-depleted cells were co-transfected with SFB-tagged VPS26, (F) VPS29, and (G) VPS35 along with Myc-SCAMP3. S-Protein beads were used for the pull-down assays, and the interaction between retromer components and SCAMP3 in control and EYA-depleted cells was determined by immunoblotting with the indicated antibodies.

Please cite this article in press as: Reshi et al., EYA protein complex is required for Wntless retrograde trafficking from endosomes to Golgi, Developmental Cell (2024), https://doi.org/10.1016/j.devcel.2024.05.021

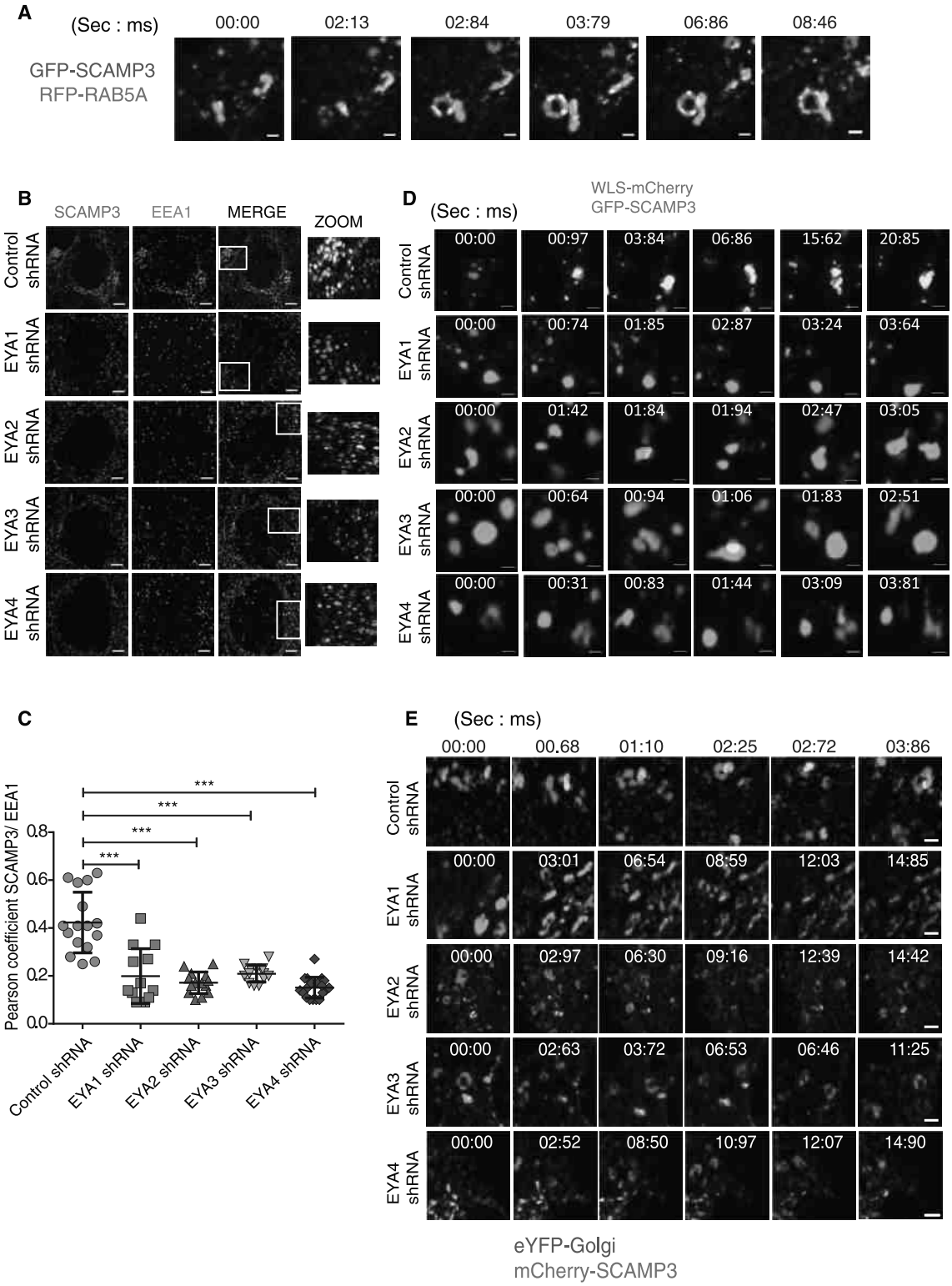

Figure 5. EYA complex incorporates SCAMP3 into WLS-positive endosomes

(A) Wild-type 293T cells co-expressing GFP-SCAMP3 and RFP-RAB5A were imaged using a Carl Zeiss ELYRA Super-resolution microscope (63× oil immersion lens, NA 1.46). Screenshots were captured from t = 00:00 to t = 08:46 post-processing. Scale bars, 2 μm.

(legend continued on next page)

Please cite this article in press as: Reshi et al., EYA protein complex is required for Wntless retrograde trafficking from endosomes to Golgi, Developmental Cell (2024), https://doi.org/10.1016/j.devcel.2024.05.021

(KO) for all Eya genes, Scamp3 and Vps35, and studied 5-day post-fertilization embryos of the F0 generation. Interestingly, embryos depleted for Eya1–4 individually or together, Scamp3 or Vps35 displayed significant craniofacial abnormalities (Figures S6Q and S6R) and lacked swim bladders, phenocopying WLS or Wnt5b KO phenotype.[36,37] Further assessment for craniofacial abnormalities was done by Alcian blue staining. Compared with control, Eya or Scamp3 showed key abnormalities in cartilage and ceratobranchial arch formation (Figure 7A). Importantly, in line with our data in human cells, loss of EYA or SCAMP3 in zebrafish embryos led to a significant reduction in WLS levels *in vivo* (Figures 7B–7D and S6S). Besides an overall decrease, WLS reduction is especially accentuated in eyes and otic vesicles. Similar to the loss of EYA-SCAMP3, WLS levels were also reduced in Vps35 KO embryos, thereby establishing a connection between retromer and EYA-SCAMP3 complex in WLS regulation *in vivo*. Wntless reduction in Eya or Scamp3 KO embryos further led to an aberrant localization of Wnt5b. Compared with control embryos where Wnt5b is concentrated in the periphery of the eye lens, Wnt5b in Eya, Scamp3, or Vps35 KO embryos displays aberrant localization in the lens (Figure S6T). Besides the eyes, Wnt5b localized specifically to intermandibular anterior and posterior muscles in the ventral head region of the fish. Compared with control, muscles in Eya, Scamp3, or Vps35 KOs, as revealed by Wnt5b staining, did not develop properly (Figure S6U), suggesting that the dysmorphic head, jaw, and other craniofacial abnormalities are a reflection of aberrant Wnt5b localization. Together, these data validate that EYA-SCAMP3-mediated WLS trafficking and Wnt signaling are outcomes of EYA complex formation, which evolved in vertebrates.

Pathogenic mutations disrupting the EYA complex fail to activate Wnt signaling

Mutations in EYA proteins are known to be associated with human diseases such as BOR syndrome, congenital cataracts, and late-onset sensorineural hearing loss.[9,38–43] However, the precise mechanisms on how these mutations contribute to the development of these disorders are unclear. Since we identified a functional EYA-retromer-SCAMP3 complex in human cells that is essential for WLS trafficking, and given that Wnt signaling plays a critical role in organ development, we speculated that some of these pathogenic mutations may disrupt the EYA complex function and thus lead to human disorders. We searched for EYA mutations using the Human Gene Mutation Database (HGMD), where all the gene lesions responsible for human inherited diseases are listed. Although no mutations were found in EYA2, several pathogenic EYA1 mutations have been reported in BOR and branchio-oto-ureteral (BOU) syndromes. We found that one of these pathogenic EYA1 variants (G533R)[44] is defective in the assembly of the EYA complex (Figures 7E–7G). Although WT EYA1 can efficiently interact with all other EYAs, its pathogenic mutant G533R was not able to participate in hetero-tetrameric EYA complex formation as it failed to interact with EYA2 (Figure 7E), EYA3 (Figure 7F), and EYA4 (Figure 7G). Consequent to its failed ability to form EYA complex, the G533R mutant was unable to activate Wnt signaling as efficiently as WT EYA1 in normal 293T cells (Figure S7A). Additionally, the expression of WT EYA1 but not the G533R mutant rescued the defective secretion of extracellular Wnt3a in EYA1 knockdown cells (Figure 7H). Only WT EYA1 but not the mutant G533R could restore β-catenin-dependent Wnt signaling in EYA1-depleted cells (Figure 7I). Among the EYA3 mutations, although one variant (N358S) did not interact with EYA2 (Figure S7C), its interaction with EYA1 (Figure S7B) and EYA4 (Figure S7D) was unaffected. No significant changes in Wnt activity were observed with N358S mutant in comparison with WT EYA3 (Figure S7E). Interestingly, a pathogenic mutation in EYA4 (G171R) near the N terminus of the protein, associated with Autosomal Dominant Non-Syndromic Hearing Loss[45] did not show any loss of interaction with other EYA members (Figures S7F–S7H) but instead shows defective binding with retromer component VPS26 (Figure 7J). None of the EYA mutants described here showed any defect in binding to SCAMP3 (Figure S7I). Importantly, defective binding of EYA1 G171R mutant with retromer component led to its failure in inducing Wnt signaling (Figure S7J) as efficiently as WT EYA4. Moreover, the expression of WT EYA4 but not the mutant G171R restored defective extracellular Wnt3a secretion in EYA4-depleted cells (Figure 7K). Compared with the WT EYA4, the mutant G171R could not restore Wnt signaling in EYA4 knockdown cells (Figure 7L). These data indicate that the above-described EYA mutations that are implicated in hearing loss phenotype in humans fail to either form a functional EYA complex or affect the interaction of EYA complex with the retromer, thus leading to defective Wnt signaling.

DISCUSSION

In conclusion, our study identified that EYA proteins form a hetero-tetrameric complex that interacts with retromer-coated early endosomes. Retromer-bound EYA complex then recruits SCAMP3, which is necessary for docking and fusion of WLS-enriched endosomes to TGN (model shown in Figure 7M). By facilitating the recycling of WLS cargo, the EYA-SCAMP3 axis ensures the ready availability of WLS which is critical for Wnt ligand secretion.

(B) The presence of SCAMP3 on early endosomes was checked by imaging control or EYA KD cells using Carl Zeiss ELYRA Super-resolution microscope (63× oil immersion lens, NA 1.46), after immunostaining with SCAMP3 and EEA1. Scale bars, 5 μm.
(C) Localization of SCAMP3 on early endosomes was measured using Pearson's coefficient of correlation for $n \geq 10$ and plotted in GraphPad Prism using one-way ANOVA. Error bars representing SD, $^{***}p < 0.001$.
(D) Control or individual EYA-knockdown cells expressing WLS-mCherry and GFP-SCAMP3 were imaged in real-time using a Carl Zeiss ELYRA Super-resolution microscope (63× oil immersion lens, NA 1.46). Screenshots highlighting the incorporation of SCAMP3 into WLS vesicles were plotted with the indicated time points post-processing. Scale bars, 2 μm.
(E) Control or individual EYA knockdown cells expressing mCherry-SCAMP3 and eYFP-Golgi were imaged in real time using Carl Zeiss ELYRA Super-resolution microscope (63× oil immersion lens, NA 1.46). The fusion of SCAMP3 vesicles with Golgi was plotted with the indicated time points post-processing. Scale bars, 2 μm.

Please cite this article in press as: Reshi et al., EYA protein complex is required for Wntless retrograde trafficking from endosomes to Golgi, Developmental Cell (2024), https://doi.org/10.1016/j.devcel.2024.05.021

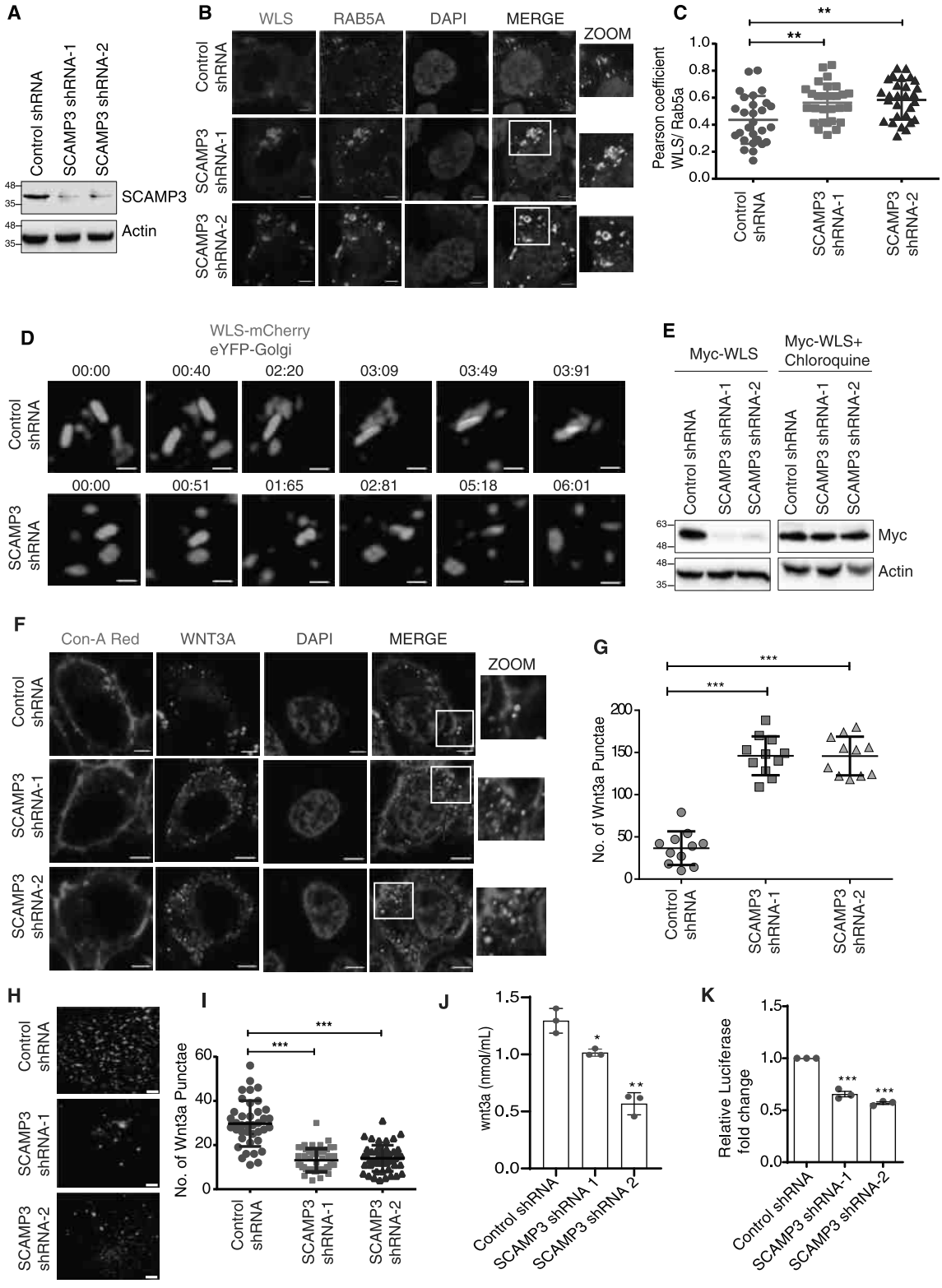

Figure 6. SCAMP3 knockdown phenocopies the trafficking defects seen in EYA depletion

(A) Stable knockdowns of SCAMP3 were generated in 293T cells by transducing lentiviral-based specific shRNAs. SCAMP3 levels in control and shRNA transduced cells were shown by immunoblotting with SCAMP3 antibody.

(legend continued on next page)

Please cite this article in press as: Reshi et al., EYA protein complex is required for Wntless retrograde trafficking from endosomes to Golgi, Developmental Cell (2024), https://doi.org/10.1016/j.devcel.2024.05.021

Wnt-secretory cells make use of a 7 pass-putative GPCR protein called WLS to carry the Wnt ligand from Golgi to the plasma membrane to be appropriately delivered in the extracellular space. Therefore, the presence of WLS at TGN is essential for receiving a newly synthesized Wnt ligand from ER. Not surprisingly, WLS depletion across various organisms shows an accumulation of Wnt inside the cells followed by ER stress and defective Wnt signaling.[7,8,27] An important step to ensure WLS presence at TGN involves retromer-mediated delivery of cargo from early endosomes to TGN via retrograde trafficking. Although the requirement of retromer-SNX3 for WLS trafficking has been well established, the underlying mechanisms of how the retromer delivers the cargo precisely to TGN are unknown. Our work identifying the EYA complex as a molecular bridge between retromer and TGN fills this gap.

Interestingly, the EYA and SCAMP3-mediated regulation of Wnt signaling is not conserved in *C. elegans* and *Drosophila*. This could be primarily because these organisms have just one EYA protein, while the higher vertebrates, including humans and other mammals, have 4 EYA proteins (EYA1–4). Phylogenetic analysis of EYA proteins from lower invertebrates to humans indicate that EYA duplication happened from the clade Euteleostomi (bony vertebrates) onward, supporting the speculation that EYAs might have acquired the Wnt regulation role later in the evolution. Our data indicate that EYA-SCAMP3-mediated regulation of Wnt signaling is an outcome of EYA complex formation and its interaction with SCAMP3. N termini of EYA proteins, which mediate interactions within the EYA complex and SCAMP3, bear almost no homology with those in *Drosophila* and *C. elegans*. The absence of such attributes in EYA proteins of lower organisms may explain this functional departure from their human counterparts. The evolution of molecular players and mechanisms to regulate complex signaling pathways in higher animals is well known. For example, in mammalian cells, primary cilia act as molecular hubs for Hedgehog signaling,[46] while no Hedgehog-specific cilia are found in lower invertebrates. The protein Costal2 (Cos2) in *Drosophila* acts primarily as a scaffolding protein for cytoplasmic protein complexes. Its mammalian homolog Kif7, however, has a motor protein function and moves from the cilia base to its tip during the activation of the Hedgehog pathway.[47]

Importantly, missense mutations in EYA found in hearing loss patients failed to form the EYA-retromer complex and could not induce Wnt signaling. These data point toward the central role of EYA proteins in Wnt signaling and could explain the hearing loss and other developmental defects in these patients. Although both EYA proteins and Wnt signaling are known to independently play an essential role in organ development, no connection has been established between these two signaling entities so far. Loss of EYA leads to defective eye and ear development[48,49] in humans. Interestingly, depletion of WLS in zebrafish also leads to defective eye development.[37,50] In early development, the expression of EYA proteins in the hearing-sensitive areas of the inner ear like hair cells and otic vesicles coincide with the initial waves of Wnt signaling.[51] Both EYA depletion and β-catenin KO in mice display similar consequences, including abnormal differentiation of inner ear cells, resulting in hearing loss.[16,52–54] Although these observations point toward a possible correlation between Wnt signaling and EYA expression, our data establish that WLS regulation might be a key node connecting EYA and Wnt signaling for appropriate organ development. In addition to various EYA mutations found in developmental disorders, several EYA somatic mutations have been listed in the COSMIC (Catalogue Of Somatic Mutations In Cancer) database. Besides that, the role of EYAs has been implicated in several human cancers.[55–59] Given that hyperactive Wnt signaling positively contributes to tumorigenesis, it is highly possible that some of these EYA mutations found in cancer samples may contribute to the activation of Wnt signaling by forming either a constitutively active EYA complex or via enhanced binding with retromer/SCAMP3, which needs to be tested in future studies.

Limitations of the study

Our data here demonstrate that retomer-EYA complex-SCAMP3 axis ensures accurate delivery of WLS from endosomes to Golgi.

(B) Control or SCAMP3 knockdown 293T cells were transfected with Myc-WLS. Localization of WLS with RAB5A endosomes was determined by confocal imaging (Carl Zeiss LSM 700, 63× oil immersion lens, NA 1.4) after co-staining with RAB5A and Wntless antibodies. Scale bars, 10 μm.

(C) RAB5a co-localization with Myc-WLS was assessed by comparing the Pearson's correlation coefficient values of control or SCAMP3 knockdown cells ($n \geq 30$) using Zen Blue software. Error bars represent standard deviation, ** $p < 0.01$ (one-way ANOVA).

(D) Control or SCAMP3 knockdown cells expressing WLS-mCherry and eYFP-Golgi were imaged in real time using Carl Zeiss ELYRA Super-resolution microscope (63× oil immersion lens, NA 1.46). Fusion of WLS vesicles with Golgi was plotted with the indicated time points. Scale bars, 2 μm.

(E) Protein levels of Myc-WLS in control and SCAMP3 knockdown conditions were evaluated by immunoblotting in the absence or presence of a lysosomal inhibitor, chloroquine. Actin was used as a loading control.

(F) Control or SCAMP3 knockdown HeLa cells were immunostained using endogenous Wnt3a antibody, and the imaging was done using Carl Zeiss LSM 700 microscope (63×, oil immersion, NA 1.4). Scale bars, 10 μm. The peripheries of the cells were marked by fluorescent lectin, concanavalin A red.

(G) The number of Wnt3a punctae inside the cells was counted using ImageJ software. Statistical significance was calculated using GraphPad Prism software ($n \geq 10$, one-way ANOVA, ***$p < 0.001$). Error bars represent SD.

(H) Control or SCAMP3 knockdown 293T cells were transfected with EGFP-Wnt3a. Raw images were captured using Carl Zeiss ELYRA Super-resolution microscope (63× oil immersion lens, NA 1.46) equipped with a TIRF imaging facility. The surface of the cells was focused by setting appropriate critical angles. TIRF-SIM images showing surface localized Wnt3a for various conditions were shown. Scale bars, 2 μm.

(I) The number of EGFP-Wnt3a punctae present in sections of the plasma membrane after TIRF-SIM was counted using ImageJ software and analyzed using GraphPad Prism ($n \geq 50$, one-way ANOVA, ***$p < 0.001$). Error bars represent SD.

(J) Wnt3a ELISA was used to measure the secreted Wnt3a levels. 96 well plates precoated with Wnt3a antibody were incubated with spent media from control or SCAMP3 knockdown stable cell lines. Wnt3a levels were determined by measuring the absorbance at 450 nm. The comparisons were plotted in GraphPad Prism using one-way ANOVA with n = 3 biological replicates, *$p < 0.05$, ***$p < 0.001$, and error bars representing SEM.

(K) The effect of SCAMP3 depletion on Wnt-dependent β-catenin transcriptional activity was measured using SuperTopFlash (STF) luciferase assay with Renilla luciferase as an internal control. The plot was made using GraphPad Prism, n = 3 biological replicates, error bars represent standard error of the mean (SEM) with one-way ANOVA, ***$p < 0.001$.

Please cite this article in press as: Reshi et al., EYA protein complex is required for Wntless retrograde trafficking from endosomes to Golgi, Developmental Cell (2024), https://doi.org/10.1016/j.devcel.2024.05.021

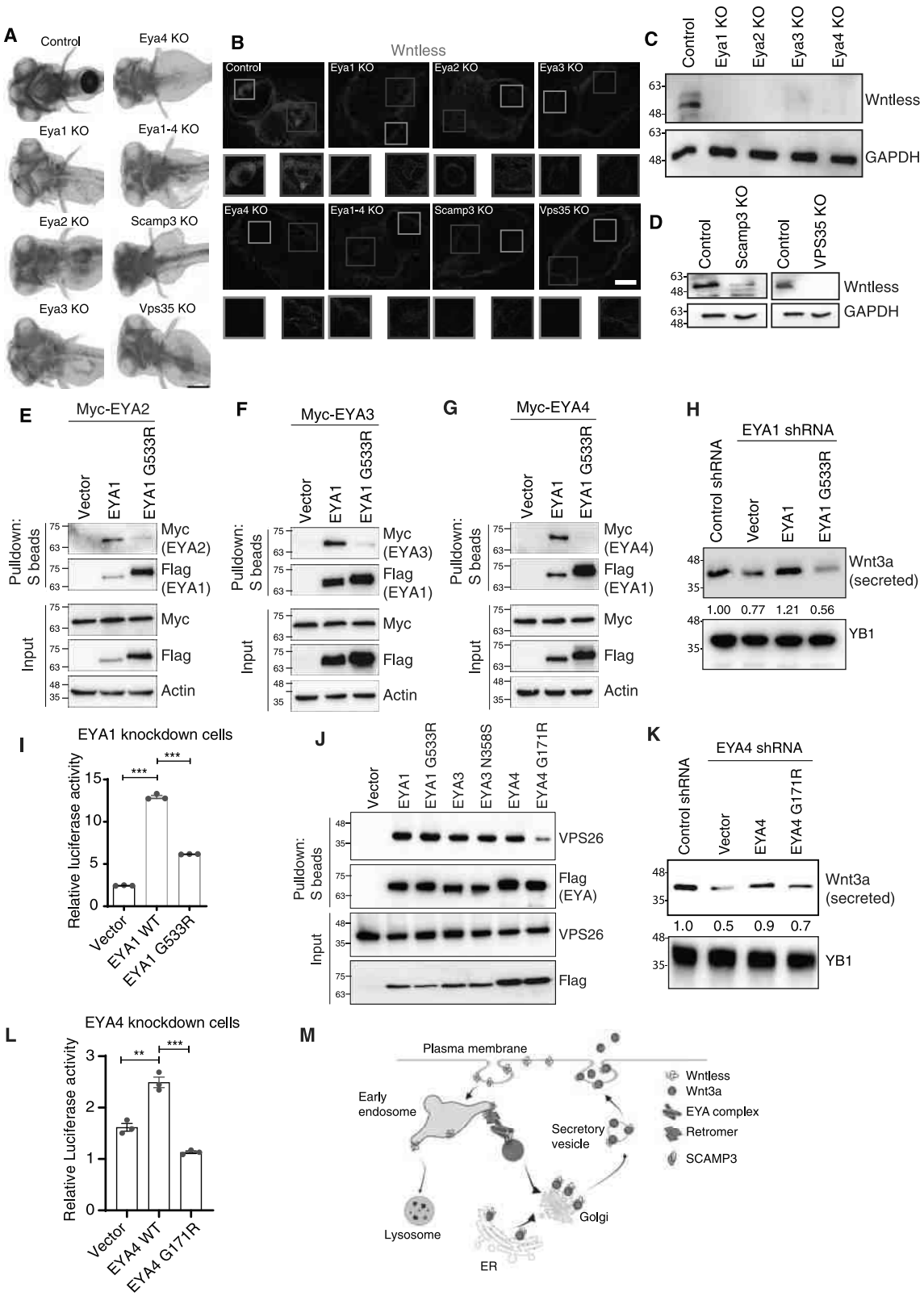

Figure 7. EYA-SCAMP3 axis is evolved in vertebrates, and pathogenic mutations disrupting the EYA complex fail to activate Wnt signaling

(A) Control 5 days post-fertilization (5 dpf) zebrafish embryos or those with CRISPR-mediated knockout of the genes Eya1, Eya2, Eya3, Eya4, Eya1–4, Scamp3, or VPS35 were stained with Alcian blue dye, bleached, and imaged with dissecting epifluorescence microscope with 10× magnification. Scale bars, 50 μM.

(legend continued on next page)

However, it is currently unknown if these complexes participate in trafficking of other cargoes as well, which needs to be tested in future studies. Also, although we have shown an essential role of SCAMP3 in the transport of WLS from endosomes to Golgi, the precise source of SCAMP3 that is recruited to the EYA complex is currently unclear, which needs to be identified further.

STAR★METHODS

Detailed methods are provided in the online version of this paper and include the following:

- KEY RESOURCES TABLE
- RESOURCE AVAILABILITY
  - Lead contact
  - Materials availability
  - Data and code availability
- EXPERIMENTAL MODEL AND STUDY PARTICIPANT DETAILS
  - Cell lines
  - C. elegans culture and maintenance
  - Drosophila culture
  - Zebrafish culture
- METHOD DETAILS
  - Plasmids
  - Immunoprecipitation
  - Cell Transfections
  - Generation of stable knockdown cell lines
  - Size exclusion chromatography
  - Recombinant Protein Purification of GST, His and MBP tagged proteins
  - Immunofluorescence and time-tracking experiments
  - Scoring for ALM and PLM polarity defects
  - Generation of knockout zebrafish
- QUANTIFICATION AND STATISTICAL ANALYSIS

SUPPLEMENTAL INFORMATION

Supplemental information can be found online at https://doi.org/10.1016/j.devcel.2024.05.021.

ACKNOWLEDGMENTS

This work was supported by the DBT/Wellcome Trust India Alliance Senior Fellowship grant (IA/S/16/2/502729 to S.M.), the DBT National Bioscience Award for Career Development (BT/HRD/NBA/39/08/2018-19), and CDFD core funds. H.A.R. acknowledges the support of Research Fellowship from the Indian Council of Medical Research (ICMR). We are grateful to Dr Sankaranarayanan and Dr Biswajit Pal from CCMB for helping with gel filtration experiments. We thank all members of LCDCS for their critical inputs. The authors thank Nanci Rani for providing technical assistance. Stocks obtained from the Bloomington Drosophila Stock Center (NIH P40OD018537) were used in this study. M.J. is supported by the Department of Atomic Energy (Project Identification No. RTI 4007), the Department of Science and Technology, SERB (CRG/2020/003275), the Department of Biotechnology (BT/PR32873/BRB/10/1850/2020), and the Government of India. K.C. and the zebrafish studies are supported by DBT/Wellcome Trust India Alliance Clinical Research Center Team Grant (IA/CRC/20/1/600002) and CSR funding from Dr Reddy's Foundation (Center for Rare Disease Models, Dr. Reddy's Institute of Life Sciences).

AUTHOR CONTRIBUTIONS

S.M. conceptualized and managed the project. S.M. and H.A.R. designed the experiments, analyzed the data, and wrote the manuscript. H.A.R. performed all the experiments. M.J. and D.B. designed and analyzed *Drosophila* experiments, and D.B. performed the *Drosophila* experiments. A.A. and K.B. designed and analyzed *C. elegans* experiments, and A.A. performed the *C. elegans* experiments. R.M., K.C., and H.A.R. designed the zebrafish experiments. R.M. and H.A.R. performed the zebrafish experiments.

DECLARATION OF INTERESTS

The authors declare no competing interests.

Received: September 24, 2022
Revised: December 1, 2023
Accepted: May 17, 2024
Published: June 12, 2024

REFERENCES

1. MacDonald, B.T., Tamai, K., and He, X. (2009). Wnt/beta-catenin signaling: components, mechanisms, and diseases. Dev. Cell *17*, 9–26. https://doi.org/10.1016/j.devcel.2009.06.016.
2. MacDonald, B.T., and He, X. (2012). Frizzled and LRP5/6 receptors for Wnt/beta-catenin signaling. Cold Spring Harb. Perspect. Biol. *4*, a007880. https://doi.org/10.1101/cshperspect.a007880.
3. Fu, J., Jiang, M., Mirando, A.J., Yu, H.M.I., and Hsu, W. (2009). Reciprocal regulation of Wnt and Gpr177/mouse Wntless is required for embryonic axis formation. Proc. Natl. Acad. Sci. USA *106*, 18598–18603. https://doi.org/10.1073/pnas.0904894106.

(B) Control or knockout 5 dpf embryos were incubated with WLS antibody and imaged with Carl Zeiss ELYRA Super-resolution microscope 10× magnification. Zoomed areas highlight eyes (green box) and otic vesicles (blue box). Scale bars, 50 μm.
(C) Control or EYA knockout zebrafish (5 dpf) embryos were lysed in 1× NETN (nuclear and cytoplasmic extraction buffer), loaded on 10% SDS gel, and immunoblotted using WLS antibody with glyceraldehyde-3-phosphate dehydrogenase (GAPDH) as an internal control.
(D) Wntless levels were assessed in Scamp3 and Vps35 knockout zebrafish embryos by immunoblotting using WLS antibody with GAPDH as an internal control.
(E–G) 293T cells co-expressing WT EYA1 or EYA1 G533R mutant along with Myc-tagged EYA2 (E), EYA3 (F), and EYA4 (G) were lysed and incubated on S-protein agarose beads. The interaction of WT and the mutant EYA1 with other EYAs was assessed by immunoblotting with Myc-antibody.
(H) Rescue of Wnt3a secretion was done by expressing either WT EYA1 or the mutant EYA1 G533R in 293T cells stably depleted for the endogenous EYA1. The collected spent media was concentrated using Amicon filters with a molecular weight cutoff (MWCO) of 30 kDa. The immunoblotting was done using the Wnt3a antibody. YB1 was used as a positive control. The quantification was done using ImageJ software.
(I) Rescue of Wnt signaling in EYA1 knockdown 293T cells by WT EYA1 or the mutant EYA1 G533R was measured by STF luciferase reporter assay. The results were plotted using GraphPad Prism with n = 3 biological replicates. Statistical analysis was done using one-way ANOVA. The error bars represent SEM and $^{***}p < 0.001$.
(J) EYA1, EYA3, EYA4, or their respective pathogenic mutants, i.e., EYA1 G533R, EYA3 N358S, and EYA4 G171R were expressed in 293T cells. Interactions between EYA proteins and VPS26 were determined by immunoblotting with VPS26 antibody after performing pull-down using S-protein agarose beads.
(K) Rescue of Wnt3a secretion in stable EYA4 knockdown 293T cells by either WT EYA4 or EYA4 G171R mutant. The collected spent media was concentrated using Amicon filters with a molecular weight cutoff (MWCO) of 30 kDa. The immunoblotting was done using the Wnt3a antibody.
(L) Rescue of Wnt signaling in EYA4 knockdown 293T cells by WT EYA4 or the mutant EYA4 G171R was measured by STF luciferase reporter assay. The results were plotted using GraphPad Prism with n = 3 biological replicates. The error bars represent SEM with $^{**}p < 0.01$, $^{***}p < 0.001$ (one-way ANOVA).
(M) A proposed model to depict the role of retromer-EYA complex-SCAMP3 in directing WLS from endosomes to TGN is shown.

4. Herr, P., and Basler, K. (2012). Porcupine-mediated lipidation is required for Wnt recognition by Wls. Dev. Biol. *361*, 392–402. https://doi.org/10.1016/j.ydbio.2011.11.003.

5. Goodman, R.M., Thombre, S., Firtina, Z., Gray, D., Betts, D., Roebuck, J., Spana, E.P., and Selva, E.M. (2006). Sprinter: a novel transmembrane protein required for Wg secretion and signaling. Development *133*, 4901–4911. https://doi.org/10.1242/dev.02674.

6. Gasnereau, I., Herr, P., Chia, P.Z.C., Basler, K., and Gleeson, P.A. (2011). Identification of an endocytosis motif in an intracellular loop of Wntless protein, essential for its recycling and the control of Wnt protein signaling. J. Biol. Chem. *286*, 43324–43333. https://doi.org/10.1074/jbc.M111.307231.

7. Port, F., Kuster, M., Herr, P., Furger, E., Bänziger, C., Hausmann, G., and Basler, K. (2008). Wingless secretion promotes and requires retromer-dependent cycling of Wntless. Nat. Cell Biol. *10*, 178–185. https://doi.org/10.1038/ncb1687.

8. McGough, I.J., de Groot, R.E.A., Jellett, A.P., Betist, M.C., Varandas, K.C., Danson, C.M., Heesom, K.J., Korswagen, H.C., and Cullen, P.J. (2018). SNX3-retromer requires an evolutionary conserved MON2:DOPEY2:ATP9A complex to mediate Wntless sorting and Wnt secretion. Nat. Commun. *9*, 3737. https://doi.org/10.1038/s41467-018-06114-3.

9. Tadjuidje, E., and Hegde, R.S. (2013). The Eyes Absent proteins in development and disease. Cell. Mol. Life Sci. *70*, 1897–1913. https://doi.org/10.1007/s00018-012-1144-9.

10. Belenkaya, T.Y., Wu, Y., Tang, X., Zhou, B., Cheng, L., Sharma, Y.V., Yan, D., Selva, E.M., and Lin, X. (2008). The retromer complex influences Wnt secretion by recycling wntless from endosomes to the trans-Golgi network. Dev. Cell *14*, 120–131. https://doi.org/10.1016/j.devcel.2007.12.003.

11. Blackburn, J.B., D'Souza, Z., and Lupashin, V.V. (2019). Maintaining order: COG complex controls Golgi trafficking, processing, and sorting. FEBS Lett. *593*, 2466–2487. https://doi.org/10.1002/1873-3468.13570.

12. Tootle, T.L., Silver, S.J., Davies, E.L., Newman, V., Latek, R.R., Mills, I.A., Selengut, J.D., Parlikar, B.E.W., and Rebay, I. (2003). The transcription factor Eyes absent is a protein tyrosine phosphatase. Nature *426*, 299–302. https://doi.org/10.1038/nature02097.

13. Pappu, K.S., and Mardon, G. (2004). Genetic control of retinal specification and determination in Drosophila. Int. J. Dev. Biol. *48*, 913–924. https://doi.org/10.1387/ijdb.041875kp.

14. Bonini, N.M., Leiserson, W.M., and Benzer, S. (1998). Multiple roles of the eyes absent gene in Drosophila. Dev. Biol. *196*, 42–57. https://doi.org/10.1006/dbio.1997.8845.

15. Orten, D.J., Fischer, S.M., Sorensen, J.L., Radhakrishna, U., Cremers, C.W.R.J., Marres, H.A.M., Van Camp, G., Welch, K.O., Smith, R.J.H., and Kimberling, W.J. (2008). Branchio-oto-renal syndrome (BOR): novel mutations in the EYA1 gene, and a review of the mutational genetics of BOR. Hum. Mutat. *29*, 537–544. https://doi.org/10.1002/humu.20691.

16. Abe, S., Takeda, H., Nishio, S.Y., and Usami, S.I. (2018). Sensorineural hearing loss and mild cardiac phenotype caused by an EYA4 mutation. Hum. Genome Var. *5*, 23. https://doi.org/10.1038/s41439-018-0023-9.

17. Azuma, N., Hirakiyama, A., Inoue, T., Asaka, A., and Yamada, M. (2000). Mutations of a human homologue of the Drosophila eyes absent gene (EYA1) detected in patients with congenital cataracts and ocular anterior segment anomalies. Hum. Mol. Genet. *9*, 363–366. https://doi.org/10.1093/hmg/9.3.363.

18. Jin, M., and Mardon, G. (2016). Distinct Biochemical Activities of Eyes absent During Drosophila Eye Development. Sci. Rep. *6*, 23228. https://doi.org/10.1038/srep23228.

19. Rayapureddi, J.P., Kattamuri, C., Steinmetz, B.D., Frankfort, B.J., Ostrin, E.J., Mardon, G., and Hegde, R.S. (2003). Eyes absent represents a class of protein tyrosine phosphatases. Nature *426*, 295–298. https://doi.org/10.1038/nature02093.

20. Jemc, J., and Rebay, I. (2007). Identification of transcriptional targets of the dual-function transcription factor/phosphatase eyes absent. Dev. Biol. *310*, 416–429. https://doi.org/10.1016/j.ydbio.2007.07.024.

21. Ohto, H., Kamada, S., Tago, K., Tominaga, S.I., Ozaki, H., Sato, S., and Kawakami, K. (1999). Cooperation of six and eya in activation of their target genes through nuclear translocation of Eya. Mol. Cell. Biol. *19*, 6815–6824. https://doi.org/10.1128/MCB.19.10.6815.

22. Cook, P.J., Ju, B.G., Telese, F., Wang, X., Glass, C.K., and Rosenfeld, M.G. (2009). Tyrosine dephosphorylation of H2AX modulates apoptosis and survival decisions. Nature *458*, 591–596. https://doi.org/10.1038/nature07849.

23. Okabe, Y., Sano, T., and Nagata, S. (2009). Regulation of the innate immune response by threonine-phosphatase of Eyes absent. Nature *460*, 520–524. https://doi.org/10.1038/nature08138.

24. Tadjuidje, E., Wang, T.S., Pandey, R.N., Sumanas, S., Lang, R.A., and Hegde, R.S. (2012). The EYA tyrosine phosphatase activity is pro-angiogenic and is inhibited by benzbromarone. PLoS One *7*, e34806. https://doi.org/10.1371/journal.pone.0034806.

25. Kumar, P., Munnangi, P., Chowdary, K.R., Shah, V.J., Shinde, S.R., Kolli, N.R., Halehalli, R.R., Nagarajaram, H.A., and Maddika, S. (2017). A Human Tyrosine Phosphatase Interactome Mapped by Proteomic Profiling. J. Proteome Res. *16*, 2789–2801. https://doi.org/10.1021/acs.jproteome.7b00065.

26. Gallon, M., and Cullen, P.J. (2015). Retromer and sorting nexins in endosomal sorting. Biochem. Soc. Trans. *43*, 33–47. https://doi.org/10.1042/BST20140290.

27. Bänziger, C., Soldini, D., Schütt, C., Zipperlen, P., Hausmann, G., and Basler, K. (2006). Wntless, a conserved membrane protein dedicated to the secretion of Wnt proteins from signaling cells. Cell *125*, 509–522. https://doi.org/10.1016/j.cell.2006.02.049.

28. Mota, L.J., Ramsden, A.E., Liu, M., Castle, J.D., and Holden, D.W. (2009). SCAMP3 is a component of the Salmonella-induced tubular network and reveals an interaction between bacterial effectors and post-Golgi trafficking. Cell. Microbiol. *11*, 1236–1253. https://doi.org/10.1111/j.1462-5822.2009.01329.x.

29. Aoh, Q.L., Castle, A.M., Hubbard, C.H., Katsumata, O., and Castle, J.D. (2009). SCAMP3 negatively regulates epidermal growth factor receptor degradation and promotes receptor recycling. Mol. Biol. Cell *20*, 1816–1832. https://doi.org/10.1091/mbc.E08-09-0894.

30. Harterink, M., Port, F., Lorenowicz, M.J., McGough, I.J., Silhankova, M., Betist, M.C., van Weering, J.R.T., van Heesbeen, R.G.H.P., Middelkoop, T.C., Basler, K., et al. (2011). A SNX3-dependent retromer pathway mediates retrograde transport of the Wnt sorting receptor Wntless and is required for Wnt secretion. Nat. Cell Biol. *13*, 914–923. https://doi.org/10.1038/ncb2281.

31. Yang, P.T., Lorenowicz, M.J., Silhankova, M., Coudreuse, D.Y.M., Betist, M.C., and Korswagen, H.C. (2008). Wnt signaling requires retromer-dependent recycling of MIG-14/Wntless in Wnt-producing cells. Dev. Cell *14*, 140–147. https://doi.org/10.1016/j.devcel.2007.12.004.

32. Pan, C.L., Baum, P.D., Gu, M., Jorgensen, E.M., Clark, S.G., and Garriga, G. (2008). C. elegans AP-2 and retromer control Wnt signaling by regulating mig-14/Wntless. Dev. Cell *14*, 132–139. https://doi.org/10.1016/j.devcel.2007.12.001.

33. Prasad, B.C., and Clark, S.G. (2006). Wnt signaling establishes anteroposterior neuronal polarity and requires retromer in C. elegans. Development *133*, 1757–1766. https://doi.org/10.1242/dev.02357.

34. Bartscherer, K., Pelte, N., Ingelfinger, D., and Boutros, M. (2006). Secretion of Wnt ligands requires Evi, a conserved transmembrane protein. Cell *125*, 523–533. https://doi.org/10.1016/j.cell.2006.04.009.

35. Franch-Marro, X., Wendler, F., Guidato, S., Griffith, J., Baena-Lopez, A., Itasaki, N., Maurice, M.M., and Vincent, J.P. (2008). Wingless secretion requires endosome-to-Golgi retrieval of Wntless/Evi/Sprinter by the retromer complex. Nat. Cell Biol. *10*, 170–177. https://doi.org/10.1038/ncb1678.

36. Wu, B.T., Wen, S.H., Hwang, S.P.L., Huang, C.J., and Kuan, Y.S. (2015). Control of Wnt5b secretion by Wntless modulates chondrogenic cell proliferation through fine-tuning fgf3 expression. J. Cell Sci. *128*, 2328–2339. https://doi.org/10.1242/jcs.167403.

37. Kuan, Y.S., Roberson, S., Akitake, C.M., Fortuno, L., Gamse, J., Moens, C., and Halpern, M.E. (2015). Distinct requirements for Wntless in habenular development. Dev. Biol. *406*, 117–128. https://doi.org/10.1016/j.ydbio.2015.06.006.

38. Li, Y., Manaligod, J.M., and Weeks, D.L. (2010). EYA1 mutations associated with the branchio-oto-renal syndrome result in defective otic development in Xenopus laevis. Biol. Cell *102*, 277–292. https://doi.org/10.1042/BC20090098.

39. Wang, Y.G., Sun, S.P., Qiu, Y.L., Xing, Q.H., and Lu, W. (2018). A novel mutation in EYA1 in a Chinese family with Branchio-oto-renal syndrome. BMC Med. Genet. *19*, 139. https://doi.org/10.1186/s12881-018-0653-2.

40. Matsunaga, T., Okada, M., Usami, S.I., and Okuyama, T. (2007). Phenotypic consequences in a Japanese family having branchio-oto-renal syndrome with a novel frameshift mutation in the gene EYA1. Acta Otolaryngol. *127*, 98–104. https://doi.org/10.1080/00016480500527185.

41. Wayne, S., Robertson, N.G., DeClau, F., Chen, N., Verhoeven, K., Prasad, S., Tranebjärg, L., Morton, C.C., Ryan, A.F., Van Camp, G., et al. (2001). Mutations in the transcriptional activator EYA4 cause late-onset deafness at the DFNA10 locus. Hum. Mol. Genet. *10*, 195–200. https://doi.org/10.1093/hmg/10.3.195.

42. Tan, M., Shen, X., Yao, J., Wei, Q., Lu, Y., Cao, X., and Xing, G. (2014). Identification of I411K, a novel missense EYA4 mutation causing autosomal dominant non-syndromic hearing loss. Int. J. Mol. Med. *34*, 1467–1472. https://doi.org/10.3892/ijmm.2014.1939.

43. Soni, U.K., Roychoudhury, K., and Hegde, R.S. (2021). The Eyes Absent proteins in development and in developmental disorders. Biochem. Soc. Trans. *49*, 1397–1408. https://doi.org/10.1042/BST20201302.

44. Castiglione, A., Melchionda, S., Carella, M., Trevisi, P., Bovo, R., Manara, R., and Martini, A. (2014). EYA1-related disorders: two clinical cases and a literature review. Int. J. Pediatr. Otorhinolaryngol. *78*, 1201–1210. https://doi.org/10.1016/j.ijporl.2014.03.032.

45. Xiao, S.Y., Qu, J., Zhang, Q., Ao, T., Zhang, J., and Zhang, R.H. (2019). Identification of a novel missense eya4 mutation causing autosomal dominant non-syndromic hearing loss in a chinese family. Cell. Mol. Biol. (Noisy-Le-Grand) *65*, 84–88.

46. Bangs, F., and Anderson, K.V. (2017). Primary Cilia and Mammalian Hedgehog Signaling. Cold Spring Harb. Perspect. Biol. *9*, a028175. https://doi.org/10.1101/cshperspect.a028175.

47. Liem, K.F., Jr., He, M., Ocbina, P.J.R., and Anderson, K.V. (2009). Mouse Kif7/Costal2 is a cilia-associated protein that regulates Sonic hedgehog signaling. Proc. Natl. Acad. Sci. USA *106*, 13377–13382. https://doi.org/10.1073/pnas.0906944106.

48. Pignoni, F., Hu, B., Zavitz, K.H., Xiao, J., Garrity, P.A., and Zipursky, S.L. (1997). The eye-specification proteins So and Eya form a complex and regulate multiple steps in Drosophila eye development. Cell *91*, 881–891. https://doi.org/10.1016/s0092-8674(00)80480-8.

49. Zou, D., Erickson, C., Kim, E.H., Jin, D., Fritzsch, B., and Xu, P.X. (2008). Eya1 gene dosage critically affects the development of sensory epithelia in the mammalian inner ear. Hum. Mol. Genet. *17*, 3340–3356. https://doi.org/10.1093/hmg/ddn229.

50. Cavodeassi, F., Carreira-Barbosa, F., Young, R.M., Concha, M.L., Allende, M.L., Houart, C., Tada, M., and Wilson, S.W. (2005). Early stages of zebrafish eye formation require the coordinated activity of Wnt11, Fz5, and the Wnt/beta-catenin pathway. Neuron *47*, 43–56. https://doi.org/10.1016/j.neuron.2005.05.026.

51. Munnamalai, V., and Fekete, D.M. (2013). Wnt signaling during cochlear development. Semin. Cell Dev. Biol. *24*, 480–489. https://doi.org/10.1016/j.semcdb.2013.03.008.

52. Shi, F., Hu, L., Jacques, B.E., Mulvaney, J.F., Dabdoub, A., and Edge, A.S.B. (2014). beta-Catenin is required for hair-cell differentiation in the cochlea. J. Neurosci. *34*, 6470–6479. https://doi.org/10.1523/JNEUROSCI.4305-13.2014.

53. Deng, D., Qian, X., Chen, B., Yang, X., Wang, Y., Chi, F., Huang, Y., Zhao, Y., and Ren, D. (2021). Canonical Wnt Signaling Pathway on Polarity Formation of Utricle Hair Cells. Neural Plast. *2021*, 9950533. https://doi.org/10.1155/2021/9950533.

54. Zhang, T., Xu, J., and Xu, P.X. (2021). Eya2 expression during mouse embryonic development revealed by Eya2^{lacZ} knockin reporter and homozygous mice show mild hearing loss. Dev. Dyn. *250*, 1450–1462. https://doi.org/10.1002/dvdy.326.

55. Kong, D., Ma, W., Zhang, D., Cui, Q., Wang, K., Tang, J., Liu, Z., and Wu, G. (2019). EYA1 promotes cell migration and tumor metastasis in hepatocellular carcinoma. Am. J. Transl. Res. *11*, 2328–2338.

56. Zhou, J.J., Huang, Y., Zhang, X., Cheng, Y., Tang, L., and Ma, X. (2017). Eyes absent gene (EYA1) is a pathogenic driver and a therapeutic target for melanoma. Oncotarget *8*, 105081–105092. https://doi.org/10.18632/oncotarget.21352.

57. Xu, H., Jiao, Y., Yi, M., Zhao, W., and Wu, K. (2019). EYA2 Correlates With Clinico-Pathological Features of Breast Cancer. Front. Oncol. *9*, 26. https://doi.org/10.3389/fonc.2019.00026.

58. Vartuli, R.L., Zhou, H., Zhang, L., Powers, R.K., Klarquist, J., Rudra, P., Vincent, M.Y., Ghosh, D., Costello, J.C., Kedl, R.M., et al. (2018). Eya3 promotes breast tumor-associated immune suppression via threonine phosphatase-mediated PD-L1 upregulation. J. Clin. Invest. *128*, 2535–2550. https://doi.org/10.1172/JCI96784.

59. Li, Z., Qiu, R., Qiu, X., and Tian, T. (2018). EYA4 Promotes Cell Proliferation Through Downregulation of p27Kip1 in Glioma. Cell. Physiol. Biochem. *49*, 1856–1869. https://doi.org/10.1159/000493631.

60. Brenner, S. (1974). The genetics of Caenorhabditis elegans. Genetics *77*, 71–94. https://doi.org/10.1093/genetics/77.1.71.

61. Abraham, C., Hutter, H., Palfreyman, M.T., Spatkowski, G., Weimer, R.M., Windoffer, R., Jorgensen, E.M., and Leube, R.E. (2006). Synaptic tetraspan vesicle membrane proteins are conserved but not needed for synaptogenesis and neuronal function in Caenorhabditis elegans. Proc. Natl. Acad. Sci. USA *103*, 8227–8232. https://doi.org/10.1073/pnas.0509400103.

62. Xu, T., and Rubin, G.M. (1993). Analysis of genetic mosaics in developing and adult Drosophila tissues. Development *117*, 1223–1237. https://doi.org/10.1242/dev.117.4.1223.

Article

SOURCE DATA | TRANSPARENT PROCESS

THE EMBO JOURNAL

SHP-1 dephosphorylates histone H2B to facilitate its ubiquitination during transcription

Prajakta Tathe[1,2], K V S Rammohan Chowdary[1], Krushna Chandra Murmu[3], Punit Prasad[3] & Subbareddy Maddika[1,*]

Abstract

Dynamic regulation of phosphorylation and dephosphorylation of histones is essential for eukaryotic transcription, but the enzymes engaged in histone dephosphorylation are not fully explored. Here, we show that the tyrosine phosphatase SHP-1 dephosphorylates histone H2B and plays a critical role during transition from the initiation to the elongation stage of transcription. Nuclear-localized SHP-1 is associated with the Paf1 complex at chromatin and dephosphorylates H2B at tyrosine 121. Moreover, knockout of SHP-1, or expression of a mutant mimicking constitutive phosphorylation of H2B Y121, leads to a reduction in genome-wide H2B ubiquitination, which subsequently causes defects in RNA polymerase II-dependent transcription. Mechanistically, we demonstrate that Y121 phosphorylation precludes H2B's interaction with the E2 enzyme, indicating that SHP-1-mediated dephosphorylation of this residue may be a prerequisite for efficient H2B ubiquitination. Functionally, we find that SHP-1-mediated H2B dephosphorylation contributes to maintaining basal autophagic flux in cells through the efficient transcription of autophagy and lysosomal genes. Collectively, our study reveals an important modification of histone H2B regulated by SHP-1 that has a role during eukaryotic transcription.

Keywords H2B ubiquitination; histone H2B; Paf1 complex; SHP-1; transcription

Subject Categories Chromatin, Transcription & Genomics

DOI 10.15252/embj.2021109720 | Received 15 September 2021 | Revised 23 June 2022 | Accepted 5 July 2022 | Published online 8 August 2022

The EMBO Journal (2022) 41: e109720

Introduction

Eukaryotic transcription is a highly complex and tightly coordinated process. Transcription cycle starts with an assembly of a preinitiation complex that promotes sequential recruitment of transcription factors and RNA Polymerase II (Pol II), followed by promoter melting, promoter escape leading to transcript elongation, and finally culminates with termination (Svejstrup, 2004). The formation of a preinitiation complex at the promoters does not always lead to productive transcription (Core *et al*, 2008). The occurrence of precise post-translational modifications on the C-terminal domain (CTD) of RNA Pol II and histone tails of the nucleosomes is vital to creating a dynamic environment for productive transcription (Li *et al*, 2007). Among many modifications of RNA Pol II CTD (Hsin & Manley, 2012), the role of ser5 and ser2 phosphorylation during transcription has been extensively characterized. CTD is phosphorylated at Ser5 residue by CDK7 to facilitate recruitment of enzymes for nascent mRNA capping and promote transition from preinitiation state to elongation (Ebmeier *et al*, 2017). Subsequently, Pol II gets phosphorylated at Ser2 by CDK9 (Marshall *et al*, 1996) and recently characterized CDK12 (Bartkowiak *et al*, 2010), during elongation step of the transcription. These two CTD modifications are dynamically regulated during transcription cycle, where phosphatases such as Scp1, Fcp1, SSU72, CDC14, Rtr1, Glc7 dephosphorylate Ser5 and Ser2 after Pol II entry to elongation state and at the end of transcription respectively to initiate a new cycle of transcription (Yeo *et al*, 2003; Fuda *et al*, 2012).

In addition to Pol II CTD modifications, histone modifications such as ubiquitination, acetylation, and methylation occur co-transcriptionally and play an essential role in productive transcription (Gates *et al*, 2017). Different histone marks recruit specific readers necessary for each step of the transcription cycle (e.g., H3K4me3/TFIID for initiation, H3K9ac/SEC for pause release, H3K36me3/DNMT3a/b for elongation, and H3K9me2/HP1γ for termination). High levels of H3K4me3 and multiple acetylated H3 and H4 lysine residues were found to be enriched at active promoters, whereas gene bodies of transcribed genes are enriched with H2BK120ub, H3K36me3, H3K79me2, and H3K79me3 (Chen *et al*, 2018). Additionally, dynamic phosphorylation of histones has been shown to play a vital role in coordinating transcription. For instance, phosphorylation of histone H3 at serine 10 and 28, and histone H2A on T120, is involved in the regulation of chromatin structure and function during transcription (Rossetto *et al*, 2012; Kim *et al*, 2013). Recent studies also highlight the importance of histone tyrosine phosphorylation during transcription regulation. For example, H2B Y37 phosphorylation was shown to attenuate the transcription of histone cluster genes and, on the other hand, H3 Y41 phosphorylation by JAK2 leads to

1 Laboratory of Cell Death and Cell Survival, Centre for DNA Fingerprinting and Diagnostics (CDFD), Hyderabad, India
2 Graduate Studies, Manipal Academy of Higher Education, Manipal, India
3 Epigenetic and Chromatin Biology Unit, Institute of Life Sciences, Bhubaneswar, India
*Corresponding author. Tel: +91 40 2721 6168. E-mail: msreddy@cdfd.org.in

transcriptional activation by preventing binding of HPIα to chromatin (Dawson *et al*, 2009; Mahajan *et al*, 2012). Interestingly, so far, all the emphasis has been given to kinases that modify histones, but little is known about the phosphatases responsible for histone dephosphorylation during transcription. Here, we report a tyrosine phosphatase SHP-1 as an important enzyme that reverses phosphorylation of Y121 residue on H2B, a new modification that plays an essential switching role during transcription.

SHP-1, a non-receptor tyrosine phosphatase encoded by the PTPN6 gene, is highly expressed in hematopoietic cells and moderately in several non-hematopoietic cell types (Craggs & Kellie, 2001). SHP-1 functions in multiple signaling pathways (growth factor and cytokine-dependent) in hematopoietic cells by controlling phosphorylation of varied substrates such as ZAP70, Syk, Crk II, Jak1, GSK3β, thus regulating a variety of cellular processes including cell proliferation, growth, and differentiation (Brockdorff *et al*, 1999; Dustin *et al*, 1999; Jiang *et al*, 2016; Azoulay-Alfaguter *et al*, 2017). Homozygous mutation in PTPN6 gene ($PTPN6^{me/me}$) shows moth-eaten phenotype in mice. These mice develop chronic inflammation of the skin, autoimmunity, and eventually succumb to fatal pneumonitis (Van Zant & Shultz, 1989). By virtue of its antagonist function to the growth-promoting tyrosine kinase signaling in hematopoietic cells, SHP-1 has been suggested to be a candidate tumor suppressor gene in lymphoma and leukemias (Zhang *et al*, 2000). In contrast, SHP-1 protein is over-expressed in some non-lymphocytic cell lines, such as prostate cancer, breast and ovarian cancers, possibly suggesting that SHP-1 can play context-dependent negative or positive roles in regulating signal transduction pathway (Varone *et al*, 2020).

Results

SHP-1 interacts with chromatin-associated proteins

SHP-1 is known to be a predominantly cytoplasmic phosphatase in cells of hematopoietic origin; however, by virtue of a nuclear localization signal on its C-terminus, it has the potential to localize to the nucleus (Yang *et al*, 2002). We screened a panel of cells from hematopoietic and non-hematopoietic origin to understand the localization of SHP-1. While SHP-1 is majorly found in the cytoplasm of different hematopoietic cells (THP-1, Jurkat and U937), interestingly, it shows distinct nuclear localization in epithelial cells of non-hematopoietic origin derived from different human cancer tissues (breast epithelial line: MCF-7, colon epithelial cells: HCT116, Lung epithelial cell line: A549, embryonic kidney cells: 293T and cervical epithelial cells: HeLa) (Fig 1A). Similar nuclear localization of SHP-1 was also seen in epithelial cells of non-cancerous origin (Retinal pigment epithelial cells: RPE1, human mammary epithelial cells: MCF10A) (Fig EV1A). To test if the nuclear localization signal is specific for SHP-1, we generated an SHP-1 knockout line in MCF-7 breast epithelial cells using CRISPR (Fig EV1B). Wild-type MCF-7 cells display predominant SHP-1 nuclear localization, but the signal is completely lost in SHP-1 knockout cells (Fig EV1C). In addition, no SHP-1 signal was detected in MDA-MB-231 cell line (Fig EV1D), a breast cancer epithelial line that loses SHP-1 expression due to promoter hypermethylation (Yip *et al*, 2000), suggesting that the nuclear localization is specific for SHP-1. Furthermore, we observed that SHP-1 displays a distinct punctate-like localization in the nucleus, prompting us to hypothesize that SHP-1 might be localizing to chromatin. Indeed, our biochemical fractionation experiments confirmed SHP-1 association with chromatin in different epithelial cells (Fig EV1E and F). Although SHP-1 was predominantly seen in the cytoplasm of different hematopoietic cells during our immunofluorescence studies, cell fractionation experiments revealed significant enrichment of SHP-1 at chromatin (Fig EV1G). Together, these data indicate that SHP-1 displays chromatin localization in a broad range of cells derived from hematopoietic as well as non-hematopoietic origin.

To investigate the role of chromatin-associated nuclear SHP-1 in cells, we analyzed the list of SHP-1-associated proteins derived through an interaction proteomics approach in our earlier study (Kumar *et al*, 2017). Tandem affinity purification with streptavidin-agarose beads and S-protein-agarose beads using lysates derived from cells expressing a triple-tagged SFB-SHP-1 followed by mass spectrometry analysis allowed us to discover several chromatin proteins associated with SHP-1. Among these proteins, we consistently found the components of Paf1 complex along with histone H2B in SHP-1 purified complex (Fig 1B). Paf1 complex (Paf1C) is a conserved multi-subunit complex (with Paf1, Ctr9, Cdc73, Rtf1, hSki8, and Leo1 as integral components) that plays a very critical role in various stages of RNA Polymerase II-dependent transcription cycle (Van Oss *et al*, 2017). Several studies have clearly established that Paf1C regulates transcription elongation as well as transcription termination via promoting different co-transcriptional histone modifications such as H2B ubiquitination (Van Oss *et al*, 2017). By using exogenously expressed proteins, we confirmed the interaction of Paf1 complex components specifically with SHP-1 (Fig 1C). Also, we confirmed the interaction of overexpressed myc-tagged histone H2B specifically with SHP-1 in cells (Fig 1D). Furthermore, we validated the interaction of endogenous SHP-1 with endogenous Paf1 complex proteins (Fig 1E) as well as histone H2B (Fig 1F) in cells by performing immunoprecipitation with SHP-1 specific antibody. Interaction of SHP-1 is with chromatin-bound H2B and not free histone, as other histones such as H2A, H3, and H4 were readily found in the immunoprecipitated complexes of SHP-1 (Fig EV1H). Bacterially purified recombinant GST-tagged H2B and MBP-tagged SHP-1 proteins interacted with each other, suggesting a direct interaction between SHP-1 and histone H2B (Fig 1G). Together, these data indicate that SHP-1, a well-known cytoplasmic phosphatase, localizes to nucleus where it is associated with new complexes at chromatin such as Paf1 complex and histones.

Nuclear SHP-1 is necessary for H2B ubiquitination

Paf1 complex is essential for histone H2B ubiquitination (Chen *et al*, 2021), but how exactly it promotes H2B ubiquitination in cells is not completely understood. Since we found that SHP-1 is associated with both Paf1 complex as well as histone H2B, we hypothesized that SHP-1 by associating with Paf1 complex might contribute to H2B ubiquitination. To test this hypothesis, we generated CRISPR-based SHP-1 knockout lines in 293T cells. While H2B ubiquitination is readily detected in wild-type 293T cells, SHP-1 knockout cells display severely diminished histone ubiquitination (Fig 2A and Appendix Fig S1A). Furthermore, to understand if nuclear-localized SHP-1 is necessary for mediating histone ubiquitination,

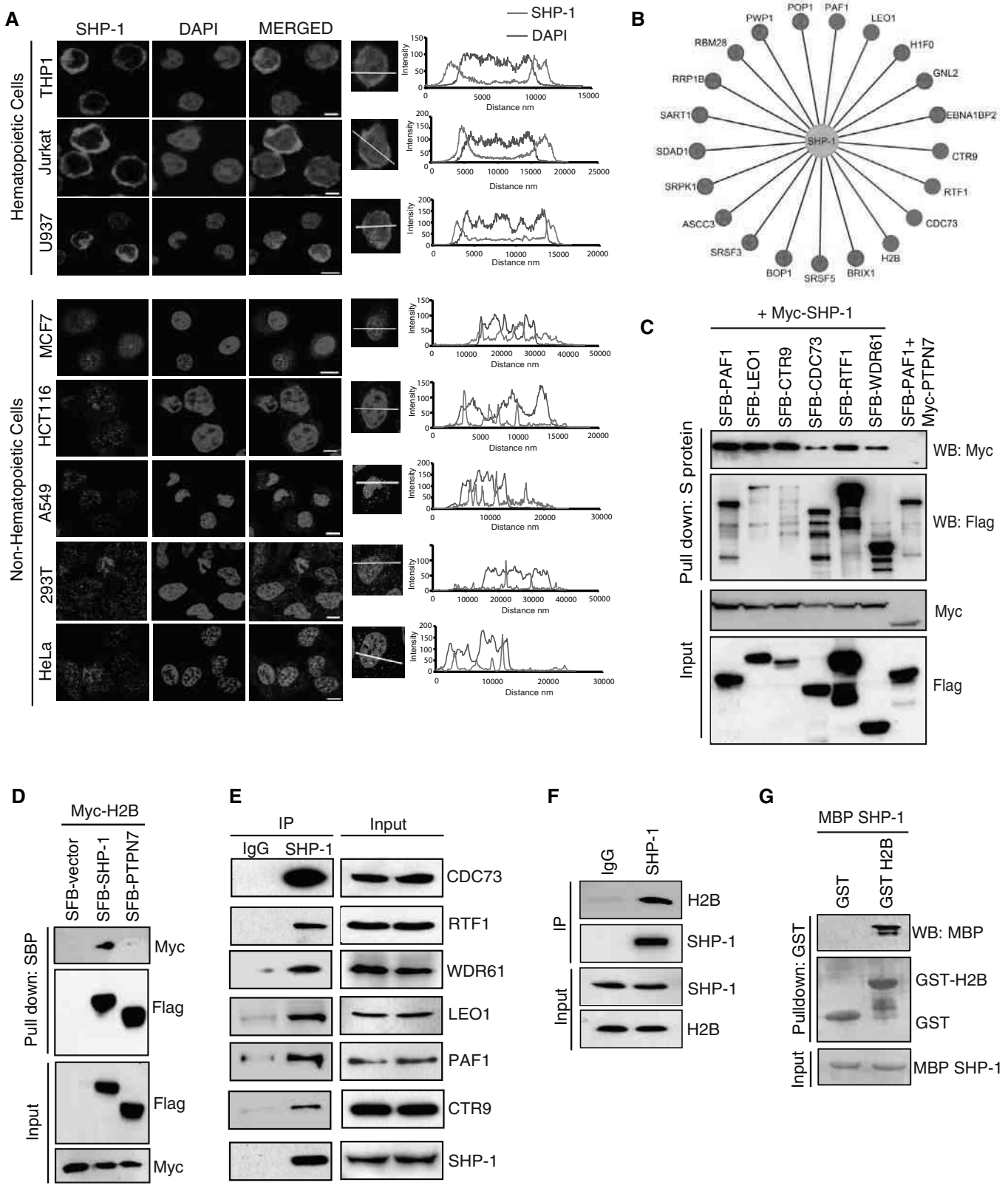

Figure 1.

Figure 1. Nuclear localized SHP-1 is associated with Paf complex and Histone H2B.

A Localization of endogenous SHP-1 in hematopoietic and non-hematopoietic cells was determined by confocal imaging after staining with SHP-1 antibody. DAPI was used for nuclear staining, Scale bar: 5 μm. Fluorescence intensities along the line drawn in a representative cell were obtained using Zen software and the co-localization plots were made using GraphPad (Red: SHP-1, Blue: DAPI).

B Network of nuclear proteins associated with SHP-1 is shown. SFB-GFP purification was used as control to filter out non-specific interactions. The list of SFB-SHP-1 and SFB-GFP-associated proteins was derived from our earlier study (Kumar *et al*, 2017). Paf complex components and Histone H2B are highlighted in blue in the network.

C SFB tagged PAF1, SFB-LEO1, SFB-CTR9, SFB-CDC73, SFB-RTF1, SFB-WDR61 along with Myc SHP-1 or Myc PTPN7 were transfected in 293T cells and interaction of SHP-1 with PAF complex components was detected by immunoblotting with Myc antibody after S protein beads pulldown in the presence of TurboNuclease.

D SFB empty vector, SFB SHP-1, or SFB PTPN7 was co-transfected with Myc tagged H2B in 293T cells. The interaction of H2B with SHP-1 was detected through immunoblotting using Myc antibody after pulldown with streptavidin sepharose beads.

E Endogenous association of SHP-1 with Paf1 complex subunits (CDC73, RTF1, WDR61, LEO1, Paf1, CTR9) was detected by immunoblotting after performing immunoprecipitation with either IgG or SHP-1 antibody.

F Immunoprecipitation (IP) with control IgG or anti-SHP-1 antibody was performed with extracts prepared from MCF7 cells and endogenous association of H2B with SHP-1 was detected by immunoblotting.

G Glutathione Sepharose beads immobilized with bacterially expressed recombinant GST or GST-H2B proteins were incubated with bacterially purified recombinant MBP-SHP-1. The association of SHP-1 with H2B was detected by immunoblotting with MBP antibody. Expression of GST, GST-H2B, and MBP SHP-1 was shown by Coomassie staining.

Source data are available online for this figure.

we generated an SHP-1 NLS mutant that is defective in nuclear localization (Fig EV2A) and unable to interact with histone H2B (Fig EV2B). Expression of constitutively active SHP-1 (ΔSH2) with intact NLS, but not NLS mutant, rescues H2B ubiquitination that was lost in SHP-1 knockout cells, suggesting that nuclear localization of SHP-1 is required for histone ubiquitination (Fig 2B and Appendix Fig S1B). SHP-1 being a phosphatase, we next tested if its catalytic activity in the nucleus is required for promoting H2B ubiquitination. Expression of wild-type, but not catalytically inactive mutant of SHP1 (C453S), could enhance H2B ubiquitination in SHP-1 knockout cells (Fig 2C and Appendix Fig S1C), thus suggesting the requirement of phosphatase activity in the nucleus to mediate H2B ubiquitination. Given that SHP-1 is a tyrosine phosphatase and its activity is required for H2B ubiquitination, we next tested if mutation of any tyrosine residue on H2B would alter its ubiquitination. H2B has 5 tyrosine residues and conversion of any of the tyrosines to phenyl alanine has no impact on its ubiquitination. However, mutation of Y121 residue to aspartic acid (a phosphomimetic variant) completely abolished H2B ubiquitination (Figs 2D and EV2C), similar to that of H2B K120R (ubiquitination site) mutant. Mutation of Y121 to aspartic acid neither affected H2B presence in the nucleosome fraction (Fig EV2D) nor its ability to interact with other histones such as H2A, H3, and H4 (Fig EV2E), thus suggesting that the loss of ubiquitination in Y121D mutant is a direct effect of Y121 modification. Interestingly, Y121 is located adjacent to the site of H2B ubiquitination and our data suggest that the presence of a negative charge on this residue might negatively hamper the ubiquitination of K120 residue. To further test if this is indeed true, we performed *in vitro* ubiquitination assays using various bacterially purified recombinant H2B proteins. While wild-type H2B could be readily ubiquitinated *in vitro*, no ubiquitination was detected with Y121D mutant (Fig 2E). Loss of ubiquitination in Y121D mutant *in vitro* is not restricted to free histone as H2B Y121D mutant in H2A-H2B dimer also shows a similar defect in ubiquitination (Fig EV2F and Appendix Fig S1D). Furthermore, *in vitro* ubiquitination assays using synthesized histone peptides revealed that a non-phosphopeptide could be ubiquitinated efficiently, whereas phosphopeptide (pY121) fails to accept ubiquitin on K120 residue (Fig 2F). Therefore, these data suggest that a phosphate group on Y121 residue hampers H2B K120 ubiquitination and the nuclear-localized SHP-1 might assist in H2B ubiquitination by removing the phosphate on H2B.

SHP-1 dephosphorylates histone H2B at Y121 residue

Since SHP-1 phosphatase activity is required for promoting H2B ubiquitination, we next sought to identify if histone H2B or any of the components of Paf1 complex are novel SHP-1 substrates in the nucleus. Previously, CDC73, one of the components of Paf1 complex, was shown to be dephosphorylated by SHP-2, a closely related phosphatase to SHP-1(Takahashi *et al*, 2011). In line with the earlier study, we observed that SHP-2 could readily dephosphorylate CDC73 *in vitro*; however, SHP-1 could not dephosphorylate CDC73 (Fig EV3A). We next tested if any of the other components of Paf1 complex are substrates of SHP-1. All the components of Paf1 complex purified individually from bacteria (Fig EV3B) were *in vitro* phosphorylated using 293T lysate and used as substrates for phosphatase assay. *In vitro* phosphatase assay using active SHP-1 (ΔSH2) (Fig EV3C) revealed that none of the Paf1 components were dephosphorylated by SHP-1 (Fig EV3D). Lack of phosphate release in the *in vitro* malachite green assay also confirmed that none of the Paf1 components are bona fide substrates of SHP-1 (Fig EV3E). Next, we tested if H2B is a new substrate of SHP-1. Tyrosine kinase SYK was shown to have the ability to transfer phosphate groups on various tyrosine residues on H2B (Sakai *et al*, 1991). Bacterially purified recombinant H2B was phosphorylated *in vitro* by using SYK and we utilized this phosphorylated H2B as a substrate in our phosphatase assays. We found that bacterially purified active SHP-1 readily releases phosphatase from H2B (Fig 3A). While active SHP-1 could dephosphorylate tyrosine residues, phosphatase inactive C/S mutant could not do so under *in vitro* conditions (Fig 3B and Appendix Fig S1E). Furthermore, *in vitro* phosphatase assay using the custom synthetic peptide containing phosphorylated residue at Y121 site confirmed that SHP-1 releases phosphate from H2B Y121 residue (Fig 3C). Tyrosine phosphorylation of H2B is also readily observed in cells, and deletion of SHP-1 in cells enhanced tyrosine phosphorylation (Fig EV4A and Appendix Fig S1F). Furthermore, while tyrosine phosphorylation on wild-type H2B is readily detected in cells, phosphorylation is severely hampered in Y121F mutant, clearly suggesting that Y121 residue is a bona fide tyrosine

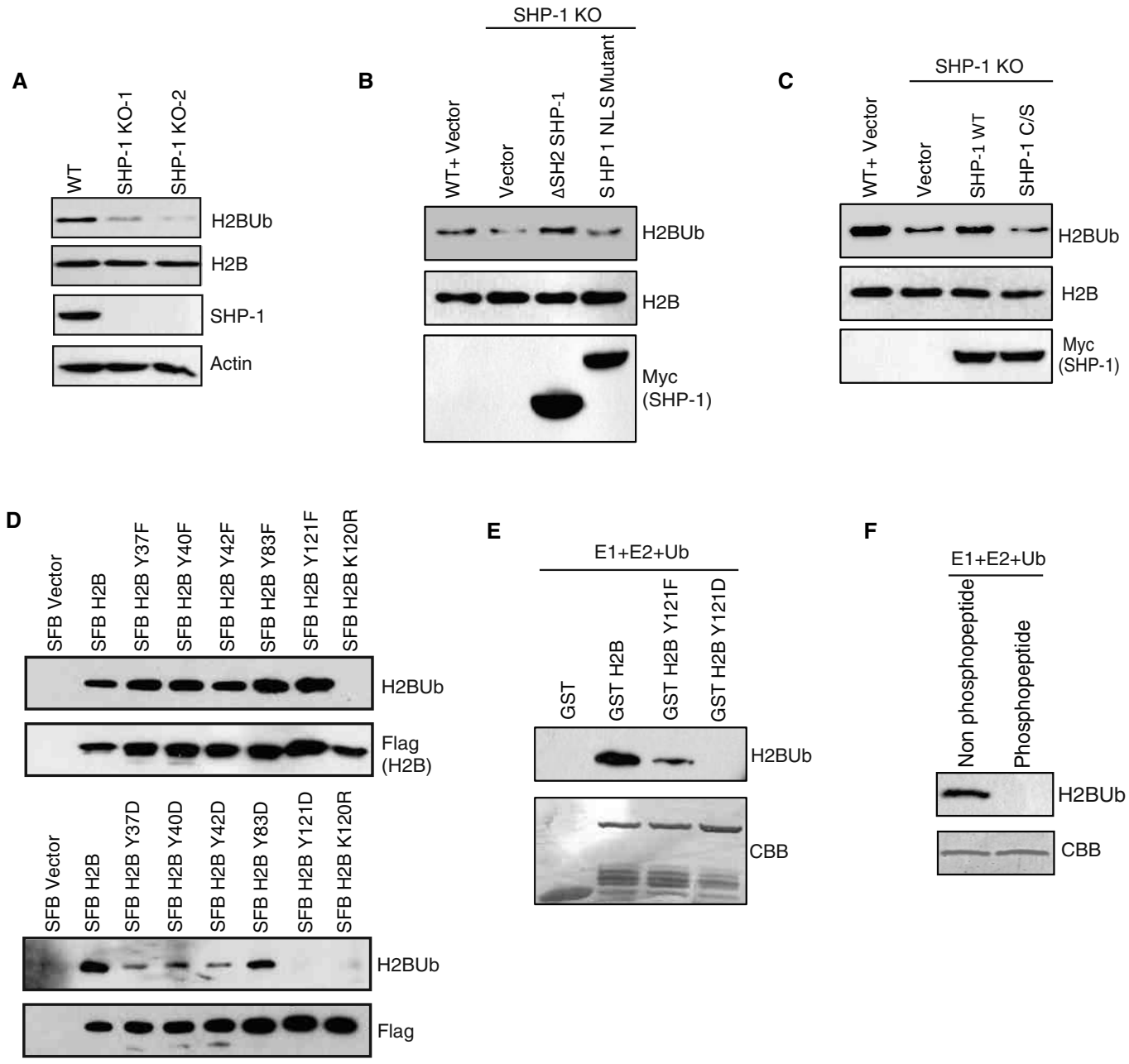

Figure 2. SHP-1 is required for efficient H2B ubiquitination.

A Nuclear extracts of WT and SHP-1 knockout cells (derived from two independent guide RNAs) were made and the levels of H2BUb were detected.

B Wild-type (WT) 293T cells along with SHP-1 KO cells transfected with either Myc vector, Myc SHP-1 ΔSH2, or Myc SHP-1 NLS mutant were lysed. H2BUb levels were determined using specific antibody.

C WT and SHP-1 KO 293T cells transfected with Myc vector, Myc SHP-1, or Myc SHP-1 C/S (C453S) mutant were lysed. H2BUb levels were determined using specific antibody.

D H2B WT along with the indicated Y/F and Y/D mutants were transfected into 293T cells. Histone extract was prepared from cells transfected with each construct and subjected to Western blotting with anti-H2B and anti-H2BUb antibodies.

E *In vitro* ubiquitination assay was performed using bacterially purified GST, GST-tagged H2B, and its mutants as substrates. Recombinant E1, E2(UBE2A), and ubiquitin were included in each reaction. Ubiquitination was detected by H2BUb antibody.

F *In vitro* ubiquitination was performed using biotin-tagged non-phospho and phospho (pY121) peptide of H2B as substrates in the presence of E1 and E2. H2BUb was detected by immunoblotting with specific antibody.

Source data are available online for this figure.

phosphorylation site in cells (Fig EV4B and Appendix Fig S1G). To further understand if SHP-1 dephosphorylates H2B at Y121 residue, we generated a polyclonal Y121 phospho-specific antibody. We validated the antibody *in vitro* using phospho-specific Y121 synthetic peptide (Fig EV4C) and in cells using an Y121F mutant (Fig EV4D and Appendix Fig S1H). We found that the newly generated antibody specifically detects H2B phosphorylated at Y121 residue. Phospho-Y121 signal was lost upon treatment of H2B with λ-phosphatase (Fig EV4E and Appendix Fig S1I). In addition, preincubation of antibody with phosphospecific Y121 synthetic peptide,

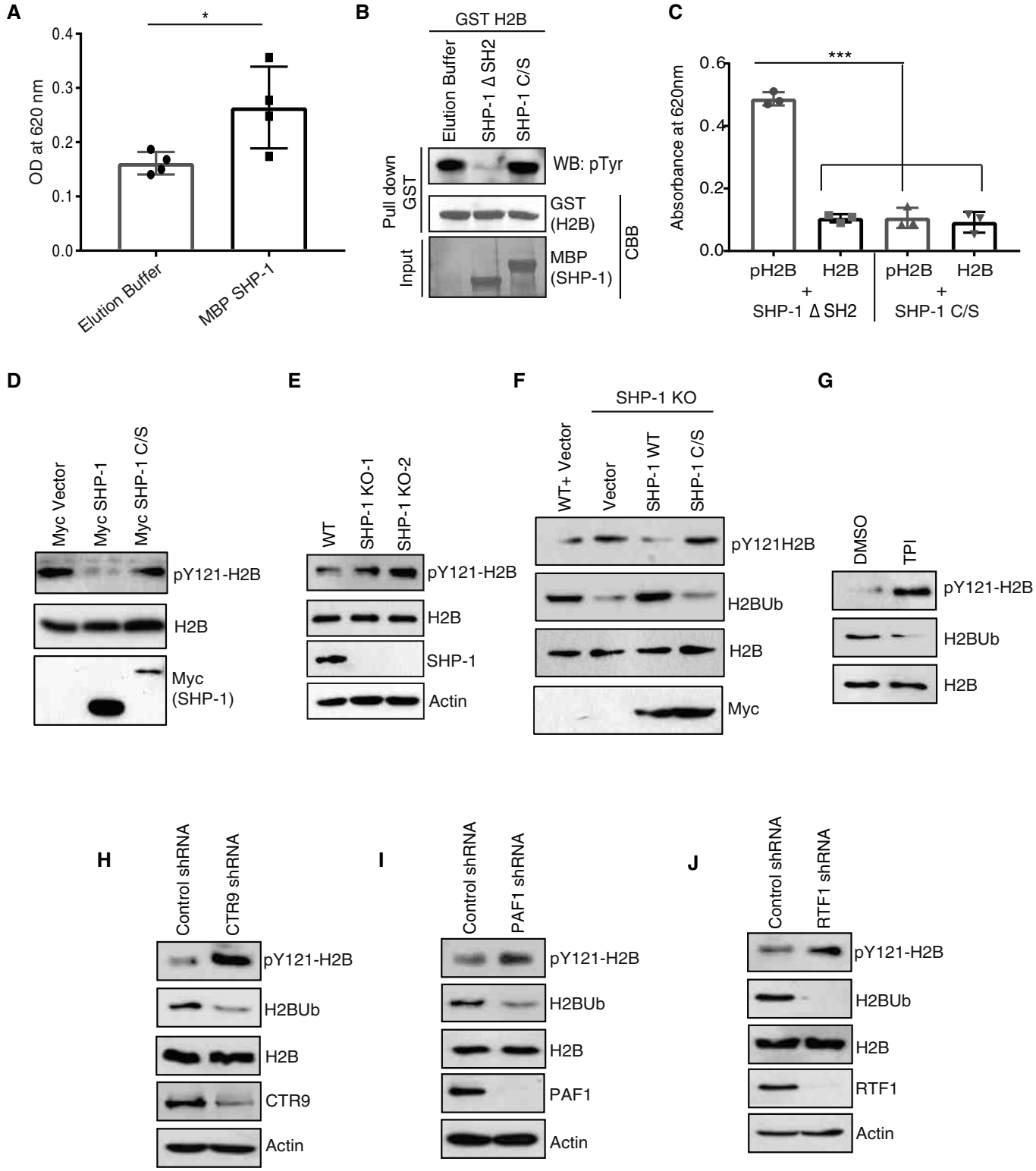

Figure 3.

Figure 3. Histone H2B is a new substrate for SHP-1.

A *In vitro* phosphorylated GST H2B by Syk kinase was incubated with bacterially purified recombinant wild-type SHP-1 or elution buffer and the amount of released phosphate was assayed colorimetrically using the malachite green reagent (A620 nm). Data represent mean absorbance from four independent experiments. Error bar indicates SD; *$P < 0.05$, by Student's *t* test.

B Bacterially purified GST H2B was subjected to *in vitro* kinase assay using HEK293T-cell lysate, and then phosphorylated proteins were incubated with either bacterially purified MBP tagged constitutively active (SHP-1 ΔSH2), or catalytically inactive SHP-1 C/S mutant. The phosphorylation status of recombinant H2B was detected by immunoblotting with phospho-tyrosine antibody.

C Phospho (pH2B) Y121 and non-phospho peptide of H2B was incubated with constitutively active (SHP-1 ΔSH2) or catalytically inactive mutant (C/S) of SHP-1 and the released phosphate was assayed colorimetrically using the malachite green reagent (A620 nm). $n = 3$ independent experiments, Error bars indicate SD; ***$P < 0.001$ (one-way ANOVA, Tukey's multiple comparison test).

D 293T cells were transfected with vector, Myc tagged SHP-1 WT or C/S mutant. The phosphorylation status of endogenous H2B was detected by immunoblotting with pY121-H2B antibody.

E Nuclear extracts of 293T WT and SHP-1 KO cells were made and the levels of H2B phosphorylation were detected using pY121-H2B antibody.

F Wild-type (WT) along with SHP-1 KO 293T cells transfected with either Myc vector, Myc SHP-1 or Myc SHP-1 C/S mutants were lysed. Levels of pY121-H2B and H2BUb were determined using specific antibodies.

G 293T Cells were treated with SHP-1 inhibitor TPI (50 nM) for 1 h and levels of pY121-H2B were determined using pY121H2B antibody.

H–J MCF7 cells were transduced with (H) CTR9 shRNA, (I) Paf1 shRNA, or (J) RTF1 shRNA along with control shRNA. Post 72 h, cells were collected and lysed to isolate soluble and nuclear fractions. Levels of phosphorylated and ubiquitinated H2B were detected by immunoblotting with indicated specific antibodies.

Source data are available online for this figure.

but not non-phospho peptide, failed to detect a phospho-signal on H2B in wild-type and SHP-1 KO cells, thus indicating that the newly generated antibody specifically detects phosphorylated H2B (Fig EV4F). Furthermore, the antibody detects phosphorylation on histone H2B, but not on any other histones (Fig EV4G), thus confirming the specificity of the antibody. By using a phospho-specific antibody, we found that phosphorylation at H2B Y121 residue is reduced in cells expressing wild-type SHP-1, but not catalytically inactive C/S mutant (Fig 3D and Appendix Fig S2A). Similar data were obtained under *in vitro* conditions, where active SHP-1, but not the catalytically inactive mutant, dephosphorylates H2B at Y121 residue (Fig EV4H and Appendix Fig S2B). On the other hand, deletion of SHP-1 in cells enhanced phosphorylation of Y121 residue (Fig 3E and Appendix Fig S2C). The enhanced phosphorylation in knockout cells is due to specific deletion of SHP-1 since re-expression of wild-type SHP-1, but not inactive C/S mutant, reduced pY121 levels in SHP-1 knockout cells (Fig 3F and Appendix Fig S2D). In addition, we demonstrated that pharmacological inhibition of SHP-1 by treating cells with a specific inhibitor TPI enhanced pY121 levels (Fig 3G and Appendix Fig S2E), followed by reduced H2B ubiquitination in cells. Together, these data clearly suggest that histone H2B is a novel substrate of SHP-1 in cells and the dephosphorylation occurs specifically at Y121 residue on H2B. Furthermore, as SHP-1 is associated with H2B along with Paf1 complex, we next tested if Paf complex participates in SHP-1 mediated H2B dephosphorylation. Depletion of CTR9 (Fig 3H), Paf1 (Fig 3I), or RTF1 (Fig 3J) (Appendix Fig S2F–H) using individual shRNAs significantly enhanced the phosphorylation levels of H2B Y121 in cells. Thus, these data indicate that Paf1 complex-associated SHP-1 removes phosphate group from H2B Y121 residue and thereby promotes efficient H2B K120 ubiquitination.

H2B Y121 dephosphorylation is required for E2 binding

We next sought to understand the molecular mechanism on how phosphorylation at Y121 residue prevents H2B ubiquitination in cells. H2B ubiquitination in cells is carried out by concerted action of E2 (Ube2A in humans or Rad6 in yeast) and E3 (RNF20/40 in humans or BRE1 in yeast) enzymes. Firstly, we tested if H2B Y121 phosphorylation modulates the binding of E3 enzymes. No detectable changes were observed in binding of RNF20 with Y121F and Y121D mutants in comparison with wild-type H2B (Fig 4A), thereby suggesting that Y121 phosphorylation has no effect on E3 ligase binding with H2B. Next, we tested if Y121 phosphorylation modulates E2 binding with the substrate. While Y121F mutant binds with Ube2A as efficiently as wild-type H2B, mutation of Y121D that mimics phosphorylation led to severe loss of interaction between H2B and Ube2A in cells (Fig 4B and Appendix Fig S3A and B). On the other hand, we also confirmed the loss of interaction between H2B Y121D mutant and Ube2A under *in vitro* conditions using bacterially purified recombinant proteins (Fig 4C and Appendix Fig S3C). Furthermore, we tested if indeed addition of phosphate group on H2B impedes its binding to Ube2A. While Ube2A efficiently interacts with unphosphorylated H2B, phosphorylation of H2B at Y121 residue *in vitro* hampered its interaction with Ube2A (Fig 4D and Appendix Fig S3D), thus clearly suggesting that phosphorylation of H2B at Y121 residue prevents its association of E2 enzyme. As we have demonstrated that SHP-1 dephosphorylates H2B at Y121 residue, we next tested if SHP1 activity is necessary for H2B binding with E2 enzyme. While no detectable changes in total protein levels of either E3 or E2 enzymes were seen (Appendix Fig S3E), interaction of H2B with Ube2A is severely hampered in SHP-1 knock out cells in comparison to wild-type cells (Fig 4E and Appendix Fig S3F). Furthermore, pharmacological inactivation of SHP-1 activity by treating cells with a specific inhibitor TPI also caused loss of H2B interaction with Ube2A (Fig 4F and Appendix Fig S3G). Together, these results suggest that H2B phosphorylation at Y121 residue precludes its interaction with E2 enzyme and therefore SHP-1-mediated dephosphorylation of this residue is necessary for providing substrate access to E2 enzyme that leads to H2B ubiquitination. Thus, loss of SHP1 protein or its activity leads to loss of H2B ubiquitination due to inability of H2B to interact with E2 enzymatic machinery.

SHP-1 localizes to sites of transcription and facilitates cellular transcription

H2B K120 ubiquitination is critical for cellular transcription. As we have shown that SHP-1 is necessary for efficient H2B ubiquitination in cells, we next tested if SHP-1 localizes to sites of active

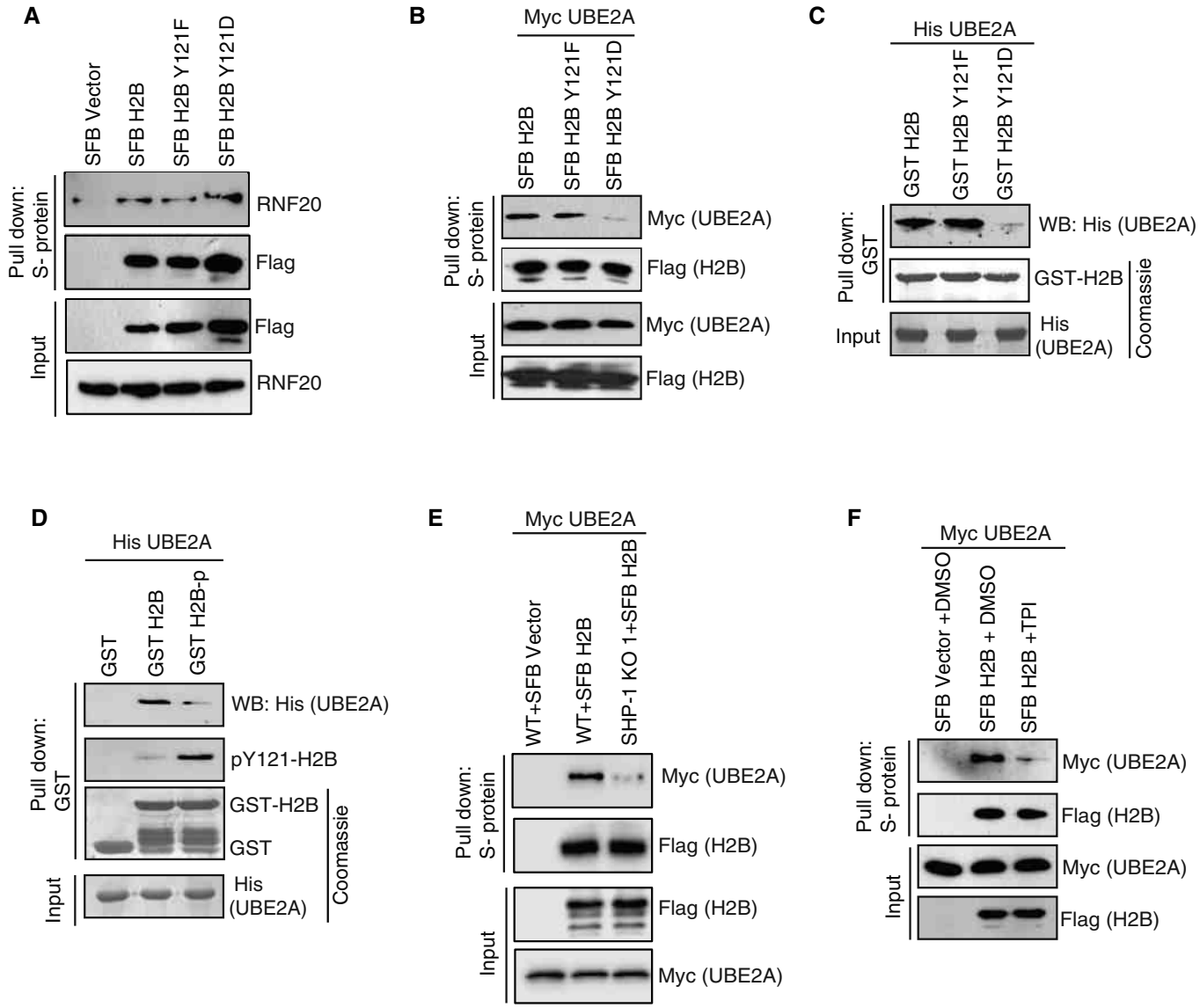

Figure 4. H2B Y121 dephosphorylation by SHP-1 is necessary for E2 binding.

A Cell lysates derived from 293T cells transfected with empty vector, SFB-tagged H2B, H2B Y121F, or H2B Y121D constructs were pulled down with S-protein agarose beads. RNF20 interaction with H2B was detected by immunoblotting with specific antibody.

B HEK293T cells were co-transfected with the SFB-tagged H2B, H2B Y121F, or H2B Y121D constructs along with Myc-tagged UBE2A. Cell lysates were pulled down with S-protein beads, and interaction was detected by immunoblotting with Myc antibody.

C Glutathione Sepharose beads bound with bacterially expressed recombinant GST-H2B, GST H2B Y121F and GST-H2B Y121D proteins were incubated with bacterially purified recombinant His UBE2A, and interaction of UBE2A with H2B was detected by immunoblotting with His antibody. Recombinant protein expression and pull-down were shown by Coomassie staining.

D Bacterially purified GST, GST H2B, and GST H2B-p (phosphorylated using Syk) were incubated with recombinant His UBE2A, and interaction of UBE2A with H2B was detected by immunoblotting with His antibody. Recombinant protein expression and pulldown were shown by Coomassie staining.

E WT 293T cells along with SHP-1 KO were co-transfected with SFB vector or SFB H2B along with Myc UbE2A. Cell lysates were pulldown using S-protein beads, and interaction of UBE2A with H2B was determined by Western blotting with the indicated antibodies.

F HEK293T cells were transfected with SFB vector or SFB H2B along with Myc UBE2A. Cells were treated with SHP-1 inhibitor TPI (50 nM) for 1 h after 24 h of transfection. Cell lysates were subjected to pulldown with S-protein beads, and Western blotting was performed using specific antibodies.

Source data are available online for this figure.

transcription on chromatin. In order to determine if SHP-1 co-localizes to transcription machineries in cells, we performed immunofluorescence staining with specific antibodies against CDK9, RNA Pol II, RNA Pol II Ser5P, and RNA Pol II Ser2P. Our super-resolution imaging analysis has revealed that SHP-1 readily localizes to CDK9 along with RNA Pol II, RNA Pol II Ser5P, and RNA Pol II Ser2P (Fig 5A). Several studies have clearly shown that CDK9 and RNA Pol II Ser5P mostly occupy the promoter/transcription start site

of genes and that RNA Pol II Ser2P is enriched over the gene body and is associated with transcriptional elongation (Komarnitsky *et al*, 2000). Although SHP-1 co-localizes with RNA Pol II Ser5P as well as RNA Pol II Ser2P, we noted that co-localization co-efficiency of SHP-1 is significantly higher in CDK9 and RNA Pol II Ser5P in comparison to RNA Pol II Ser2P (Fig 5B), possibly suggesting an important role of SHP-1 during the early stages of transcription. Also, we found that SHP-1 readily interacts with the RNA Pol II and CDK9 in cells (Fig 5C). To further determine if SHP-1 is indeed required for cellular transcription, we analyzed the levels of active transcription marks upon loss of SHP-1. Interestingly, we found that deletion of SHP-1 in cells led to a significant reduction in RNA Pol II Ser2P levels coupled with RNA Pol II Ser5P accumulation (Fig 5D and Appendix Fig S4A). Furthermore, pharmacological inactivation of SHP-1 activity by treating cells with a specific inhibitor TPI also shows similar defects in active RNA Pol II (Fig 5E and Appendix Fig S4B). Importantly, the changes in RNA Pol II phosphorylation detected in SHP-1 KO cells could be rescued by expression of a non-phosphorylatable H2B Y121F mutant but not a phosphomimetic Y121D mutant (Fig 5F and Appendix Fig S4C). These data suggest that SHP-1 is required for transition of RNA Pol II into productive elongation stage from initiation phase of the transcription and loss of SHP-1 may lead to stalling of RNA Pol II at early phases of transcription. Moreover, reduced RNA Pol II Ser2P levels after SHP-1 deletion is associated with an overall reproducible and quantifiable decrease in the incorporation of 5-ethynyl uridine (EU) into nascent RNA detected by immunofluorescence staining (Fig 5G and H). Similar reduction in nascent RNA synthesis was also observed upon pharmacological inhibition of SHP-1 activity via TPI treatment (Fig 5I and J), thus suggesting that transcription elongation is attenuated across the transcriptome upon SHP-1 loss.

Loss of SHP-1 results in genome wide changes in H2B ubiquitination and pol II distribution

To gain more insights into how loss of SHP-1 impacts Pol II-dependent transcription and if SHP-1 coexists with RNAPII transcription factories, we first determined the genome-wide occupancy of SHP-1 by chromatin immunoprecipitation (ChIP) coupled with deep sequencing. As no ChIP-grade antibodies were available for SHP-1 so far, we generated a rabbit polyclonal antibody for this purpose. Analysis of chromatin immunoprecipitate from MCF-7 cells demonstrated the proficiency of our antibody, albeit very weak, in specifically pulling down SHP-1 in ChIP experiments (Appendix Fig S5A). Our ChIP-Seq analysis revealed that SHP-1 is distributed across various regions of the genome (Appendix Fig S5B), however, predominantly at promoter (16%), first exon (22%) and distal intergenic regions (39%). Motif discovery analysis performed with the findMotifsGenome function of the HOMER retrieved several known and *de novo* motifs for SHP-1 binding (Appendix Fig S5C), suggesting a broad coverage of SHP-1 association across the genomic regions in cells with no bias for a particular transcription factor/site. Consistent with our observation that SHP-1 might be important during early events of Pol II-dependent transcription, we found that SHP-1 is highly enriched at the transcription start sites (Fig 6A and B). To further validate our ChIP-Seq data, we randomly picked two independent genes (SETD1A and SMARCE1) where SHP-1 has shown enrichment in the ChIP-Seq analysis (Appendix Fig S5D). Chromatin immunoprecipitation followed by q-RT-PCR analysis has clearly indicated that SHP-1 is readily enriched at the transcription start sites of these genes (Appendix Fig S5E), thus validating our SHP-1 ChIP-Seq data.

Furthermore, to understand how loss of SHP-1 impacts Pol II-dependent transcription, we analyzed H2B ubiquitination and Pol II occupancy at genome-wide level by performing ChIP-seq experiments in wild-type and SHP-1 knockout cells. Deletion of SHP-1 drastically reduced global H2B ubiquitination at the gene body (Fig 6C and D). Consistent with the role of H2Bub in regulating Pol II movement during transcription, reduction in global H2Bub in SHP-1 KO cells further led to alterations in Pol II occupancy at the coding regions (Fig 6E). SHP-1 knockout cells display significant enrichment of Pol II adjacent to TSS, suggesting impaired Pol II movement upon SHP-1 loss (Fig 6F). In fact, the pausing index

Figure 5. SHP-1 participates in Pol II-mediated transcription.

A Representative super-resolution images of MCF7 cells immunostained with SHP-1 in combination with CDK9, total RNA Polymerase II, RNA polymerase II Ser2P, and RNA Polymerase II Ser5P. Scale bar: 5 μm. Fluorescence intensities along the line drawn in a representative section of cell were obtained using Zen software and the co-localization plots were made using GraphPad.

B Co-localization of SHP-1 with CDK9, total RNA Polymerase II, RNA Polymerase II S2P, and RNA Polymerase II S5P was measured by Pearson correlation coefficient using ImageJ. Values are presented as the mean ± SD, $n = 10$ (from three independent experiments). ***P value <0.001. (One-way ANOVA).

C Endogenous interaction of SHP-1 with RNA Polymerase II, RNA polymerase II Ser2P, and RNA Polymerase II Ser5P and CDK9 was detected by immunoblotting after performing immunoprecipitation with either IgG or SHP-1 antibody using TurboNuclease-treated cell lysate.

D Nuclear extracts of MCF-7 WT and SHP-1 knockout cells were made and the levels of RNA Polymerase II, RNA Polymerase II Ser2P and RNA Polymerase II Ser5P were detected by immunoblotting using specific antibodies.

E Nuclear extracts of cells treated with either DMSO or SHP-1 inhibitor TPI (50 nM) were used to detect total RNA Polymerase II and its modifications by immunoblotting using specific antibodies.

F Nuclear extracts of MCF-7 WT and SHP-1 knockout cells transfected with Myc vector, H2B Y121F, or H2B Y121D constructs were made and the levels of RNA Polymerase II, RNA Polymerase II Ser2P, RNA Polymerase II Ser5P, and Lamin B1 were detected by immunoblotting using specific antibodies.

G Immunofluorescence of WT or SHP-1 knockout MCF7 cells labeled with the 5-Ethynyl Uridine (EU) for 60 min to capture nascent RNA synthesis. Scale bars 10 μm.

H The EU incorporation in MCF-7 WT and SHP-1 KO cells was quantified in three independent experiments. Values are presented as the mean ± SD, ***indicates $P < 0.001$ (One-way ANOVA).

I Representative images of immunofluorescence of DMSO or TPI-treated (50 nM) MCF7 cells labeled with EU for 60 min are shown. Scale bar: 40 μm.

J The EU incorporation in MCF7 cells treated with DMSO or TPI was quantified in three independent experiments. Values are presented as the mean ± SD, ***indicates $P < 0.001$ (One-way ANOVA).

Source data are available online for this figure.

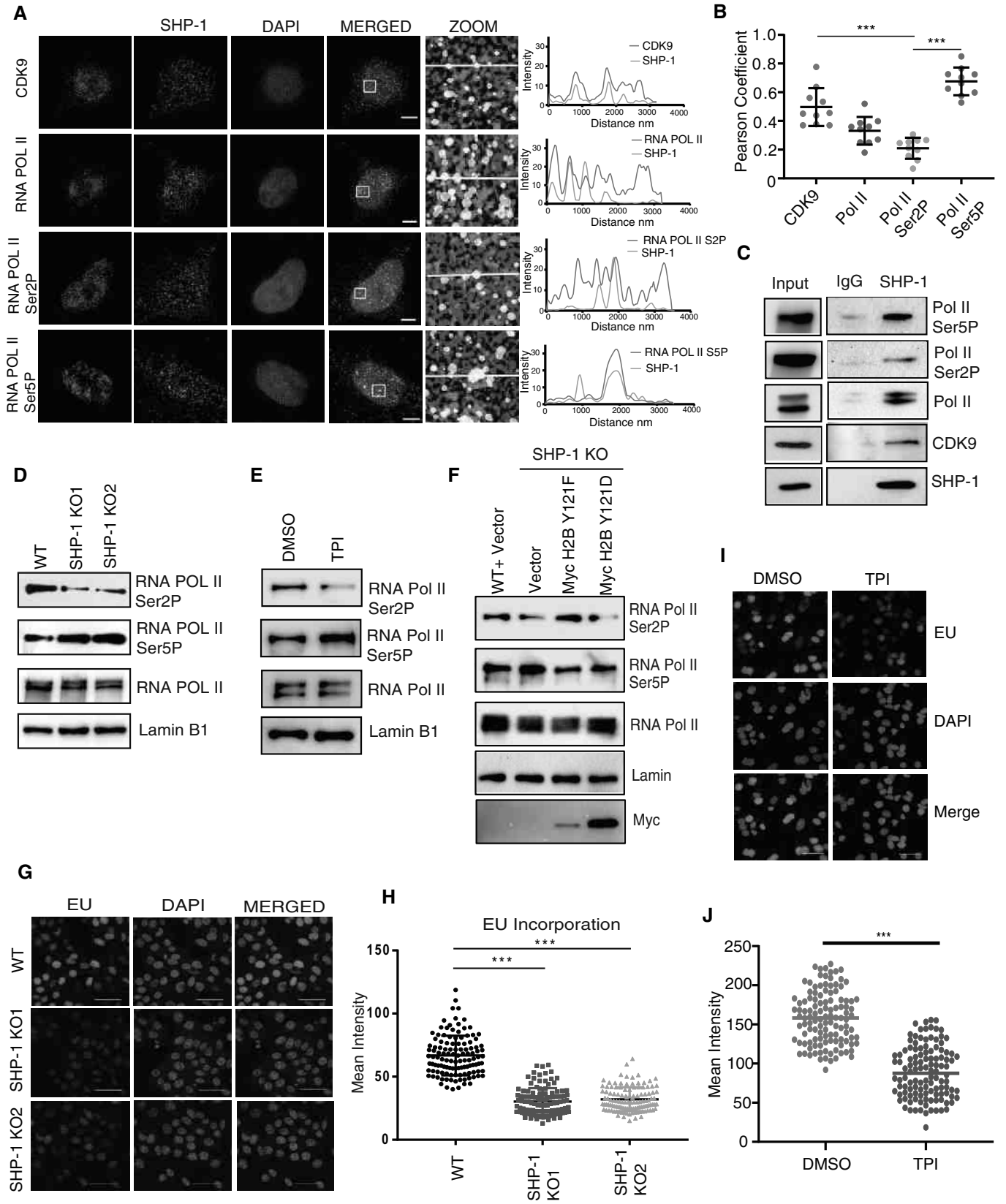

Figure 5.

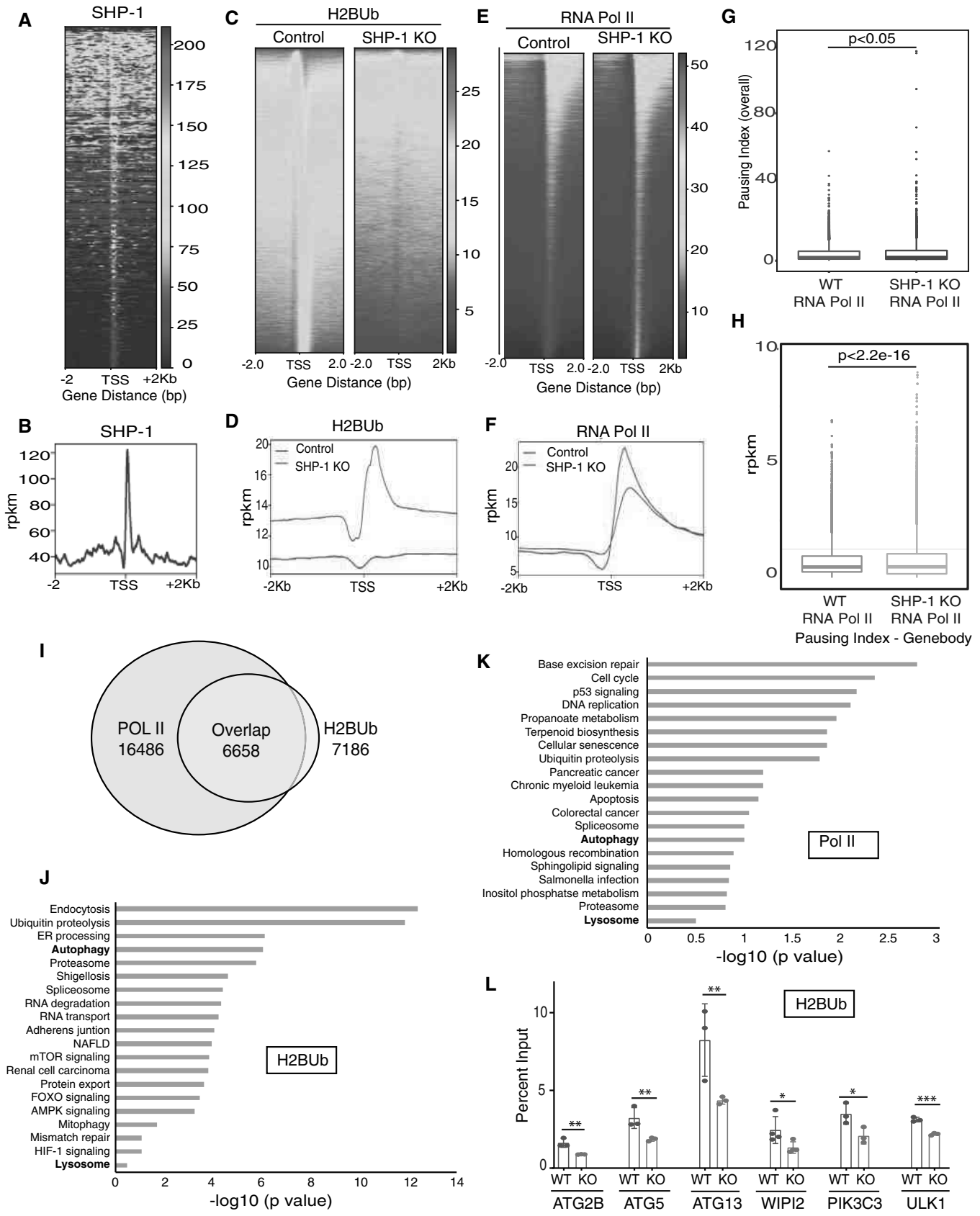

Figure 6.

Figure 6. Deletion of SHP-1 leads to global changes in H2Bub and Pol II occupancy.

A ChIP-seq density heatmap of SHP-1 occupancy within the extended gene regions (−2 kb to +2 kb around TSS) is shown.
B Genome-wide enrichment profile for SHP-1 determined by ChIP Seq in MCF7 cells is shown (−2 kb to +2 kb around TSS).
C Normalized ChIP-seq density heatmap of H2BUb occupancy over 2 kb upstream and downstream of TSS in SHP-1 WT and knockout MCF7 cells is shown.
D Genome-wide H2Bub enrichment profiles around ± 2 kb TSS determined by ChIP-seq using H2Bub-specific antibodies in MCF7 WT, and SHP-1 KO cells are shown. Color-scaled intensities are in units of rpkm.
E Heatmaps of the RNA Polymerase II occupancy around TSS (−2 kb to +2 kb) region determined by ChIP-seq using Pol II-specific antibodies in MCF7 WT and SHP-1 KO cells are shown. Heatmaps were ordered by descending ChIP-Seq signal intensity.
F Genome-wide ChIP Seq density plot of RNA Polymerase II around the TSS in SHP-1 WT and knockout MCF7 cells is shown.
G, H Box plot showing RNA Polymerase II (G) overall pausing index and (H) pausing index at gene body in MCF-7 WT and SHP-1 KO cells (n = 28,256 annotated regions). Data represent two independent experiments. Box represents overall signal distribution and line as the median. The upper and lower whiskers extend to the largest and smallest value, respectively. Significance was calculated using the Wilcoxon rank test.
I Venn diagram showing number of distinct and common ChIP seq peak-associated genes from H2Bub and RNA Pol II ChIP-seq data in SHP-1 knockout cells.
J, K Bar graphs showing the −log10 P-values of the most significant pathways enriched in (J) H2Bub ChIP-Seq and (K) Pol II ChIP-Seq derived from KEGG pathway analysis using Enrichr.
L WT and SHP-1 knockout MCF7 cells were subjected to ChIP analysis using H2BUb antibody. H2BUb enrichment in the middle region of ATG2B, ATG5, ATG13, PIK3C3, WIPI2, and ULK1 with respect to WT is shown. The data shown are derived from three independent experiments. Error bars indicate the mean ± SD; $^{**}P < 0.01$; $^{*}P < 0.05$, one-way ANOVA.

measurements has confirmed that there is an overall Pol II stalling in SHP-1 KO cells (Fig 6G). Specifically, while pausing in the promoter regions was undetected (Appendix Fig S6A), we found significant Pol II pausing in the gene bodies of SHP-1 knockout cells (Fig 6H), suggesting that SHP-1 activity is necessary for transcription elongation. Analysis of H2Bub altered genes in SHP-1 KO cells revealed 92% overlap with genes having altered Pol II occupancy (Fig 6I), again strongly suggesting the dependency of Pol II activity on H2B ubiquitination in these cells. To further understand the functional significance of alterations caused by SHP-1 loss, we annotated the H2Bub (Fig 6J) and Pol II gene list (Fig 6K) with KEGG pathway. Analysis with Enrichr tool revealed genes associated with multiple cellular processes being affected by SHP-1 loss (Fig 6J and K). Although we found global changes in H2Bub and Pol II in SHP-1 KO cells, thereby focusing on specific cellular processes, we next sought to understand the physiological relevance of H2Bub and Pol II changes caused by SHP-1 loss in cells. Among the most significantly altered processes, interestingly, the genes associated with autophagy and lysosomes were commonly found to be affected in H2Bub and Pol II list. By analyzing a set of specific candidate gene loci associated with various steps of autophagy process (ATG2B, ATG5, ATG13, WIPI2, PIK3C3 and ULK1), we validated consistent reduction in H2Bub levels on these genes upon SHP-1 loss (Fig 6L and Appendix Fig S6B).

Next, we tested if SHP-1 is associated with these candidate gene loci. Indeed, chromatin immunoprecipitation with SHP-1 specific antibody followed by q-RT-PCR analysis has clearly indicated that SHP-1 is readily enriched at the transcription start sites of the autophagy-related genes (Fig 7A). Furthermore, reduced H2B ubiquitination at these gene loci followed by Pol II occupancy changes (Appendix Fig S6C) caused by SHP-1 loss led to their decreased gene expression (Fig 7B). Importantly, decrease in H2Bub levels at these gene loci in SHP-1 KO cells could be rescued by expression (Fig 7C) of a non-phosphorylatable H2B Y121F mutant, but not a phosphomimetic Y121D mutant (Fig 7D). Also, stalling of RNA Pol II at this autophagy-related gene loci (Fig 7E) and reduced expression of these genes (Fig 7F) in SHP-1 KO cells could be rescued by expression of a non-phosphorylatable H2B Y121F mutant, but not a phosphomimetic Y121D mutant. Therefore, these data fully support our hypothesis that SHP-1 participates in promoting H2B ubiquitination during transcription by dephosphorylating Y121 residue.

SHP-1-dependent H2B dephosphorylation is required for maintenance of basal autophagy

To further assess the functional role of SHP-1-dependent changes in the autophagy genes, we analyzed the autophagic process in MCF-7 breast epithelial cells (known to exhibit higher basal autophagy) (Gavilan *et al*, 2013). Consistent with defective gene expression, SHP-1 KO cells display reduced ability in the conversion of LC3-I to LC3-II (Fig 8A and B), suggestive of defective basal autophagy. Reduced conversion of LC3 is followed by significant accumulation of LC3 puncta in SHP-1 KO cells (Fig 8C and D). Furthermore, a significant accumulation of an autophagic cargo adaptor p62 in SHP-1 KO cells substantiated the role of SHP-1 in maintenance of autophagic flux in cells (Fig EV5A–C and Appendix Fig S7A). Interestingly, expression of wild-type SHP-1 with intact NLS, but not NLS mutant, rescues basal autophagy that was lost in SHP-1 knockout cells, suggesting that nuclear SHP-1 is required for the maintenance of autophagy (Fig 8E, Appendix Fig S7B, Fig EV5D and Appendix Fig S7C). On the other hand, H2B Y121F mutant, but not Y121D mutant, could reverse p62 levels (Fig 8F and G, EV5E, and Appendix Fig S7D) and defective LC3 conversion (Fig EV5F and Appendix Fig S7E) in SHP-1 KO cells, suggesting that SHP-1 maintains basal cellular autophagy via H2B dephosphorylation. Accumulation of LC3 and p62 in SHP-1 KO cells prompted us to propose two possibilities: firstly, the defective autophagosomes might have failed to fuse with lysosomes in these cells or, alternatively, the autophagic cargo is not efficiently degraded possibly due to defective lysosomes as well. We found that LC3 puncta co-localizes with LAMP2 and is significantly accumulated in lysosomes of SHP-1 KO cells (Fig 8H and I) compared to wild-type cells, thus supporting the second possibility of defective lysosomes. Indeed, in line with this hypothesis, we found that H2Bub levels were significantly reduced on multiple gene loci coding for lysosomal genes (Appendix Fig S8). Moreover, lysotracker staining suggested that SHP-1 KO cells has significantly reduced acidic lysosomes (Fig EV5G and H). Together, these data suggest that SHP-1 maintains basal autophagic flux by controlling various genes involved in multiple steps of autophagy and lysosomal pathways.

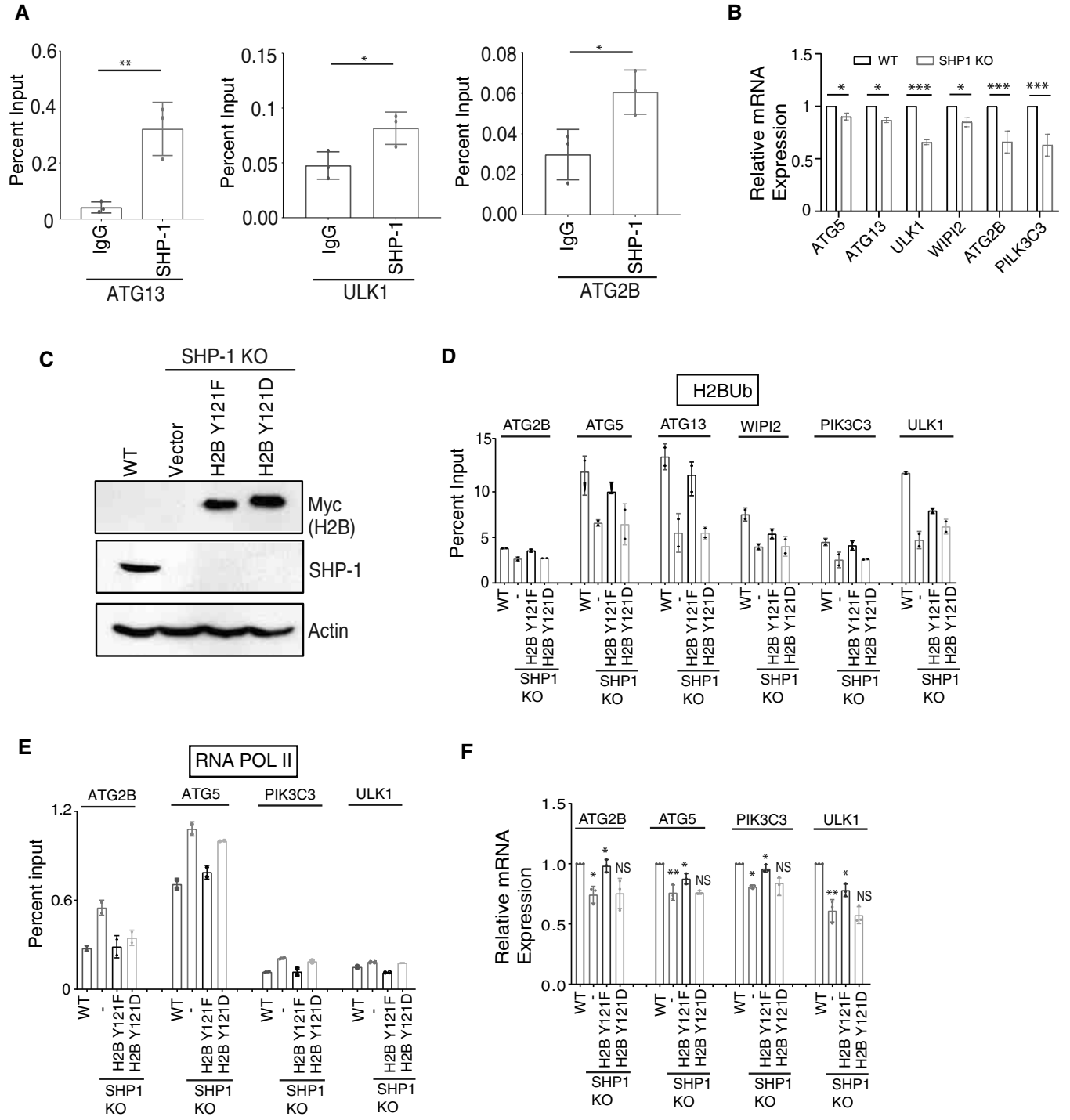

Figure 7. SHP-1 facilitates H2Bub and Pol II occupancy at transcriptional sites via H2B dephosphorylation.

A ChIP-qPCR using either anti-IgG or anti-SHP-1 antibody was performed in MCF-7 cells and the binding of SHP-1 at TSS region adjacent to the promoter region of the ATG2B, ATG13, and ULK1 genes was determined. The Y-axis represents the percentage input signal. The data shown are derived from three independent experiments. Error bars indicate the mean ± SD; $^{**}P < 0.01$; $^{*}P < 0.05$, Student's *t*-test.

B Expression of indicated genes in WT and SHP-1 knockout MCF7 cells was measured by qRT-PCR from three independent experiments. Values are presented as the mean ± SD. $^{*}P < 0.05$ and $^{***}P$ value <0.001, Student's *t*-test.

C, D MCF-7 WT cells along with SHP-1 KO cells transfected with either vector, H2B Y121F, or H2B Y121D mutant were used for ChIP q-PCR analysis of the H2BUb at indicated genes. The data shown are derived from two independent experiments. Error bars indicate the mean ± SD.

E MCF-7 WT cells along with SHP-1 KO cells transfected with either Myc vector, H2B Y121F or H2B Y121D mutant were used for ChIP-qPCR analysis of the RNA Pol II at indicated genes. The data are derived from two independent experiments. Error bars indicate the mean ± SD.

F Expression of indicated genes in WT and SHP-1 knockout MCF7 cells transfected with Myc vector, Myc H2B Y121F, or Myc H2B Y121D mutant was measured by qRT-PCR from three independent experiments. Values are presented as the mean ± SD. $^{*}P < 0.05$, $^{**}P < 0.01$, one-way ANOVA.

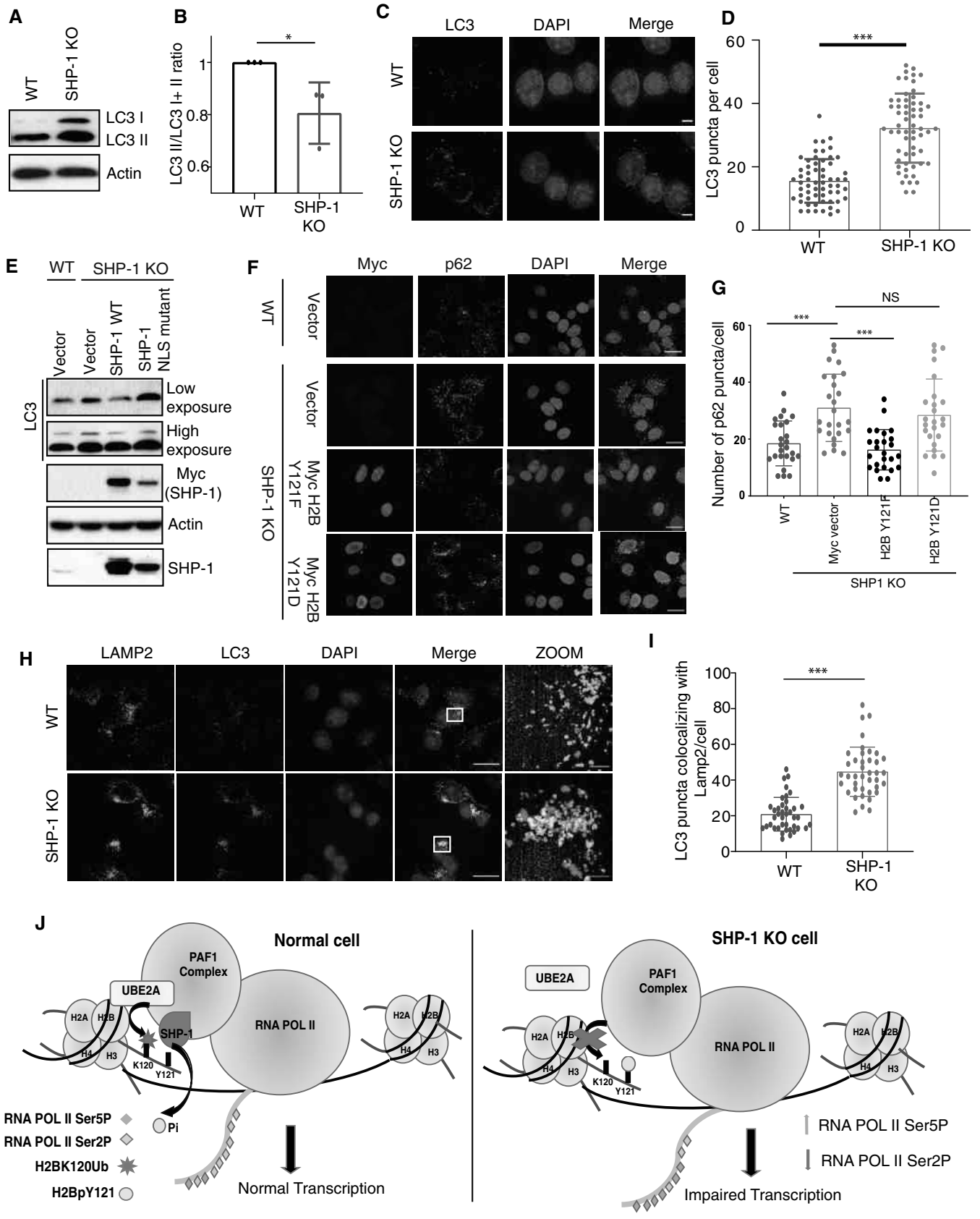

Figure 8.

Figure 8. SHP-1 is required for maintenance of basal autophagic flux.

A Lysates of WT and SHP-1 knockout MCF7 cells were made and the levels of LC3-I and II were detected by immunoblotting.

B Levels of LC3 II were normalized against total LC3 (LC3 I + LC3 II). The data shown are derived from three independent experiments. Error bars indicate the mean ± SD. *P value < 0.05, Student's t-test.

C Representative super-resolution images of WT and SHP-1 KO MCF7 cells immunostained with LC3 antibody, (Scale bar: 5 μm).

D Quantification of LC3 puncta accumulation per cell done by using ImageJ is shown. Bars represent mean ± SD (N = 60). ***P value < 0.001, Student's t-test.

E WT along with SHP-1 KO MCF7 cells transfected with either Myc vector, Myc SHP-1, or Myc SHP-1 NLS mutant were lysed. Levels of LC3 and actin were determined using specific antibodies.

F WT and SHP-1 knockout MCF7 cells transfected with the Myc vector or Myc-tagged H2B, H2B Y121F, or H2B Y121D constructs were immunostained with endogenous p62 and Myc antibody. Image acquisition was done using LSM 700, (Scale bar: 20 μm).

G Accumulation of p62 was quantified by counting p62 positive puncta per cell (N = 25); values are presented as the mean ± SD. ***P value < 0.001 (One-way ANOVA).

H Representative super-resolution images of LC3 and LAMP2 immunostaining in WT and SHP-1 KO MCF7 cells. (Scale bar: 20 μm for merge and 5 μm for Zoom).

I LC3 puncta co-localizing with LAMP2 per cell were quantified using ImageJ (N = 45); values are presented as the mean ± SD. ***P value < 0.001, Student's t-test.

J A proposed model to depict the role of nuclear SHP-1 during active transcription. SHP-1 dephosphorylates H2B at Y121 residue, thereby allowing ubiquitination of K120 site and productive transcription. Loss of SHP-1 leads to impaired transcription as H2B stays in a constitutively phosphorylated state at Y121, thus precluding interaction of E2 enzyme and failure to ubiquitinate H2B.

Source data are available online for this figure.

Discussion

Histones are subjected to diverse posttranslational modifications such as phosphorylation, acetylation, methylation, ubiquitination, SUMOylation, ADP ribosylation, deamination, proline isomerization, serotonylation, and lactylation to provide dynamic environment for precise regulation of gene expression in eukaryotes (Shilatifard, 2006; Farrelly *et al*, 2019; Zhang *et al*, 2019). The list of these modifications is constantly growing and the intricacies of their functions are only just beginning to be understood. Identification of new histone modifications, specifically the tyrosine modifications, critical for transcriptional control has gained immense interest in recent years. So far, a handful of tyrosine modifications like H3pY41 (Dawson *et al*, 2009), H2ApY57 (Basnet *et al*, 2014), H2BY37 (Mahajan *et al*, 2012), and H4pY88 (Mahajan *et al*, 2017) are reported to have a positive role in genome-wide as well as context-dependent transcription. In this study, we identified a new histone tyrosine modification that acts as a regulatory switch during eukaryotic transcription. We found that phosphorylation on tyrosine 121 residue negatively influences transcriptional outcome by inhibiting covalent attachment of ubiquitin to adjacent K120 residue (H2Bub). Tyrosine phosphatase SHP-1 dephosphorylates Y121 and allows H2B ubiquitination, thereby permitting productive transcription (model shown in Fig 8J).

One of the important features of histone modifications is the existence of crosstalk between different modifications. The earliest examples of histone modification that promotes the generation of another modification on the same histone tail were observed in the budding yeast *Saccharomyces cerevisiae*. Phosphorylation of serine 10 (S10) on histone H3 by the Snf1 kinase promoted the Gcn5-mediated acetylation of H3 lysine 14 (K14) during gene activation (Cheung *et al*, 2000; Lo *et al*, 2000). Subsequently, several crosstalks between histone modifications have emerged (Suganuma & Workman, 2008). However, undoubtedly, there are more modifications and mechanisms of histone crosstalk to be discovered. In contrast to promoting another modification, histone modification crosstalks can also direct the loss of certain modifications. For instance, H3 lysine 36 (K36) methylation leads to the removal of acetyl groups from H3 and H4 (Lee & Shilatifard, 2007). In addition to the crosstalk between modifications on the same histone, some of the most exciting examples involve trans-histone effects, where modifications on histone affect the modification of a different histone. Of specific interest is the role of H2B monoubiquitination in regulating multiple downstream modifications on other histones. H2B ubiquitination by the Rad6 enzyme is necessary to trigger H3 lysine 4 (H3K4) methylation by the Set1 methyltransferase subunit of the COMPASS complex and H3 lysine 79 (H3K79) methylation by the Dot1 methyltransferase, which is critical for transcriptional process (Zhu *et al*, 2005). Interestingly, however, an upstream regulatory event that participates in the cross talk with H2B ubiquitination is unknown so far. Therefore, our study identifying Y121 phosphorylation as an upstream control switch for H2B K120 ubiquitination adds another important layer of regulation during transcription.

Histone modifications in general exert their effects either by directly influencing the chromatin structure or by regulating (positively or negatively) the binding of downstream effector proteins. For example, phosphorylation of Histone H3 at S10 residue that occurs during mitosis leads to condensed chromatin (Wei *et al*, 1998). Similarly, modifications such as histone acetylation were also indicated to alter the chromatin structure under certain conditions (Bannister & Kouzarides, 2011). On the other hand, multiple examples exist wherein chromatin-associated proteins have been demonstrated to specifically interact with modified histones via distinct domains such as Tudor domain, Chromodomain, PHD fingers, and Bromodomain (Bannister & Kouzarides, 2011). It is possible that SHP-1 controlled H2B Y121 phosphorylation that we identified here might alter the chromatin structure at specific stages of transcription, thereby regulating the accessibility of effector proteins and the transcriptional machineries. Identification of differential binding partners using the phosphorylated versus non-phosphorylated H2B at Y121 residue, which is being actively pursued in the lab, may provide us further clues on how Y121 phosphorylation/dephosphorylation cycle alters the downstream processes. Furthermore, to fully appreciate the role of H2B Y121 phosphorylation during specific steps of transcription, it is important to map the landscape of Y121 phosphorylation at the genomic level, in future studies.

While here we demonstrated the functional significance of SHP-1-dependent H2B dephosphorylation during regulation of autophagic gene expression, it is quite clear from our H2Bub and Pol II ChIP-seq data that SHP-1 may participate in regulation of several other cellular processes. To understand the role of chromatin-

bound SHP-1:H2B connection in different cellular processes, it is imperative to identify and map the binding regions of SHP-1 on various genes known to be involved in these cellular processes. Non-availability of ChIP grade antibodies for SHP-1 is a limitation in this process. Although we utilized a custom-generated polyclonal antibody to demonstrate the association of SHP-1 at TSS regions of certain genes, we believe that genomic coverage for SHP-1 binding is low due to poor efficiency of the antibody. Therefore, generation of a high-quality ChIP grade monoclonal SHP-1 antibody is essential to fully appreciate the functional repertoire of chromatin-associated SHP-1 in cells. In addition to its role in transcription, H2Bub has been demonstrated to have an important role in events such as DNA damage response and repair, maintenance of genome stability, and tumorigenesis (Meas & Mao, 2015). Given that H2B Y121 phosphorylation controls H2B ubiquitination, it would be interesting to test if Y121 phosphorylation participates in these processes as well. Interestingly, SHP-1, the enzyme that we have shown to control Y121 phosphorylation, displays aberrations in different human cancers. For example, due to promoter hypermethylation, SHP-1 expression is reduced in the hematological malignancies like lymphoma and leukemia (Zhang *et al*, 2000). On the contrary, increased SHP-1 levels were detected in a subset of breast and in ovarian cancers (Yip *et al*, 2000). Thus, we speculate that there might be important roles of H2B Y121 phosphorylation in human cancers, which need to be unveiled in future studies.

Materials and Methods

Plasmids, shRNAs, and guide RNA

cDNA of SHP-1, Paf1, LEO1, CDC73, CTR9, WDR61, RTF1 and UbE2A were purchased from Dharmacon. H2B plasmid was purchased from addgene. All cDNAs were PCR amplified and cloned into SFB (S protein tag, FLAG tag, streptavidin-binding protein tag) triple tagged destination vector using gateway cloning. All clones were verified by sequencing. SHP-1 and H2B were cloned into Myc, MBP and GST destination vectors using the same cloning system. Point mutants (H2B Y37F, Y41F, Y43F, Y83F Y121F, Y37D, Y41D, Y43D, Y83D, Y121D, K120R) for H2B, SHP-1 ΔSH2 (comprising residues 248–597), SHP-1 C453S, SHP-1 NLS mutant (595 KRK597 mutated to AAA) were generated by site-directed mutagenesis and cloned into SFB, Myc, GST, and MBP-tagged destination vectors. Lentiviral-based shRNAs for SHP-1, Paf1, LEO1, CDC73, CTR9, WDR61, and RTF1 were purchased from open biosystems. Lentiviral vectors coding SHP-1 guide RNAs were purchased from transOMIC technologies inc.

Antibodies

Following antibodies were used in this study: SHP-1 (Abcam ab32559, WB 1:1,000), SHP-1 (Biolegend 620301, IF 1:200), SHP-1 (Bioklone, IP 2 μg), pY121-H2B (Bioklone, WB 1:50), RNA Polymerase II S2P (Abcam ab5095, WB 1:5,000 and IF 1:200), RNA Polymerase II S5P (ab5131, WB 1:5,000 and IF 1:200), RNA Polymerase II (CST 14958, WB, ChIP), RNA Polymerase II (Santa Cruz Biotechnologies sc9001; IF 1:100, Paf1 (CST 12883, WB 1:1,000), Leo1 (Bethyl A300-174A, WB 1:500), CTR9 (Bethyl A301-395A, WB 1:1,000), RTF1(Bethyl A300-179A, WB 1:1,000), WDR61(Bethyl A305-191A, WB 1:1,000), CDC73 (Novus NB200-184, WB 1:5,000), FLAG (Sigma F3165, WB 1:10,000), Actin (Sigma A5441; WB 1:10,000), Lamin B1(Abcam Ab16048 WB 1:5,000), Syk (CST 13198, WB 1:1,000), GST (Santa Cruz Biotechnologies, WB 1:5,000), HIS (Bethyl, WB 1:1,000), MBP (NEB, WB 1:5,000), Myc-tag (Santa Cruz Biotechnologies. WB 1:1,000), H2B (Millipore 07–371, WB 1:5,000); H2B (Abcam ab52484, 5 μg for endogenous IP), H2B ubiquitylated at Lys120 (H2BUb; CST 5546, WB 1:1,000), Anti p62 (CST 5114, WB 1:2,000); Abcam ab56416, IF 1:200), Anti Tubulin (Sigma T6074, WB 1:1,000), Phospho tyrosine (CST 9416, WB 1:1,000), CDK9 (Santa Cruz Biotechnologies, IF 1:100), LC3B (CST 83506, WB 1:5,000 and CST 4108, IF 1:200), LAMP2 (DSHB GL2A7 IF 1:200), Histone H4 (Abcam Ab10158, WB 1:5,000), H2A (Abcam Ab177308, WB 1:1,000), UbE2A (Bethyl A300-281A, WB 1:5,000), Myc Tag (Abcam ab9106, IF 1:200). Polyclonal anti-SHP-1 antibodies were raised by immunizing rabbits with GST-SHP-1 fusion protein (Bioklone, India). Antisera were affinity-purified using Amino Link plus Immobilization and purification kit (ThermoFisher). Antibodies for H2B-pY121 were generated by immunizing rabbits with a peptide having phosphate at Y121 position (KAVTK(pY)TSAK). After clearing through non-phospho peptide (KAVTKYTSAK) column, antibodies were affinity-purified using the column immobilized with the phospho-peptide.

Cell lines and transfections

MCF7, MDA-MB 231, HEK 293T, HCT116, A549, HeLa, THP-1, Jurkat, U937, RPE1, MCF10A and BOSC23 cell lines were used in this study. Except, MCF7, MCF10A and MDA-MB 231 cells, all cells were grown in RPMI containing 10% donor bovine serum (DBS) and 1% penicillin and streptomycin. MCF7 and MDA-MB-231 cells were maintained in DMEM plus 10% DBS with 1% penicillin and streptomycin. MCF10A cells were maintained in DMEM/F12 medium supplemented with 5% FBS, 20 ng/ml EGF, 0.5 mg/ml hydrocortisone, 100 ng/ml cholera toxin, 10 μg/ml insulin along with penicillin and streptomycin. Cells were continuously checked by microscopy for their original morphology and tested for mycoplasma contamination by using DAPI staining. Transfection of cells with different plasmids was carried out with PEI (Polysciences) according to the manufacturer's protocol. Briefly, the plasmid diluted in serum-free RPMI medium was mixed with PEI (1 mg/ml) in 1:3 ratio. After incubating the DNA–PEI mixture at room temperature for 15 min, the complexes were added to cells to allow the transfection of plasmid.

Lentiviral infection

Lentivirus-based Paf1, RTF1, and CTR9 shRNA clones were purchased from Open Biosystems. shRNAs were transfected transiently using PEI (Invitrogen) in BOSC23 packaging cells along with packaging vectors (psPAX2 and pMD2.G); 48 h post transfection, the viral medium was collected, filtered through 0.45 μM filter, and added to the target cells along with polybrene (8 mg/ml); 72 h post infection, cells were collected and processed for various assays and immunoblotting was performed with the specific antibodies to check the efficiency of knockdown.

Generation of SHP-1 knockout cell lines

SHP-1 knockout MCF7 and 293T cell lines were established using the CRISPR/Cas9 system. In brief, guide RNAs (TEVH-1119886 and TEVH-1187028) targeting SHP-1 and non-targeting control (TELA1011) were purchased from transOMIC technologies (pCLIP-All-EFS-Puro vector). Plasmids were transfected into cells with Turbofect according to the manufacturer's protocol. After 48 h, cells were treated with puromycin (2 μg/ml) and further subjected to clonal selection. Positive clones were verified by Western blot for the absence of SHP-1 protein expression.

Immunoprecipitation

For immunoprecipitation assays, cells were harvested and lysed with NETN buffer (20 mM Tris- HCl at pH 8.0, 100 mM NaCl, 1 mM EDTA, 0.5% Nonidet P-40) containing 1 mg/ml each of pepstatin A and aprotinin, centrifuged at 13,000 rpm for 15 min at 4°C. The whole-cell lysates obtained by centrifugation were incubated with 5 μg of specific antibody bound to protein G sepharose beads for 4 h at 4°C. TurboNuclease (50 U/ml) treatment for 30 min in the presence of 1 mM $MgCl_2$ was carried out on cell lysates before immunoprecipitation in specific experiments to rule out the interference from DNA contamination during protein–protein interactions. The immunocomplexes were then washed with NETN buffer six times and eluted by boiling in 1× laemmli buffer. Samples were resolved by SDS-PAGE and immunoblotted with indicated antibodies.

Denaturing immunoprecipitation

The 293T whole cell lysate was prepared by boiling the cells in denaturing lysis buffer (20 mM Tris pH 8.0, 1% SDS, 10 mM dithiothreitol) for 10 min. The SDS concentration of cell lysate was adjusted to 0.1% by adding 1× NETN buffer and incubated on ice for 20 min. The whole-cell lysates obtained by centrifugation were incubated with streptavidin–sepharose for 4 h at 4°C. The immunocomplexes were then washed with NETN buffer six times and applied to SDS–PAGE.

Peptide competition assay

To validate the specificity of Y121 phospho antibody, the peptide competition experiment was performed according to the following protocol (http://docs.abcam.com/pdf/protocols/peptide_competition_assay_protocol.pdf). Briefly, 2 μg of primary antibody (pY121 specific antibody) was left with no peptide or incubated with 100 μM of either non-phospho or phospho-peptide of H2B for overnight. The pre-incubated antibody in each of these samples was used in immunblotting of nuclear cell lysates to detect Y121 phosphorylation signal.

In vitro ubiquitination assay

In vitro ubiquitination assay was performed according to the protocol described earlier (Kim & Roeder, 2011; Yao *et al*, 2015). Briefly, ubiquitination reactions containing 100 ng E1, 100 ng E2, 2.5 μg ubiquitin, and 2.0 μg recombinant WT H2B, H2B Y121F, or H2B Y121D mutants or 1 μg of phospho or non-phosphopeptides or 2 μg His H2A: H2B, His H2A: H2BY121F and His H2A: H2B dimers in 20 μl reaction buffer (50 mM Tris–HCl pH 7.9, 5 mM $MgCl_2$, 2 mM NaF, 0.4 mM DTT, and 4 mM ATP) was incubated at 37°C for 1.5 h and then subjected to SDS–PAGE and Western blot using the H2BK120Ub antibody.

H2A: H2B Dimer preparation

H2A: H2B dimers were prepared as described earlier (Tachiwana *et al*, 2008). *Escherichia coli* BL21 (DE3) cells producing His H2A, His H2B, His H2B Y121F, and His H2B Y121D were collected and suspended in buffer containing 50 mM Tris pH 8, 500 mM NaCl, 1 mM PMSF, and 5% glycerol. Samples were sonicated for 20 cycles in Diagenode Bioruptor at high power (30 s on 30 s off). After centrifugation at 27,000 *g* for 20 min at 4°C, the pellets containing His tagged histones were re-suspended in urea buffer (Tris pH 8, 6 M Urea) and cleared by centrifugation at 27,000 *g* for 20 min at 4°C. Cell lysates were pulled down with Ni-NTA beads for 1 h at 4°C. The beads were then washed with a urea buffer containing 5 mM imidazole and bound proteins were eluted with the tris-urea buffer containing 300 mM imidazole. His tagged H2A and H2B proteins were mixed in the equimolar ratio in tris-urea buffer and dialyzed overnight against reconstitution buffer (20 mM Tris pH 8, 5 mM DTT, 1 mM EDTA, 1 mM PMSF, and 5% glycerol) containing 2 M NaCl. To lower the concentration of NaCl, stepwise dialysis was performed against the reconstitution buffer (1 M NaCl for 4 h, 0.5 M NaCl for 4 h and 0.1 M NaCl overnight) at 4°C. After dialysis, samples were cleared by centrifugation at 27,000 *g* for 10 min to remove insoluble aggregates.

Micrococcal nucleosome preparation

Nucleosomes were prepared as described earlier (Khan *et al*, 2020). Briefly, cells were harvested by centrifugation at 4°C for 5 min at 300 *g*, washed twice with ice-cold PBS and once with buffer A (10 mM HEPES pH 8, 10 mM KCl, 1.5 mM $MgCl_2$, 340 mM sucrose, 10% glycerol, and 1 mM DTT). Cells were resuspended in buffer A containing 0.2% Triton-X100 and incubated on ice for 5 min. The nuclei were pelleted by centrifugation (1,300 *g*, for 5 min, at 4°C) and washed once with ice-cold buffer A, followed by centrifugation (1,300 *g*, 5 min at 4°C). Then, nuclei were digested with 40 units/ml micrococcal nuclease (NEB) in digestion buffer (15 mM NaCl, 60 mM KCl and 10 mM $CaCl_2$) for 2 h at 37°C. The micrococcal nuclease reaction was quenched by the addition of EGTA to a final concentration of 20 mM. Then, samples were centrifuged at 13,000 *g* for 5 min at 4°C. The supernatant containing soluble nucleosomes was collected and stored at −80°C before use. The quality of the purified nucleosomes was analyzed by gel electrophoresis.

Immunofluorescence staining

Cells were grown on glass coverslips and fixed with 3% paraformaldehyde solution in PBS at room temperature for 10 min. Permeabilization of the cells was carried out with ice-cold methanol for 10 min and cells were incubated with 5% BSA for blocking at room temperature for 60 min. After this step, cells were washed

with PBS and incubated with primary antibodies overnight at 40C followed by washing thrice with 1× PBS. Cells were then incubated with Alexa488 or rhodamine-conjugated secondary antibodies at 37°C for 60 min followed by washing thrice with 1× PBS. Nuclei were stained with 4′,6-diamidino-2-phenylindole (DAPI). After a final wash with PBS, coverslips were mounted with glycerin-containing para- phenylenediamine, and imaging was done using a confocal microscope (LSM Meta 510, Zeiss). For LC3 and LAMP2 staining, cells were fixed with ice-cold methanol for 10 min and 4% paraformaldehyde fixative was used for p62 staining as well as lysotracker staining. Super-resolution images were acquired with LSM 980 Airyscan 2 microscope using Plan-Apochromat 63×/1.4 Oil DIC M27. Images were obtained using Z-stacks with a step size of 0.5 μm. Raw images were processed using the Zen Black software.

Histone extraction

Histone extraction was performed according to the protocol described earlier (Shechter *et al*, 2007). Briefly, cells were collected in 1× PBS and lysed in hypotonic lysis buffer to obtain nuclei. Histones were extracted by incubating nuclear pellets in 0.4 N H_2SO_4 overnight at 4°C. The supernatant containing histones was precipitated using chilled trichloroacetic acid (33%). The precipitate was washed with acetone to remove residual TCA. The pellets were air dried and 1× NETN was added to dissolve histones. Histone fractions were subjected to SDS-PAGE followed by Western blotting with antibodies of interest.

Subcellular fractionation

After washing twice with ice cold PBS, the cell pellets were resuspended in CE buffer (20 mM Tris, pH 7.6, 50 mM ß-mercaptoethanol, 0.1 mM EDTA, 2 mM $MgCl_2$, 1 mM PMSF supplemented with protease and phosphatase inhibitors) and incubated for 2 min at room temperature and for another 10 min on ice. After incubation, NP-40 was added at a final concentration of 1% (v/v) and lysates were homogenized by passing through a 22-G needle for three times. Nuclei were pelleted by centrifugation at 600 *g* for 5 min at 4°C and supernatant containing cytoplasmic fraction was collected. The remaining nuclei pellets were washed three times in CE buffer containing 1% NP-40. The nuclear pellets were lysed in NE buffer (20 mM HEPES, pH 7.9, 2.5% glycerol, 1 mM EDTA, 0.4 M NaCl, 1 mM PMSF, 10 mM NaF, 2 mM Na_3VO_4, 0.5 mM DTT, supplemented with protease inhibitors) by repeated freezing and thawing. Supernatant containing soluble nuclear fraction was collected by centrifugation at 20,000 *g* for 20 min. The chromatin pellets obtained following centrifugation were resuspended in SDS loading dye and boiled for 10 min at 90°C.

In vitro phosphatase assay

The bacterially purified H2B was incubated in the presence of 0.1 μg Syk and 10 μM ATP in reaction buffer (30 mM HEPES pH 7.5, 2 mM $MnCl_2$, 10 mM $MgCl_2$, 2 mM DTT and 0.1 mM Sodium Orthovandate) at 30°C for 60 min. For the kinase reaction on Paf1 components, bacterially purified proteins were incubated with 293T lysate in the presence of 25MM HEPES (pH 7.5), 25 mM β-glycerophosphate, 25 mM $MgCl_2$, 2 mM DTT, 0.1 mM sodium orthovandate, and 1 mM ATP. The phosphorylated substrates were then incubated with constitutively active mutant (SHP-1 ΔSH2) or catalytically inactive mutant (SHP-1 C/S) in reaction buffer (25 mM HEPES pH 7.4, 2.5 mM EDTA, 5 mM DTT, and 50 mM NaCl) at 37°C for 60 min. After phosphatase assay, beads were washed three times with 1× NETN and run on SDS-PAGE followed by transfer onto PVDF membrane. After incubating the membrane with blocking buffer (1 h), pIMAGO-Biotin reagent was added and further incubated for 1 h. After three washes with 1× wash buffer, the membrane was incubated with avidin-HRP for 1 h. After washing three times with 1× TBST, phosphorylation signals were detected by ECL reagent. On the other hand, the released phosphate was also detected using malachite green assay kit (Cayman) by measuring the absorbance at 620 nm.

In vitro binding assay

Bacterially expressed GST–H2B or control GST immobilized to Glutathione-Sepharose beads (GE Healthcare) was incubated with bacterially purified MBP SHP-1 for 2 h at 4°C. Further beads were washed five times and the washed complexes were eluted by boiling in 2× SDS sample buffer and then separated by SDS–PAGE; the interactions were analyzed by Western blotting.

EU incorporation and IF

SHP-1 WT and knockout MCF7 cells were incubated with a modified nucleotide Ethynyl Uridine (EU) at 2 mM concentration for 30 min for incorporation into nascent RNA prior to fixation. Detection with the Click-iT RNA Alexa Fluor 594 Imaging Kit (Thermo Fisher, C10330) was done according to the manufacturer's instructions. Image acquisition was done using Leica SP8.

Quantitative real-time PCR

Total RNA was isolated using Macherey-Nagel RNA isolation kit as per the manufacturer's instructions. Reverse transcription was performed using cDNA synthesis kit (Takara). qRT-PCR was then performed using the TB Green Premix Ex Taq II (Tli RNaseH plus) kit (Takara Bio) in Biorad real-time PCR systems as per the manufacturer's protocol. The threshold cycle (Ct) values for particular genes were normalized to GAPDH for each sample. Sequences for primers used for qRT-PCR analysis are included in Appendix Table S1.

ChIP assay

The 3 μg rabbit IgG (Bethyl Laboratories), 4 μl of H2BUb (CST 5546; dilution 1:200), 4 μl (RNA Polymerase II; CST 14958) or 20 μl of SHP-1 (In house purified) antibodies were used for chromatin immunoprecipitation (ChIP) assay. Briefly, MCF7 cells were cross-linked with 1% formaldehyde for 10 min at room temperature. Crosslinking was quenched by the addition of glycine to a final concentration of 125 mM. Cells were then spun down and washed twice with ice-cold 1 × PBS and lysed in cell lysis buffer (5 mM PIPES pH 8.8, 5 mM KCl, 0.5% NP-40, and protease inhibitors) followed by nuclei lysis buffer (50 mM Tris pH 8.1, 10 mM EDTA, 1% SDS, and protease inhibitors). Isolated chromatin was sheared to a range of 500–200 bp by sonicating for 20 cycles (30 s on, 30 s off)

using a Diagenode Bioruptor at medium power. After centrifugation, the supernatant was diluted with 1 × IP dilution buffer and preclearing was performed using Protein G beads for 1 h. Then, equal amount of antibody was added and incubated on a nutator overnight at 4°C. Next day, protein G beads were added to chromatin. Beads were washed twice with IP Dialysis buffer (2 mM EDTA and 50 mM Tris pH 8) and three times with IP wash buffer (100 mM Tris pH 8, 250 mM LiCl, 1% NP-40, and 1% Na deoxycholate) for 5 min at room temperature. Then, beads were quickly washed with 1 × TE and bound DNA fragments were eluted twice using elution buffer (50 mM $NaHCO_3$ and 1% SDS) at 65°C. Input and eluted DNA was heated at 65°C overnight for reverse crosslinking which was followed by RNase treatment and finally the proteinase K treatment. DNA samples were purified using Phenol Chloroform extraction method.

ChIP-seq analysis

The ChIP DNA (10 ng) was used for making ChIP-sequencing libraries using NEB Next Ultra II DNA Library preparation kit. Paired-end sequencing (2 × 100 bp) was performed on the Illumina HiSeq 2500/4000 for H2Bub and RNA Pol II ChIP Seq and Illumina Nextseq 2000 platform for SHP1 ChIP Seq. Fastqc of chip-seq data was done using babraham fastqc tools (https://www.bioinformatics.babraham.ac.uk/projects/fastqc/). Bowtie2 (version 2.3.2) was used to perform alignment of the respective paired-end samples using hg38 reference genome. Sorting and indexing of bam files were done using samtools (version 1.9). Duplicate reads were removed using picard tool (version 2.9.4). To generate the matrix for genomic regions and heatmaps, Deeptool functions "computeMatrix" and "plotheatmap" were used. Macs2 (version 2.2.7.1) was used for peak calling of respective samples. Those peaks were filtered for the blacklist region using hg38-blacklist.v2.bed, which was obtained from the ENCODE consortium. Bedops (version 2.4.27) was used for overlaping genomic regions. The "annotatePeaks.pl" and "analyzerepeats.pl" scripts from HOMER suite (version 4.6) (using gencode hg38) were used to annotate peaks and to calculate the pausing index for RNA polymerase II datasets. Statistical analysis was performed in R (version 3.6.0) using "ggpubr" library (version 0.4.0) along with ggplot2 (version 3.3.3).

Data availability

ChIP seq data for H2Bub, RNA Pol II, and SHP-1 are available at array express (E-MTAB-10295). https://www.ebi.ac.uk/arrayexpress/experiments/E-MTAB-10295/

Expanded View for this article is available online.

Acknowledgments
This work was supported by DBT/Wellcome Trust India Alliance senior fellowship grant (IA/S/16/2/502729 to S.M) and CDFD core funds. PP acknowledges the funding support (Grant reference no. CRG/2018/002052) from Science and Engineering Research Board (SERB), India. PT acknowledges the fellowship support (Sr. No. 2121430486, Ref No. 21/12/2014(ii)EU-V) from University Grants Commission (UGC), India. We thank all members of LCDCS, CDFD for their critical inputs. We thank Dr. Sanjeev Khosla for providing purified histones. We thank Dr. Ravi Manjithaya for providing p62 antibodies and Dr. Sunil Manna for LC3 IF-grade antibody. We thank Dr. Rupinder Kaur for providing micrococcal nuclease. We thank Nanci Rani for providing technical assistance, sophisticated equipment facility at CDFD for assistance in imaging, and the National Genomics Core at CDFD for assistance in ChIP-Seq.

Author contributions
Prajakta Tathe: Data curation; formal analysis; investigation; methodology; writing – original draft; writing – review and editing. **K V S Rammohan Chowdary:** Investigation; methodology. **Krushna Chandra Murmu:** Data curation; formal analysis; methodology. **Punit Prasad:** Data curation; formal analysis; methodology. **Subbareddy Maddika:** Conceptualization; resources; formal analysis; funding acquisition; writing – original draft; project administration; writing – review and editing.

In addition to the CRediT author contributions listed above, the contributions in detail are:

SM conceptualized and managed the project. SM and PT designed the experiments, analyzed the data, and wrote the manuscript. PT performed most of the experiments; KVSRC contributed to Paf complex interaction experiments. KCM and PP analyzed the ChIP-Seq data and also contributed to writing of the manuscript.

Disclosure and competing interest statement
The authors declare that they have no conflict of interest.

References

Azoulay-Alfaguter I, Strazza M, Peled M, Novak HK, Muller J, Dustin ML, Mor A (2017) The tyrosine phosphatase SHP-1 promotes T cell adhesion by activating the adaptor protein CrkII in the immunological synapse. *Sci Signal* 10: eaal2880

Bannister AJ, Kouzarides T (2011) Regulation of chromatin by histone modifications. *Cell Res* 21: 381 – 395

Bartkowiak B, Liu P, Phatnani HP, Fuda NJ, Cooper JJ, Price DH, Adelman K, Lis JT, Greenleaf AL (2010) CDK12 is a transcription elongation-associated CTD kinase, the metazoan ortholog of yeast Ctk1. *Genes Dev* 24: 2303 – 2316

Basnet H, Su XB, Tan Y, Meisenhelder J, Merkurjev D, Ohgi KA, Hunter T, Pillus L, Rosenfeld MG (2014) Tyrosine phosphorylation of histone H2A by CK2 regulates transcriptional elongation. *Nature* 516: 267 – 271

Brockdorff J, Williams S, Couture C, Mustelin T (1999) Dephosphorylation of ZAP-70 and inhibition of T cell activation by activated SHP1. *Eur J Immunol* 29: 2539 – 2550

Chen FX, Smith ER, Shilatifard A (2018) Born to run: control of transcription elongation by RNA polymerase II. *Nat Rev Mol Cell Biol* 19: 464 – 478

Chen F, Liu B, Guo L, Ge X, Feng W, Li DF, Zhou H, Long J (2021) Biochemical insights into Paf1 complex-induced stimulation of Rad6/Bre1-mediated H2B monoubiquitination. *Proc Natl Acad Sci USA* 118: e2025291118

Cheung P, Tanner KG, Cheung WL, Sassone-Corsi P, Denu JM, Allis CD (2000) Synergistic coupling of histone H3 phosphorylation and acetylation in response to epidermal growth factor stimulation. *Mol Cell* 5: 905 – 915

Core LJ, Waterfall JJ, Lis JT (2008) Nascent RNA sequencing reveals widespread pausing and divergent initiation at human promoters. *Science* 322: 1845 – 1848

Craggs G, Kellie S (2001) A functional nuclear localization sequence in the C-terminal domain of SHP-1. *J Biol Chem* 276: 23719 – 23725

Dawson MA, Bannister AJ, Gottgens B, Foster SD, Bartke T, Green AR, Kouzarides T (2009) JAK2 phosphorylates histone H3Y41 and excludes HP1alpha from chromatin. *Nature* 461: 819 – 822

Dustin LB, Plas DR, Wong J, Hu YT, Soto C, Chan AC, Thomas ML (1999) Expression of dominant-negative src-homology domain 2-containing protein tyrosine phosphatase-1 results in increased Syk tyrosine kinase activity and B cell activation. *J Immunol* 162: 2717 – 2724

Ebmeier CC, Erickson B, Allen BL, Allen MA, Kim H, Fong N, Jacobsen JR, Liang K, Shilatifard A, Dowell RD *et al* (2017) Human TFIIH kinase CDK7 regulates transcription-associated chromatin modifications. *Cell Rep* 20: 1173 – 1186

Farrelly LA, Thompson RE, Zhao S, Lepack AE, Lyu Y, Bhanu NV, Zhang B, Loh YE, Ramakrishnan A, Vadodaria KC *et al* (2019) Histone serotonylation is a permissive modification that enhances TFIID binding to H3K4me3. *Nature* 567: 535 – 539

Fuda NJ, Buckley MS, Wei W, Core LJ, Waters CT, Reinberg D, Lis JT (2012) Fcp1 dephosphorylation of the RNA polymerase II C-terminal domain is required for efficient transcription of heat shock genes. *Mol Cell Biol* 32: 3428 – 3437

Gates LA, Foulds CE, O'Malley BW (2017) Histone marks in the 'driver's seat': functional roles in steering the transcription cycle. *Trends Biochem Sci* 42: 977 – 989

Gavilan E, Sanchez-Aguayo I, Daza P, Ruano D (2013) GSK-3beta signaling determines autophagy activation in the breast tumor cell line MCF7 and inclusion formation in the non-tumor cell line MCF10A in response to proteasome inhibition. *Cell Death Dis* 4: e572

Hsin JP, Manley JL (2012) The RNA polymerase II CTD coordinates transcription and RNA processing. *Genes Dev* 26: 2119 – 2137

Jiang M, Zheng C, Shou P, Li N, Cao G, Chen Q, Xu C, Du L, Yang Q, Cao J *et al* (2016) SHP1 regulates bone mass by directing mesenchymal stem cell differentiation. *Cell Rep* 17: 2161

Khan KA, Ng MK, Cheung P (2020) The use of Mononucleosome immunoprecipitation for analysis of combinatorial histone post-translational modifications and purification of nucleosome-interacting proteins. *Front Cell Dev Biol* 8: 331

Kim J, Roeder RG (2011) Nucleosomal H2B ubiquitylation with purified factors. *Methods* 54: 331 – 338

Kim K, Kim JM, Kim JS, Choi J, Lee YS, Neamati N, Song JS, Heo K, An W (2013) VprBP has intrinsic kinase activity targeting histone H2A and represses gene transcription. *Mol Cell* 52: 459 – 467

Komarnitsky P, Cho EJ, Buratowski S (2000) Different phosphorylated forms of RNA polymerase II and associated mRNA processing factors during transcription. *Genes Dev* 14: 2452 – 2460

Kumar P, Munnangi P, Chowdary KR, Shah VJ, Shinde SR, Kolli NR, Halehalli RR, Nagarajaram HA, Maddika S (2017) A human tyrosine phosphatase Interactome mapped by proteomic profiling. *J Proteome Res* 16: 2789 – 2801

Lee JS, Shilatifard A (2007) A site to remember: H3K36 methylation a mark for histone deacetylation. *Mutat Res* 618: 130 – 134

Li B, Carey M, Workman JL (2007) The role of chromatin during transcription. *Cell* 128: 707 – 719

Lo WS, Trievel RC, Rojas JR, Duggan L, Hsu JY, Allis CD, Marmorstein R, Berger SL (2000) Phosphorylation of serine 10 in histone H3 is functionally linked in vitro and in vivo to Gcn5-mediated acetylation at lysine 14. *Mol Cell* 5: 917 – 926

Mahajan K, Fang B, Koomen JM, Mahajan NP (2012) H2B Tyr37 phosphorylation suppresses expression of replication-dependent core histone genes. *Nat Struct Mol Biol* 19: 930 – 937

Mahajan K, Malla P, Lawrence HR, Chen Z, Kumar-Sinha C, Malik R, Shukla S, Kim J, Coppola D, Lawrence NJ *et al* (2017) ACK1/TNK2 regulates histone H4 Tyr88-phosphorylation and AR gene expression in castration-resistant prostate cancer. *Cancer Cell* 31: 790 – 803

Marshall NF, Peng J, Xie Z, Price DH (1996) Control of RNA polymerase II elongation potential by a novel carboxyl-terminal domain kinase. *J Biol Chem* 271: 27176 – 27183

Meas R, Mao P (2015) Histone ubiquitylation and its roles in transcription and DNA damage response. *DNA Repair (Amst)* 36: 36 – 42

Rossetto D, Avvakumov N, Cote J (2012) Histone phosphorylation: a chromatin modification involved in diverse nuclear events. *Epigenetics* 7: 1098 – 1108

Sakai K, Tanaka Y, Asahi M, Shimomura R, Taniguchi T, Hashimoto E, Yamamura H (1991) Identification of the phosphorylation sites of H2B histone by a catalytic fragment of p72syk from porcine spleen. *FEBS Lett* 294: 104 – 108

Shechter D, Dormann HL, Allis CD, Hake SB (2007) Extraction, purification and analysis of histones. *Nat Protoc* 2: 1445 – 1457

Shilatifard A (2006) Chromatin modifications by methylation and ubiquitination: Implications in the regulation of gene expression. *Annu Rev Biochem* 75: 243 – 269

Suganuma T, Workman JL (2008) Crosstalk among histone modifications. *Cell* 135: 604 – 607

Svejstrup JQ (2004) The RNA polymerase II transcription cycle: cycling through chromatin. *Biochim Biophys Acta* 1677: 64 – 73

Tachiwana H, Osakabe A, Kimura H, Kurumizaka H (2008) Nucleosome formation with the testis-specific histone H3 variant, H3t, by human nucleosome assembly proteins in vitro. *Nucleic Acids Res* 36: 2208 – 2218

Takahashi A, Tsutsumi R, Kikuchi I, Obuse C, Saito Y, Seidi A, Karisch R, Fernandez M, Cho T, Ohnishi N *et al* (2011) SHP2 tyrosine phosphatase converts parafibromin/Cdc73 from a tumor suppressor to an oncogenic driver. *Mol Cell* 43: 45 – 56

Van Oss SB, Cucinotta CE, Arndt KM (2017) Emerging insights into the roles of the Paf1 complex in gene regulation. *Trends Biochem Sci* 42: 788 – 798

Van Zant G, Shultz L (1989) Hematologic abnormalities of the immunodeficient mouse mutant, viable motheaten (mev). *Exp Hematol* 17: 81 – 87

Varone A, Spano D, Corda D (2020) Shp1 in solid cancers and their therapy. *Front Oncol* 10: 935

Wei Y, Mizzen CA, Cook RG, Gorovsky MA, Allis CD (1998) Phosphorylation of histone H3 at serine 10 is correlated with chromosome condensation during mitosis and meiosis in Tetrahymena. *Proc Natl Acad Sci USA* 95: 7480 – 7484

Yang W, Tabrizi M, Yi T (2002) A bipartite NLS at the SHP-1 C-terminus mediates cytokine-induced SHP-1 nuclear localization in cell growth control. *Blood Cells Mol Dis* 28: 63 – 74

Yao X, Tang Z, Fu X, Yin J, Liang Y, Li C, Li H, Tian Q, Roeder RG, Wang G (2015) The mediator subunit MED23 couples H2B mono-ubiquitination to transcriptional control and cell fate determination. *EMBO J* 34: 2885 – 2902

Yeo M, Lin PS, Dahmus ME, Gill GN (2003) A novel RNA polymerase II C-terminal domain phosphatase that preferentially dephosphorylates serine 5. *J Biol Chem* 278: 26078 – 26085

Yip SS, Crew AJ, Gee JM, Hui R, Blamey RW, Robertson JF, Nicholson RI, Sutherland RL, Daly RJ (2000) Up-regulation of the protein tyrosine phosphatase SHP-1 in human breast cancer and correlation with GRB2 expression. *Int J Cancer* 88: 363 – 368

Zhang Q, Raghunath PN, Vonderheid E, Odum N, Wasik MA (2000) Lack of phosphotyrosine phosphatase SHP-1 expression in malignant T-cell lymphoma cells results from methylation of the SHP-1 promoter. *Am J Pathol* 157: 1137 – 1146

Zhang D, Tang Z, Huang H, Zhou G, Cui C, Weng Y, Liu W, Kim S, Lee S, Perez-Neut M *et al* (2019) Metabolic regulation of gene expression by histone lactylation. *Nature* 574: 575 – 580

Zhu B, Zheng Y, Pham AD, Mandal SS, Erdjument-Bromage H, Tempst P, Reinberg D (2005) Monoubiquitination of human histone H2B: The factors involved and their roles in HOX gene regulation. *Mol Cell* 20: 601 – 611